THE UNIVERSITY OF TEXAS SOUTHWESERN MEDICAL CENTER AT DALLAS
GRADUATE SCHOOL OF BIOMEDICAL SCIENCES

As members of the Dissertation Committee, we certify that we have read the dissertation prepared by Shanna Alexandria Arnold

entitled

SPARC: A MATRICELLULAR REGULATOR OF THE TUMOR MICROENVIRONMENT

and recommend that it be accepted as fulfilling the dissertation requirement for the Degree of Doctor of Philosophy

Rolf A. Brekken Date: 12/03/2009
Rolf A. Brekken, Ph.D., Associate Professor

Kristine E. Kamm Date: 12/03/2009
Kristine E. Kamm, Ph.D., Professor

Philip E. Thorpe Date: 12/03/2009
Philip E. Thorpe, Ph.D., Professor

Michelle Tallquist Seidel Date: 12/03/2009
Michelle Tallquist Seidel, Ph.D., Associate Professor

Final approval and acceptance of this dissertation is contingent upon the candidate's submission of the final copies of the dissertation to the Graduate School of Biomedical Sciences.

I would like to dedicate this to my mother, LaRita Keel, for teaching me by example unconditional love, as well as unwavering strength, will and determination. Thank you to all of my friends, both old and new, who have contributed greatly to my success. I would like to extend a special thanks to Sandy VanderVleit and Cindi Nipp for their generosity and love when it was most needed. Lastly, I dedicate my thesis work to those loved ones that have lost their battle with cancer, but have inspired me to pursue cancer research in hopes of improving therapy for future generations. In loving memory of Carolyn Castleman, Edward Watson, Brenda Calicoat, Jackie Duck and Julie Sutterfield.

SPARC: A MATRICELLULAR REGULATOR OF THE TUMOR MICROENVIRONMENT

By

SHANNA ALEXANDRIA ARNOLD

DISSERTATION

Presented to the Faculty of the Graduate School of Biomedical Sciences

The University of Texas Southwestern Medical Center at Dallas

In Partial Fulfillment of the Requirements

For the Degree of

DOCTOR OF PHILOSOPHY

The University of Texas Southwestern Medical Center at Dallas

Dallas, Texas

December, 2009

SPARC: A MATRICELLULAR REGULATOR OF THE TUMOR MICROENVIRONMENT

Shanna Alexandria Arnold, Ph.D.

The University of Texas Southwestern Medical Center at Dallas, 2009

Rolf Andrew Brekken, Ph.D.

SPARC, secreted protein acidic and rich in cysteine, is a matricellular protein that governs extracellular matrix (ECM) deposition and maturation during times of tissue remodeling such as wound healing and tumorigenesis. The function of host-derived SPARC in an orthotopic model of pancreatic cancer was assessed. Pancreatic tumors grown in *SPARC-null* mice were more invasive than tumors grown in *wild-type* counterparts. Active TGFβ1 was found to be increased significantly in tumors grown in *SPARC-null* mice. TGFβ1 is known to contribute to many aspects of tumor development including metastasis, endothelial cell permeability, inflammation and fibrosis, all of which were altered in the absence of host SPARC. Given these results, we performed a survival study to assess the contribution of increased TGFβ1 activity to tumor progression in *SPARC-null* mice using Losartan, an AT1 angiotensin II receptor antagonist that diminishes TGFβ1 production *in vivo*. Tumors grown in *SPARC-null* mice progressed more quickly than those grown in *wild-type* littermates resulting in a median survival of 28.0 days and 35.5 days, respectively (p=0.018). Losartan therapy extended median survival of *SPARC-null* animals to 40.0 days, equivalent to losartan treated *wild-type* controls. Furthermore, *SPARC-null* mice treated with Losartan experienced a reduction in local invasion, metastatic incidence and metastatic burden. These results confirm that aberrant TGFβ1 activation in the absence of host SPARC contributes significantly to tumor progression and suggests that SPARC, by controlling ECM deposition and maturation, can regulate cytokine availability and activation.

TABLE OF CONTENTS

PRIOR PUBLICATIONS

Peer-Reviewed:

Arnold*, S., Mira*, E., Muneer*, S., Korpanty, G., Beck, AW., Holloway, SE., Manes, S., and Brekken, RA. Forced expression of MMP9 rescues the loss of angiogenesis and abrogates metastasis of pancreatic tumors triggered by the absence of host SPARC. *Experimental Biology and Medicine;* 233(7):860-873 (2008) (* Equal Contribution) **PMID: 18445772** (Cited as SEBM Best Paper for 2008 in the category experimental biology/basic research)

Bull-Phelps, SL., Carbon, JG., Miller, AF., Castro-Rivera, E., **Arnold, S.**, Miller, DS., Brekken, RA., and Lea, JS. Secreted protein acidic and rich in cysteine as a regulator of murine ovarian cancer growth and chemosensitivity. *Am J Obstet Gynecol*. 2009 Feb; 200(2):180.e1-7. **PMID: 18992864**

Shanna A. Arnold, Lee B. Rivera, Andrew F. Miller, Juliet G. Carbon, Sean P. Dineen, Yang Xie, Diego H. Castrillon, E. Helene Sage, Pauli Puolakkainen, Amy D. Bradshaw and Rolf A. Brekken. Lack of host SPARC enhances vascular function and tumor spread in an orthotopic murine model of pancreatic carcinoma. (In press at *Disease Models and Mechanisms*)

Invited Review*:*

Shanna A. Arnold and Rolf A. Brekken. SPARC: a matricellular regulator of tumorigenesis. *J Cell Commun Signal*. 2009 Oct 7. **PMID: 19809893**

LIST OF FIGURES

LIST OF TABLES

ABBREVIATIONS

bFGF – Basic fibroblast growth factor

ECM – Extracellular matrix

FAK – Focal adhesion kinase

ILK– Integrin-linked kinase

MMP – Matrix metalloproteinase

NSCLC – Non-small cell lung cancer

PDAC – Pancreatic ductal adenocarcinoma

PDGF – Platelet-derived growth factor

SCLC – Small cell lung cancer

siRNA – Small-interfering ribonucleic acid

SPARC – Secreted Protein, Acidic and Rich in Cysteine

TGFβ – Transforming growth factor beta

VEGF – Vascular endothelial growth factor

CHAPTER ONE: INTRODUCTION

SPARC: A matricellular regulator of tumorigenesis

Shanna A. Arnold and Rolf A. Brekken*

Hamon Center for Therapeutic Oncology Research, Division of Surgical Oncology and Departments of Surgery and Pharmacology, University of Texas Southwestern Medical Center, Dallas, TX 75390 USA

*Corresponding author:

Rolf A. Brekken, PhD
Hamon Center for Therapeutic Oncology Research
UT Southwestern Medical Center
6000 Harry Hines Blvd.
Dallas, TX 75390-8593
Tel: 214 648 5151 Fax: 214 648 4940
e-mail: rolf.brekken@utsouthwestern.edu

Running header 'SPARC as a regulator of tumorigenesis'

Supported by The Effie Marie Cain Scholarship in Angiogenesis Research (RAB), NIH grant R01CA118240 (RAB) and NIH training grant GM007062 (SA).

Abstract

Although many clinical studies have found a correlation of SPARC expression with malignant progression and patient survival, the mechanisms for SPARC function in tumorigenesis and metastasis remain elusive. The activity of SPARC is context- and cell-type-dependent, which is highlighted by the fact that SPARC has shown seemingly contradictory effects on tumor progression in both clinical correlative studies and in animal models. The capacity of SPARC to dictate tumorigenic phenotype has been attributed to its effects on the bioavailability and signaling of integrins and growth factors/chemokines. These molecular pathways contribute to many physiological events affecting malignant progression, including extracellular matrix remodeling, angiogenesis, immune modulation and metastasis. Given that SPARC is credited with such varied activities, this review presents a comprehensive account of the divergent effects of SPARC in human cancers and mouse models, as well as a description of the potential mechanisms by which SPARC mediates these effects. We aim to provide insight into how a matricellular protein such as SPARC might generate paradoxical, yet relevant, tumor outcomes in order to unify an apparently incongruent collection of scientific literature.

Keywords: angiogenesis; extracellular matrix; matricellular protein; metastasis; microenvironment; osteonectin; SPARC; tumor

Introduction

Historically, cancer research has focused on the molecular genetics and cell-autonomous behavior of malignant cells. However, understanding the interaction of cancer cells with their microenvironment has emerged as an essential step towards deciphering pathways that control transformation, primary tumor growth, metastasis, immune tolerance and therapeutic response [1-9]. Cancer cells communicate with and elicit responses from the microenvironment at every stage of malignant progression. The tumor microenvironment is composed of tumor cells, extracellular matrix (ECM), stromal cells, microvessels and immune cells [10, 11]. The ECM is an extracellular protein scaffold that determines tissue architecture and provides the structural framework for cells [12]. Furthermore, the ECM is a remodeling network that regulates cell differentiation, survival, proliferation and migration [13].

Deposition and remodeling of the ECM is regulated by a functional family of extracellular proteins known as matricellular proteins. Although primarily non-structural, matricellular proteins define and contribute to the structural integrity and composition of the ECM [14]. The capacity to influence assembly and turn-over of the ECM is a governing attribute of matricellular proteins, which is emphasized by their enhanced expression at sites of tissue remodeling and during wound-healing [14, 15]. Matricellular proteins can also direct cell fate, survival, adhesion and motility by functioning as adaptors between the ECM and the cell surface [14-16].

SPARC (secreted protein acidic and rich in cysteine), also known as osteonectin and BM-40, is a multifunctional secreted glycoprotein that exemplifies the matricellular class of proteins [17]. Expression of SPARC during mammalian development and tissue

differentiation is robust but declines in the majority of organs after maturation [18]. Ultimately, the expression of SPARC is limited post-development to tissues with high ECM turnover, such as bone and gut epithelia [18]. However, SPARC is induced during wound-healing, at sites of angiogenesis, and by the stroma during tumorigenesis [19-23]. These observations suggest that SPARC functions as a regulator of tissue remodeling. In fact, the phenotype of SPARC-deficient mice validates the findings that SPARC controls tissue remodeling and is required for proper collagen matrix assembly and maturation [24-26]. Mice lacking SPARC exhibit early cataractogenesis, lax skin, progressive osteopenia and a characteristic curly tail reminiscent of ECM defects [17]. Furthermore, collagen deposition and fibrillogenesis are altered in the dermis and lens capsule of SPARC-deficient mice [24, 27].

Consistent with its participation in ECM assembly and turn-over, SPARC directly binds ECM proteins such as collagen and influences the secretion and activation of matrix metalloproteinases (MMPs) [28-34]. Moreover, SPARC interacts with or indirectly regulates several growth factors involved in angiogenesis and tissue remodeling including fibroblast growth factor (FGF), vascular endothelial growth factor (VEGF), platelet-derived growth factor (PDGF), and transforming growth factor β (TGFβ) [35-40].

By directing ECM deposition, cell-ECM interactions, and growth factor signaling, SPARC is well placed to regulate multiple hallmarks of cancer including angiogenesis, migration, proliferation and survival. As it is suggested that the tumor microenvironment is reminiscent of a wound that never heals and because SPARC is a prominent participant in wound-healing, it is not surprising that many cancers exhibit

altered expression of SPARC [17, 21, 41, 42]. However, published data on the function of SPARC during tumorigenesis are inconsistent and often contradictory, even among the same tumor types. Thus, it seems that the capacity of SPARC to promote or inhibit tumor progression is dependent on the initiating cell-type, the tumor stage, and the context of the tumor microenvironment.

This article provides a comprehensive review of the literature on SPARC in human cancers and mouse models. We explore the function of SPARC in extracellular matrix deposition and fibrillogenesis, as well as in integrin and growth factor signaling. In an attempt to unify a divergent field, we conclude by proposing a working model to rationalize how SPARC contributes to seemingly paradoxical tumor outcomes.

Tumor Promotion

SPARC displays oncogenic properties in many tumor types including gliomas, astrocytomas, melanomas, ductal carcinoma of the breast, colorectal carcinoma, clear-cell renal cell carcinoma, pancreatic ductal adenocarcinoma, and carcinoma of the prostate. Table 1 provides a list of those human correlative studies, along with associated mouse models and *in vitro* studies, which show evidence of SPARC as a tumor promoter.

Extensive data are available that show an increase in the expression of SPARC in glioblastomas, astrocytomas and meningiomas relative to that in normal brain, and reveal SPARC expression as a negative predictor of survival [22, 43-45]. Furthermore, *in vitro* experiments demonstrate that endogenous and exogenous SPARC increase survival, adhesion, migration and invasion of glioblastoma cell lines [33, 45-54]. Forced expression of SPARC by non-invasive glioma cells induces an invasive phenotype in

mouse models of glioblastoma [50, 54]. On the other hand, down-regulation of SPARC by siRNA in invasive glioma cell lines abrogates dissemination into surrounding brain regions after intracerebral injection into mice [53].

In invasive ductal carcinoma of the breast, the expression of SPARC is enhanced in tumor tissue compared to normal controls and an increased level of SPARC is associated with higher histological grade and advanced pathological stage [55-68]. Both exogenous administration and endogenous upregulation of SPARC enhance *in vitro* breast cancer cell invasion [32, 69-72]. In orthotopic and intravenous lung metastasis mouse models of breast cancer, SPARC expression is increased at metastatic sites and confers enhanced metastatic potential [73]. Moreover, orthotopic breast tumor growth and lung metastasis are impaired in SPARC-deficient mice [74, 75].

Non-small cell lung cancers (NSCLC), including squamous cell carcinoma and adenocarcinoma, display an increased expression of SPARC relative to that in normal lung [55, 76]. Elevated SPARC expression by tumor stroma is associated with a poor prognosis in NSCLC [77]. Coculture of NSCLC cell lines with normal fibroblasts stimulates expression of SPARC [78]. Furthermore, SPARC is upregulated during carcinogen-induced transformation of bronchial epithelial cells and is associated with enhanced anchorage-independent colony formation [76].

SPARC is expressed highly in pancreatic ductal adenocarcinoma (PDAC) at both primary and metastatic sites [79-81]. In addition, patients with PDAC, whose tumor-associated stroma express high levels of SPARC, have a worse prognosis compared to those with no stromal SPARC expression, which results in a relative hazard ratio of 1.89

[82, 83]. *In vitro*, exogenous SPARC enhances, while SPARC knock-down reduces, invasion of human pancreatic cancer cells [81, 83].

An elevated expression of SPARC is also found in primary and metastatic melanoma [84, 85]. The expression of SPARC in cutaneous melanomas correlates significantly with an increase in disease progression and metastatic incidence, as well as with a decrease in survival [85, 86]. Elevated SPARC levels are found in the serum of patients with malignant melanoma, a marker used to successfully identify 33% of melanoma patients including those with early stage disease [87]. Human melanoma cell lines also express high levels of SPARC [84]. Forced expression of SPARC induces motility of normal human melanocytes and enhances invasion of melanoma cells [88, 89]. Antisense suppression of SPARC reduces the *in vitro* adhesive and invasive capacity of melanoma cell lines, and abrogates *in vivo* tumor formation [88-93]. Lastly, metastatic variants of mouse melanoma cell lines show differential expression of SPARC; whereby, those with higher metastatic potential or those that demonstrate aggressive behavior express and/or secrete increased amounts of SPARC relative to low-metastatic variants [94, 95].

Table 1. SPARC as a Tumor Promoter

Cancer		Human Biopsies			Mouse Models or Cell Culture	
Site	**Classification**	**Detection**	**Expression[a]**	**References**	**Description**	**References**
Bladder	Carcinoma	RT-PCR; IHC	Increased stromal SPARC; Positive Correlation	[96, 97]		
Blood	Leukemia	Microarray	Increased SPARC expression	[98, 99]		
Bone	Osteosarcoma	Microarray; RT-PCR; IHC	Positive Correlation	[100-102]		
Brain	Glioblastoma, Astrocytoma & Meningioma	Northern Blot; IHC; Microarray; RT-PCR	Positive Correlation; SPARC expression increased in invasive benign and malignant tumors	[22, 43-45, 103]	SPARC increased invasion and survival; Endogenous SPARC increased adhesion and migration but decreased proliferation	[33, 45-54]
Breast	Invasive Ductal Carcinoma	Microarray; IHC; RT-PCR; SAGE; ISH	High stromal SPARC; Positive Correlation	[55-68]	Exogenous SPARC increased cancer cell invasion; Tumor growth reduced in SPARC deficient mice; SPARC expression increased in metastasis	[32, 69-75]
Colon	Colorectal Adenocarcinoma	Microarray; Western Blot; Northern Blot; ISH; IHC; RT-PCR	SPARC expression increased in tumor, tumor stroma and at metastatic sites	[65, 104-110]	Increased SPARC expression associated with increased invasive capacity; Reduced tumor development in SPARC deficient	[111, 112]
Esophagus	Squamous Cell Carcinoma (ESCC) & Adenocarcinoma (EA)	Western Blot; Microarray; IHC; Northern Blot; RT-PCR	Positive Correlation	[113-120]		

Table 1 (Continued). SPARC as a Tumor Promoter

Cancer		Human Biopsies			Mouse Models or Cell Culture	
Site	**Classification**	**Detection**	**Expression[a]**	**References**	**Description**	**References**
Head & Neck	Squamous Cell Carcinoma (HNSCC)	IHC; Microarray	Positive Correlation	[121-123]		
Kidney	Sarcomatoid & Clear-cell renal cell carcinoma	Microarray; IHC; Northern Blot	SPARC expression increased in tumors	[55, 124, 125]	SPARC increased cancer cell invasion	[39]
Liver	Hepatocellular Carcinoma (HCC)	RT-PCR; IHC; ISH; Western Blot; Microarray	Positive Correlation	[126-128]		
Lung	NSCLC, Squamous Cell Carcinoma, Adenocarcinoma	IHC; Microarray	High stromal SPARC; Positive Correlation	[55, 76, 77]	SPARC expression increased during transformation and increased colony formation; Coculture of NSCLC lines & fibroblasts induced SPARC	[76, 78]
Ovary	Carcinoma	IHC; ISH	High stromal SPARC; Positive Correlation	[65, 129, 130]		
Pancreas	Ampullary Carcinoma	Microarray; IHC	Positive Correlation	[131]		
Pancreas	Ductal Adenocarcinoma (PDAC)	SAGE; Microarray; IHC; RT-PCR; ELISA	High stromal SPARC; Positive Correlation	[79-83, 132]	Exogenous SPARC increased cancer cell invasion	[81, 83]
Prostate	Carcinoma	Microarray; IHC; ISH; RT-PCR	Increased SPARC expression at the metastatic site; Positive Correlation	[133-135]	Exogenous SPARC increased cancer cell invasion and bone metastasis	[71, 136, 137]

Table 1 (Continued). SPARC as a Tumor Promoter

Cancer		Human Biopsies			Mouse Models or Cell Culture	
Site	**Classification**	**Detection**	**Expression[a]**	**References**	**Description**	**References**
Skin	Melanoma	IHC; Western Blot; ELISA	Positive Correlation; Serum SPARC levels useful as a diagnostic indicator	[84-87]	SPARC knock-down inhibited tumor formation; Increased SPARC expression by metastatic cell lines; SPARC expression correlated with EMT	[88-95, 138, 139]
Skin	Squamous Cell Carcinoma				SPARC deficient mice refractory to UV induced carcinogenesis	[140]
Stomach	Gastric Cancer	Northern Blot; ISH; IHC; RT-PCR; Microarray	High stromal SPARC; Positive Correlation	[109, 141-144]	SPARC expression increased during transformation	[145]
Thyroid	Anaplastic Carcinoma	RT-PCR	High stromal SPARC expression in poorly differentiated tumors	[146]		
Uterus	Cervical & Endometrial Carcinoma	RT-PCR; IHC; ISH; Western Blot	High stromal SPARC	[147, 148]		

[a] Positive Correlation refers to one of the following: 1) Tumors had increased SPARC expression compared to normal tissue 2) Increased SPARC expression correlated with increased tumor stage, grade or metastasis 3) Increased SPARC expression correlated with decreased survival or a negative prognosis 4) Decreased SPARC expression correlated with increased survival or a positive prognosis. This table combines, updates and expands the data presented in several previous reviews [17, 21, 41].

Tumor Suppression

SPARC also shows characteristics of a tumor suppressor in many cancers including acute myeloid leukemia, neuroblastoma, carcinoma of the breast, colorectal adenocarcinoma, hepatocellular carcinoma, non-small cell and small cell lung cancer, carcinoma of the ovaries and pancreatic ductal adenocarcinoma. Table 2 presents a comprehensive list of human correlative studies, associated mouse models and *in vitro* studies that support the capacity of SPARC to impede tumor progression.

The promoter of the SPARC gene is hypermethylated in many epithelial cancers, effectively reducing SPARC production by tumor cells and supporting the idea that SPARC is tumor-suppressive in a variety of cancers (Table 2). SPARC promoter methylation is reported in colorectal, non-small cell and small cell lung, ovarian, pancreatic, prostate and uterine cancers [132, 148-156]. In most cases, SPARC promoter methylation correlates with a poor prognosis and/or decreased survival.

The SPARC promoter is hypermethylated in 80-100% of colorectal adenocarcinomas and correlates with a worse prognosis [149, 150]. In addition, approximately 71% of human colorectal cancer cell lines are methylated within the SPARC locus [149, 150]. Further evidence comes from data showing chemoresistant human colorectal cancer cells significantly downregulate SPARC production [157]. More importantly, reexpression of SPARC or exogenous administration of SPARC restores chemosensitivity in resistant cell lines and leads to tumor regression in xenograft models when combined with chemotherapy [149, 157, 158].

Table 2. SPARC as a Tumor Suppressor

Cancer		Human Biopsies				Mouse Models or Cell Culture	
Site	**Classification**	**Detection**	**Expression[a]**	**References**	**Methylation**	**Description**	**References**
Bladder	Carcinoma	Genetic mapping	Locus deletion associated with neoplasia	[159]			
Blood	Acute Myeloid Leukemia (AML) with MLL Translocation	Microarray; RT-PCR; Western Blot	SPARC expression decreased	[160-162]		Exogenous SPARC inhibited proliferation; SPARC silencing associated with promoter methylation	[161]
Brain	Neuroblastoma	IHC	Inverse Correlation	[163]		SPARC inhibited migration and angiogenesis but activated apoptosis	[163, 164]
Breast	Carcinoma	Microarray	Inverse Correlation; Increased stromal SPARC	[58, 165]		SPARC overexpression inhibited proliferation; Endogenous SPARC expression reduced metastasis	[166, 167]
Colon	Colorectal Adenocarcinoma	IHC; methylation specific PCR; Microarray; RT-PCR	Inverse Correlation	[149, 150, 157]	**80-100%**	SPARC expression decreased in chemoresistant cancer cells; SPARC treatment restored sensitivity to chemotherapy; SPARC methylated in **71%** cell lines	[149, 150, 157, 158]
Kidney	Transformed Cells					Endogenous SPARC inhibited tumor growth	[168, 169]

Table 2 (Continued). SPARC as a Tumor Suppressor

Cancer		Human Biopsies				Mouse Models or Cell Culture	
Site	**Classification**	**Detection**	**Expression[a]**	**References**	**Methylation**	**Description**	**References**
Liver	Hepatocellular Carcinoma (HCC)					SPARC overexpression reduced tumor growth and angiogenesis	[127]
Lung	NSCLC & SCLC	RT-PCR; IHC	Inverse Correlation	[151]	**69%**	SPARC methylated in **55%** cancer cell lines; SPARC promoter demethylation inhibited invasion; Increased tumor growth in SPARC deficient mice	[25, 151, 170]
Nose & Pharynx	Nasopharyngeal Carcinoma					Endogenous SPARC inhibited proliferation	[171]
Ovary	Carcinoma	IHC; Western Blot; RT-PCR	Inverse Correlation	[153, 172]	**68%**	Reduced SPARC expression and secretion in cancer cells; SPARC inhibited tumor growth; Exogenous SPARC inhibited cancer cell proliferation, adhesion and invasion; enhanced apoptosis; Tumor growth and carcinomatosis augmented in SPARC deficient mice	[153, 172-177]

Table 2 (Continued). SPARC as a Tumor Suppressor

Cancer		Human Biopsies				Mouse Models or Cell Culture	
Site	**Classification**	**Detection**	**Expression[a]**	**References**	**Methylation**	**Description**	**References**
Pancreas	Ductal Adenocarcinoma (PDAC)	SAGE; Microarray; IHC; RT-PCR	SPARC methylation; Inverse Correlation	[132, 154, 155]	**88-92%**	SPARC methylated in **94%** cancer cell lines; SPARC inhibited cancer cell proliferation; Increased tumor growth in SPARC deficient mice	[81, 132, 178, 179]
Prostate	Carcinoma					SPARC hypermethylated in cancer cell lines compared to normal cells	[152]
Skin	Melanoma					Endogenous SPARC inhibited migration and spheroid tumor cell growth; SPARC knock-down enhanced spheroid formation	[92]
Uterus	Cervical & Endometrial Carcinoma	Microarray; RT-PCR	Inverse Correlation	[148, 156, 180]	**66-86%**		
Skin	Melanoma					Endogenous SPARC inhibited migration and spheroid tumor cell growth; SPARC knock-down enhanced spheroid formation	[92]
Uterus	Cervical & Endometrial Carcinoma	Microarray; RT-PCR	Inverse Correlation	[148, 156, 180]	**66-86%**		

[a] Inverse Correlation refers to one of the following: 1) Tumors had decreased SPARC expression compared to normal tissue 2) Decreased SPARC expression correlated with increased tumor stage, grade or metastasis 3) Decreased SPARC expression correlated with decreased survival or a negative prognosis 4) Increased SPARC expression correlated with increased survival or a positive prognosis. This table combines, updates and expands the data presented in several previous reviews [17, 21, 41].

SPARC gene methylation occurs in 71% of non-small cell lung cancers (NSCLC) and 33% of small cell lung cancers (SCLC) [151]. The promoter methylation status of SPARC is an independent adverse prognostic factor with a relative risk of 4.65 in lung adenocarcinoma [151]. Similar to human biopsies, 75% of NSCLC and 25% of SCLC cell lines show evidence of SPARC methylation [151]. Furthermore, treatment of human lung cancer cells with the nonsteroidal anti-inflammatory drug NS398 reduces invasion by restoring SPARC expression through promoter demethylation, an effect that is blocked by an anti-SPARC antibody [170].

SPARC also functions as a tumor suppressor in ovarian carcinoma. Malignant epithelial cells in ovarian carcinoma tissue samples exhibit reduced SPARC immunoreactivity [172]. This reduction in SPARC expression in the tumor compartment is due to epigenetic silencing; whereby, 68% of ovarian carcinomas display aberrant methylation of the SPARC promoter [153]. In fact, decreasing levels of SPARC protein in the malignant cells corresponds with disease progression [153]. Ovarian cancer cell lines also show reduced expression and secretion of SPARC compared to normal ovarian epithelial cells, which express and secrete high levels of SPARC [153, 172, 174]. Moreover, forced expression or exogenous addition of SPARC attenuates *in vitro* proliferation and *in vivo* tumor growth of ovarian carcinoma cells [153, 172, 174]. In a mouse model of peritoneal ovarian carcinomatosis, *SPARC-null* mice experience diminished survival, enhanced peritoneal dissemination and increased accumulation of ascitic fluid compared to *wild-type* animals [173, 175-177].

In pancreatic ductal adenocarcinoma, malignant epithelial cells within the tumor often downregulate SPARC expression [132]. SPARC methylation occurs in 91% of

human infiltrating pancreatic adenocarcinoma, 88% of primary human pancreatic carcinoma xenografts and 94% of human pancreatic cancer cell lines [132, 154, 155]. Gradual loss of SPARC expression and methylation in pancreatic ductal epithelial cells is also seen in the progression of intraductal papillary mucinous neoplasms, precursors to invasive adenocarcinoma [154]. Treatment with exogenous SPARC reduces pancreatic cancer cell proliferation [81, 132]. Additionally, subcutaneous and orthotopic tumor growth of murine pancreatic adenocarcinoma cells is enhanced in *SPARC-null* mice relative to *wild-type* counterparts [178, 179].

Lastly, SPARC expression is disregulated in uterine cancers. In human cervical carcinoma, SPARC is aberrantly methylated in 86% of cancer specimens and only in 5% of normal tissue [156]. Furthermore, the frequency of SPARC hypermethylation is significantly increased in high-grade cervical lesions compared to low-grade neoplasias and normal cervical controls [156, 180]. Endometrial cancers also display SPARC promoter methylation in 66% of human samples, as well as, a reduction in the expression of SPARC by the malignant epithelial cell compartment [148].

Compartmentalized Expression

Several epithelial cancers present with contradictory compartmentalized SPARC expression; whereby, SPARC is upregulated by the intra- and peritumoral stroma but downregulated by the malignant cells. This paradoxical pattern of SPARC expression is observed in breast, colorectal, lung, ovarian, pancreatic and endometrial cancers [56, 60, 130, 132, 148, 150, 151, 172]. Whereas SPARC is highly expressed by normal breast and colonic epithelium, invasive ductal breast and colorectal carcinoma show dramatically

reduced expression by the malignant epithelial cells (Figure 1). However, the tumor-reactive stroma displays intense SPARC immunoreactivity (Figure 1) [56, 150]. Although the tumor compartment exhibits reduced SPARC production in lung and pancreatic cancers due to promoter hypermethylation, infiltrating stromal cells respond with a compensatory upregulation of SPARC [132, 151]. Overall SPARC levels are elevated in endometrial carcinoma, but this over-expression is limited to the stroma; whereas, the tumor cells themselves display attenuated SPARC expression [148].

In regards to colorectal, lung, ovarian, pancreatic and endometrial cancers, the contradictory compartmentalized expression of SPARC is a result of the loss of SPARC expression by the malignant epithelial cells due to promoter hypermethylation, as discussed in the previous section [56, 130, 132, 148, 150, 151, 172]. Furthermore, tumor cells may act in a paracrine fashion to induce SPARC expression by the surrounding stroma. Indeed, fibroblasts isolated from normal pancreas display augmented SPARC expression when cocultured with pancreatic cancer cells [132].

Therefore, the heterogeneity and compartmentalization of SPARC expression can explain contradictory results and correlations with SPARC among identical cancers and between differing tumor types. What the data suggest is that the effect of SPARC on tumor progression and patient outcome is both tumor-type and context dependent. In other words, the source and localization of SPARC in the tumor microenvironment contributes to the complexity of SPARC influence during tumorigenesis.

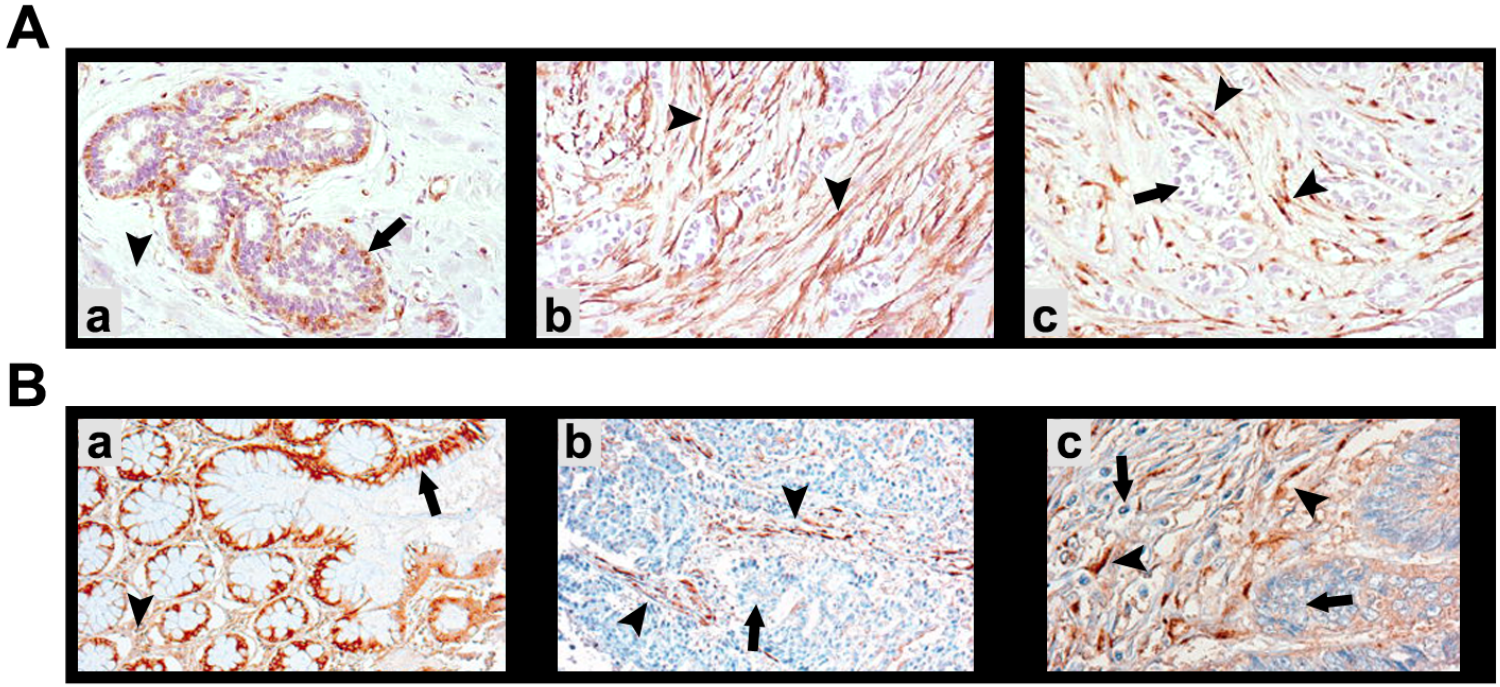

Figure 1. Compartmentalized SPARC Expression in Human Cancer. (A) Immunohistochemical staining of human biopsies of normal breast and invasive ductal adenocarcinoma, adapted from *Barth et al*. [56] (a) SPARC is expressed in myoepithelial cells (arrow) and by a few stromal cells in the ducts of normal breast. However, much of the stroma lacks SPARC expression (arrowhead) (b) Staining for α-SMA in the tumor-associated stroma (arrowheads) reveals activated fibroblasts also positive for (c) SPARC immunoreactivity (arrowheads). The arrow points to malignant epithelial cells lacking SPARC expression. (B) Immunohistochemical analysis of SPARC expression in colonic mucosae and colorectal carcinomas, adapted from *Yang et al.* [150]. (a) Normal colonic epithelial cells (arrow) strongly express SPARC, while there is only minimal SPARC expression in the surrounding stroma (arrowhead). (b,c) SPARC expression by the carcinoma cells (arrows) is dramatically reduced or absent, while tumor stromal cells display strong expression of SPARC (arrowheads) (c) Higher magnification.

Extracellular Matrix

The primary function of the ECM is to maintain tissue shape and to provide the cellular compartment with structural support [12]. However, the ECM is not just a passive bystander. It is a remodeling network that contributes substantially to tumor progression and metastasis by influencing cell adhesion, migration, differentiation, proliferation and survival [181-185]. By binding to adhesion receptors such as integrins, the ECM can communicate directly with the cell and influence signaling responses [186-189]. The ECM can also regulate cell function by harboring matrikines and dictating bioavailability of cytokines [190]. SPARC expression is increased concomitantly with activation of ECM deposition [17]. In addition, SPARC directly interacts with the ECM by binding basement membrane collagen IV and fibrillar collagens I, III and V [28-30].

There is ample evidence that SPARC is required for proper secretion, deposition and fibrillogenesis of collagen during development, wound-healing and tumor progression. SPARC-deficient mice exhibit a range of phenotypes as a result of disruption in ECM deposition and organization, including early cataract formation, accelerated dermal wound-healing, osteopenia and a curly tail [18]. Premature cataractogenesis is observed in two independently generated *SPARC-null* mouse colonies, and is caused by disorganized deposition of collagen IV and laminin in the lens epithelial basement membrane [27, 191-193]. *SPARC-null* mice also show deficiencies in connective tissue, such as decreased levels of collagen I in skin, adipose, heart and bone [194-196]. In addition to the reduction in collagen deposition, collagen fibrils in the skin of SPARC-deficient mice are uniformly smaller in diameter compared to the heterogeneous fibrils found in wild-type dermis [24]. Reduction in collagen deposition

and fibrillogenesis in *SPARC-null* mice leads to accelerated dermal wound-healing, presumably due to increased contractility [195, 197].

Not only do SPARC-deficient mice display alterations in the ECM during development and normal tissue turn-over but, in the absence of SPARC, there is also a diminished foreign-body and tumor response in regard to encapsulation. Implantation of foreign material into mice elicits a stromal response that essentially encapsulates this material in a wall of ECM. However, the collagen capsule deposited in response to foreign-body implantation is markedly reduced in thickness in *SPARC-null* compared to *wild-type* mice [198]. Furthermore, analogous to the alterations observed during development, the collagen fibrils bordering the implanted material are uniformly smaller in diameter and less mature in the absence of SPARC relative to fibers deposited in *wild-type* mice [198].

Similarly, many solid tumors show encapsulation demarcating the tumor from normal tissue. Subcutaneous tumor models of murine lung carcinoma, lymphoma and pancreatic adenocarcinoma present with enhanced growth in *SPARC-null* mice compared to *wild-type* controls [25, 179]. Moreover, tumors grown in the absence of host SPARC exhibit deficits in collagen deposition and fibrillogenesis at the tumor capsule, as well as in intratumoral connective tissue highways [25, 179]. There are also alterations in the composition of non-collagenous ECM proteins, such as laminin, in tumors grown in *SPARC-null* animals [25]. In addition, murine pancreatic cancer cells injected orthotopically into *SPARC-null* mice grow larger and metastasize more frequently than those in *wild-type* mice, thus highlighting the importance of SPARC function and ECM composition in tumor progression [178]. The fact that the tumor cells, but not the

infiltrating stromal cells, express and secrete SPARC in the aforementioned studies also supports the observation that the effect of SPARC on tumorigenesis is context- and cell-type-dependent [25, 178, 179]. Thus, SPARC can influence tumor progression and metastasis by controlling deposition and composition of the ECM. Moreover, the diverse actions of SPARC in differing tumors may be a result of distinctive ECM profiles.

Integrin Signaling

The ECM directly interacts with cells through a family of cell-surface receptors known as integrins [189]. Integrins anchor cells to the ECM, signal in response to ECM ligation ("outside-in" signaling) and regulate the interactions of the ECM in response to intracellular cues ('inside-out" signaling) [189]. Integrin signaling pathways substantially interact with growth factor receptor pathways to dictate cellular events, such as survival, proliferation, adhesion and migration, all of which contribute to tumor growth and metastasis. Integrin complexes can also cluster directly with growth factor receptors. Furthermore, proper cytokine responses require intact integrin activation and signal propagation [182, 199-201].

Numerous studies suggest that SPARC regulates integrin signaling and the ability of integrins to interact with structural components of the ECM. SPARC induces cell rounding or an intermediate state of adhesion in several cell types, *in vitro*, including endothelial and mesenchymal cells [28, 202]. This effect is due to disruption of focal adhesions [202]. In addition, many studies contribute to the emerging idea that SPARC influences downstream components of integrin signaling, specifically the activation of integrin linked kinase (ILK). Fibronectin-induced ILK activation and stress-fiber

formation are reduced in primary lung fibroblasts isolated from SPARC-null mice and restored by forced SPARC expression [203]. Furthermore, SPARC promotes cell survival of lens epithelial cells under serum-deprivation by enhancing ILK activation [204]. Moreover, recent publications report that SPARC binds integrin β1 with its copper-binding domain; thereby, directly affecting integrin/ILK signaling [204, 205].

The influence of SPARC on integrin/ILK responses is also observed in several cancer cell lines. SPARC increases survival and induces an invasive phenotype in human glioma cells [50-52]. However, targeting SPARC with short-hairpin RNA reduces cell survival and invasion, as well as attenuates the activity of ILK, focal adhesion kinase (FAK) and protein kinase B (Akt) [52]. Moreover, SPARC-induced invasion and survival is abrogated by down-regulation of ILK and FAK [52]. Total ILK expression is also found to be increased in glioma cells that are forced to express SPARC [47]. In human ovarian cancer cells, SPARC inhibits adhesion, invasion and proliferation by reducing the surface localization and/or clustering of αv, β1, β3 and β5 integrins [176]. SPARC attenuates integrin αv- and β1- induced proliferation in murine ovarian cancer cells. Furthermore, murine ovarian cancer cells adhere more readily to peritoneal explants and peritoneal mesothelial cells isolated from *SPARC-null* mice compared to *wild-type* counterparts [177]. This effect is blocked by antibodies against αvβ3 and β1 integrins [177].

Together, these data reveal that SPARC influences integrin clustering and activation, as well as the ability of integrins to interact with structural components of the ECM. Moreover, SPARC potentially dictates if and how integrins converse with and reinforce other signaling cascades. Therefore, it is not surprising that SPARC elicits such

diverse effects on tumorigenesis, given the fact that it possesses the ability to control the pleiotropic interactions and functions of integrins.

Growth Factor and Cytokine Signaling

Cross-talk between malignant cells and the surrounding stromal compartment induces ECM remodeling, angiogenesis, immune recruitment and metastasis [206]. Growth factors and their associated receptors are one way by which communication occurs between cellular compartments. It is established that SPARC modulates the activity of several growth factors including basic fibroblast growth factor (bFGF), platelet-derived growth factor (PDGF), vascular endothelial growth factor (VEGF), and transforming growth factor beta (TGFβ) [35-38]. Although SPARC does not bind bFGF directly, it inhibits bFGF-induced migration of endothelial cells [37]. SPARC binds PDGF and dose-dependently inhibits ligand binding and activation of PDGF receptors on human dermal fibroblasts [35]. In addition, PDGF-stimulated proliferation of human arterial vascular smooth muscle cells is decreased in the presence of SPARC [207].

Similar to PDGF, SPARC binds VEGF directly and prevents activation of VEGFR1 [36, 208]. This interaction attenuates VEGF-induced proliferation of microvascular endothelial cells [36]. On the other hand, VEGF induces the expression of SPARC in human vascular endothelial cells [209]. Therefore, the induction of SPARC by VEGF stimulation might be a negative regulatory feedback mechanism. In support, VEGF production is enhanced in dermal fibroblasts and subcutaneous polyvinyl alcohol sponges from *SPARC-null* mice relative to *wild-type* controls, which results in a greater angiogenic response in the absence of SPARC [210]. When injected into the brain of

nude rats, SPARC-expressing human glioblastoma cells reduce VEGF expression and angiogenesis related to tumor formation in comparison to SPARC-negative glioma cells [211]. In a mouse model of ovarian cancer, peritoneal dissemination and lethality is augmented in the absence of host-derived SPARC, which corresponds to VEGF accumulation in ascitic fluid [175, 177].

SPARC is also implicated in the regulation of TGFβ [38, 212]. TGFβ is a master regulator of wound-healing and fibrosis by inducing the synthesis of several ECM proteins including collagen and fibronectin [213]. Ample data demonstrate that TGFβ induces SPARC expression [214-217]. However, there is also evidence that SPARC regulates the expression and activity of TGFβ, suggesting that there is a reciprocal regulatory feedback loop between SPARC and TGFβ. SPARC induces the expression and secretion of TGFβ1 in rat mesangial cells *in vitro* and *in vivo* [218]. The synthesis of collagen I and TGFβ-1 is diminished in mesangial cells isolated from *SPARC-null* mice compared to those from *wild-type* mice, but is restored by the exogenous addition of SPARC [219]. Moreover, SPARC enhances the stimulatory effects of TGFβ1 on mesangial cells by directly interacting with the TGFβ/TGFβRII complex [38]. Likewise, SPARC augments the inhibitory functions of TGFβ1 in epithelial cells by stimulating smad2/3 phosphorylation [212].

Considering that growth factors such as bFGF, PDGF, VEGF and TGFβ are important contributors to tumor progression, angiogenesis and metastasis, it is clear that the interaction of SPARC with these signaling pathways influences its ability to dictate many aspects of tumorigenesis. In addition, SPARC interaction with growth factors, such

as TGFβ, that have a dichotomous effect on the progression of solid tumors, explains the ability of SPARC to influence human cancers in such apparently paradoxical ways [220].

Competing Interests

The authors have no competing interests to declare.

Author Contributions

SAA drafted the review, constructed the tables and conceptualized a working model. RAB edited and revised the review for intellectual content and continuity, as well as contributed to the development of a working model.

Acknowledgements

Supported by The Effie Marie Cain Scholarship in Angiogenesis Research (RAB), NIH grant R01CA118240 (RAB) and NIH training grant GM007062 (SAA). We gratefully acknowledge all members of the Brekken laboratory for their ongoing support. We would like to thank Lee B. Rivera, in particular, for his insightful discussion and feed-back during the development of a working model of SPARC function.

References

1. Joyce, J.A. and J.W. Pollard, *Microenvironmental regulation of metastasis.* Nat Rev Cancer, 2009. **9**(4): p. 239-52.

2. Desmouliere, A., C. Guyot, and G. Gabbiani, *The stroma reaction myofibroblast: a key player in the control of tumor cell behavior.* Int J Dev Biol, 2004. **48**(5-6): p. 509-17.

3. Zalatnai, A., *Molecular aspects of stromal-parenchymal interactions in malignant neoplasms.* Curr Mol Med, 2006. **6**(6): p. 685-93.

4. Wernert, N., *The multiple roles of tumour stroma.* Virchows Arch, 1997. **430**(6): p. 433-43.

5. Liotta, L.A. and E.C. Kohn, *The microenvironment of the tumour-host interface.* Nature, 2001. **411**(6835): p. 375-9.

6. Shan, W., G. Yang, and J. Liu, *The inflammatory network: bridging senescent stroma and epithelial tumorigenesis.* Front Biosci, 2009. **14**: p. 4044-57.

7. Kumar, S. and V.M. Weaver, *Mechanics, malignancy, and metastasis: the force journey of a tumor cell.* Cancer Metastasis Rev, 2009. **28**(1-2): p. 113-27.

8. Lorusso, G. and C. Ruegg, *The tumor microenvironment and its contribution to tumor evolution toward metastasis.* Histochem Cell Biol, 2008. **130**(6): p. 1091-103.

9. Whiteside, T.L., *The tumor microenvironment and its role in promoting tumor growth.* Oncogene, 2008. **27**(45): p. 5904-12.

10. Farrow, B., D. Albo, and D.H. Berger, *The role of the tumor microenvironment in the progression of pancreatic cancer.* J Surg Res, 2008. **149**(2): p. 319-28.

11. Jung, Y.D., et al., *The role of the microenvironment and intercellular cross-talk in tumor angiogenesis.* Semin Cancer Biol, 2002. **12**(2): p. 105-12.

12. Bosman, F.T. and I. Stamenkovic, *Functional structure and composition of the extracellular matrix.* J Pathol, 2003. **200**(4): p. 423-8.

13. Larsen, M., et al., *The matrix reorganized: extracellular matrix remodeling and integrin signaling.* Curr Opin Cell Biol, 2006. **18**(5): p. 463-71.

14. Bornstein, P. and E.H. Sage, *Matricellular proteins: extracellular modulators of cell function.* Curr Opin Cell Biol, 2002. **14**(5): p. 608-16.

15. Bornstein, P., *Thrombospondins as matricellular modulators of cell function.* J Clin Invest, 2001. **107**(8): p. 929-34.

16. Brekken, R.A. and E.H. Sage, *SPARC, a matricellular protein: at the crossroads of cell-matrix communication.* Matrix Biol, 2001. **19**(8): p. 816-27.

17. Framson, P.E. and E.H. Sage, *SPARC and tumor growth: where the seed meets the soil?* J Cell Biochem, 2004. **92**(4): p. 679-90.

18. Bradshaw, A.D. and E.H. Sage, *SPARC, a matricellular protein that functions in cellular differentiation and tissue response to injury.* J Clin Invest, 2001. **107**(9): p. 1049-54.

19. Bornstein, P., *Cell-matrix interactions: the view from the outside.* Methods Cell Biol, 2002. **69**: p. 7-11.

20. Reed, M.J., et al., *Differential expression of SPARC and thrombospondin 1 in wound repair: immunolocalization and in situ hybridization.* J Histochem Cytochem, 1993. **41**(10): p. 1467-77.

21. Podhajcer, O.L., et al., *The role of the matricellular protein SPARC in the dynamic interaction between the tumor and the host.* Cancer Metastasis Rev, 2008. **27**(4): p. 691-705.

22. Pen, A., et al., *Molecular markers of extracellular matrix remodeling in glioblastoma vessels: microarray study of laser-captured glioblastoma vessels.* Glia, 2007. **55**(6): p. 559-72.

23. Mendis, D.B., G.O. Ivy, and I.R. Brown, *SPARC/osteonectin mRNA is induced in blood vessels following injury to the adult rat cerebral cortex.* Neurochem Res, 1998. **23**(8): p. 1117-23.

24. Bradshaw, A.D., et al., *SPARC-null mice display abnormalities in the dermis characterized by decreased collagen fibril diameter and reduced tensile strength.* J Invest Dermatol, 2003. **120**(6): p. 949-55.

25. Brekken, R.A., et al., *Enhanced growth of tumors in SPARC null mice is associated with changes in the ECM.* J Clin Invest, 2003. **111**(4): p. 487-95.

26. Gruber, H.E., et al., *Targeted deletion of the SPARC gene accelerates disc degeneration in the aging mouse.* J Histochem Cytochem, 2005. **53**(9): p. 1131-8.

27. Yan, Q., et al., *Alterations in the lens capsule contribute to cataractogenesis in SPARC-null mice.* J Cell Sci, 2002. **115**(Pt 13): p. 2747-56.

28. Sage, H., et al., *SPARC, a secreted protein associated with cellular proliferation, inhibits cell spreading in vitro and exhibits Ca+2-dependent binding to the extracellular matrix.* J Cell Biol, 1989. **109**(1): p. 341-56.

29. Sasaki, T., et al., *Crystal structure and mapping by site-directed mutagenesis of the collagen-binding epitope of an activated form of BM-40/SPARC/osteonectin.* EMBO J, 1998. **17**(6): p. 1625-34.

30. Sasaki, T., N. Miosge, and R. Timpl, *Immunochemical and tissue analysis of protease generated neoepitopes of BM-40 (osteonectin, SPARC) which are correlated to a higher affinity binding to collagens.* Matrix Biol, 1999. **18**(5): p. 499-508.

31. Fujita, T., et al., *SPARC stimulates the synthesis of OPG/OCIF, MMP-2 and DNA in human periodontal ligament cells.* J Oral Pathol Med, 2002. **31**(6): p. 345-52.

32. Gilles, C., et al., *SPARC/osteonectin induces matrix metalloproteinase 2 activation in human breast cancer cell lines.* Cancer Res, 1998. **58**(23): p. 5529-36.

33. McClung, H.M., et al., *SPARC upregulates MT1-MMP expression, MMP-2 activation, and the secretion and cleavage of galectin-3 in U87MG glioma cells.* Neurosci Lett, 2007. **419**(2): p. 172-7.

34. Shankavaram, U.T., et al., *Regulation of human monocyte matrix metalloproteinases by SPARC.* J Cell Physiol, 1997. **173**(3): p. 327-34.

35. Raines, E.W., et al., *The extracellular glycoprotein SPARC interacts with platelet-derived growth factor (PDGF)-AB and -BB and inhibits the binding of PDGF to its receptors.* Proc Natl Acad Sci U S A, 1992. **89**(4): p. 1281-5.

36. Kupprion, C., K. Motamed, and E.H. Sage, *SPARC (BM-40, osteonectin) inhibits the mitogenic effect of vascular endothelial growth factor on microvascular endothelial cells.* J Biol Chem, 1998. **273**(45): p. 29635-40.

37. Hasselaar, P. and E.H. Sage, *SPARC antagonizes the effect of basic fibroblast growth factor on the migration of bovine aortic endothelial cells.* J Cell Biochem, 1992. **49**(3): p. 272-83.

38. Francki, A., et al., *SPARC regulates TGF-beta1-dependent signaling in primary glomerular mesangial cells.* J Cell Biochem, 2004. **91**(5): p. 915-25.

39. Kato, Y., et al., *Stimulation of motility of human renal cell carcinoma by SPARC/Osteonectin/BM-40 associated with type IV collagen.* Invasion Metastasis, 1998. **18**(2): p. 105-14.

40. Motamed, K., et al., *Fibroblast growth factor receptor-1 mediates the inhibition of endothelial cell proliferation and the promotion of skeletal myoblast differentiation by SPARC: a role for protein kinase A.* J Cell Biochem, 2003. **90**(2): p. 408-23.

41. Clark, C.J. and E.H. Sage, *A prototypic matricellular protein in the tumor microenvironment--where there's SPARC, there's fire.* J Cell Biochem, 2008. **104**(3): p. 721-32.

42. Dvorak, H.F., *Tumors: wounds that do not heal. Similarities between tumor stroma generation and wound healing.* N Engl J Med, 1986. **315**(26): p. 1650-9.

43. Huang, H., et al., *Gene expression profiling of low-grade diffuse astrocytomas by cDNA arrays.* Cancer Res, 2000. **60**(24): p. 6868-74.

44. Rempel, S.A., et al., *SPARC: a signal of astrocytic neoplastic transformation and reactive response in human primary and xenograft gliomas.* J Neuropathol Exp Neurol, 1998. **57**(12): p. 1112-21.

45. Rich, J.N., et al., *Gene expression profiling and genetic markers in glioblastoma survival.* Cancer Res, 2005. **65**(10): p. 4051-8.

46. Golembieski, W.A., et al., *Increased SPARC expression promotes U87 glioblastoma invasion in vitro.* Int J Dev Neurosci, 1999. **17**(5-6): p. 463-72.

47. Golembieski, W.A., et al., *HSP27 mediates SPARC-induced changes in glioma morphology, migration, and invasion.* Glia, 2008. **56**(10): p. 1061-75.

48. Kunigal, S., et al., *SPARC-induced migration of glioblastoma cell lines via uPA-uPAR signaling and activation of small GTPase RhoA.* Int J Oncol, 2006. **29**(6): p. 1349-57.

49. Rempel, S.A., et al., *SPARC modulates cell growth, attachment and migration of U87 glioma cells on brain extracellular matrix proteins.* J Neurooncol, 2001. **53**(2): p. 149-60.

50. Schultz, C., et al., *Secreted protein acidic and rich in cysteine promotes glioma invasion and delays tumor growth in vivo.* Cancer Res, 2002. **62**(21): p. 6270-7.

51. Shi, Q., et al., *Secreted protein acidic, rich in cysteine (SPARC), mediates cellular survival of gliomas through AKT activation.* J Biol Chem, 2004. **279**(50): p. 52200-9.

52. Shi, Q., et al., *Targeting SPARC expression decreases glioma cellular survival and invasion associated with reduced activities of FAK and ILK kinases.* Oncogene, 2007. **26**(28): p. 4084-94.

53. Seno, T., et al., *Downregulation of SPARC expression inhibits cell migration and invasion in malignant gliomas.* Int J Oncol, 2009. **34**(3): p. 707-15.

54. Rich, J.N., et al., *Bone-related genes expressed in advanced malignancies induce invasion and metastasis in a genetically defined human cancer model.* J Biol Chem, 2003. **278**(18): p. 15951-7.

55. Amatschek, S., et al., *Tissue-wide expression profiling using cDNA subtraction and microarrays to identify tumor-specific genes.* Cancer Res, 2004. **64**(3): p. 844-56.

56. Barth, P.J., R. Moll, and A. Ramaswamy, *Stromal remodeling and SPARC (secreted protein acid rich in cysteine) expression in invasive ductal carcinomas of the breast.* Virchows Arch, 2005. **446**(5): p. 532-6.

57. Bellahcene, A. and V. Castronovo, *Increased expression of osteonectin and osteopontin, two bone matrix proteins, in human breast cancer.* Am J Pathol, 1995. **146**(1): p. 95-100.

58. Bergamaschi, A., et al., *Extracellular matrix signature identifies breast cancer subgroups with different clinical outcome.* J Pathol, 2008. **214**(3): p. 357-67.

59. Helleman, J., et al., *Association of an extracellular matrix gene cluster with breast cancer prognosis and endocrine therapy response.* Clin Cancer Res, 2008. **14**(17): p. 5555-64.

60. Iacobuzio-Donahue, C.A., et al., *The desmoplastic response to infiltrating breast carcinoma: gene expression at the site of primary invasion and implications for comparisons between tumor types.* Cancer Res, 2002. **62**(18): p. 5351-7.

61. Jones, C., et al., *Expression profiling of purified normal human luminal and myoepithelial breast cells: identification of novel prognostic markers for breast cancer.* Cancer Res, 2004. **64**(9): p. 3037-45.

62. Lien, H.C., et al., *Molecular signatures of metaplastic carcinoma of the breast by large-scale transcriptional profiling: identification of genes potentially related to epithelial-mesenchymal transition.* Oncogene, 2007. **26**(57): p. 7859-71.

63. Parker, B.S., et al., *Alterations in vascular gene expression in invasive breast carcinoma.* Cancer Res, 2004. **64**(21): p. 7857-66.

64. Porter, D., et al., *Molecular markers in ductal carcinoma in situ of the breast.* Mol Cancer Res, 2003. **1**(5): p. 362-75.

65. Porter, P.L., et al., *Distribution of SPARC in normal and neoplastic human tissue.* J Histochem Cytochem, 1995. **43**(8): p. 791-800.

66. Sarrio, D., et al., *Epithelial-mesenchymal transition in breast cancer relates to the basal-like phenotype.* Cancer Res, 2008. **68**(4): p. 989-97.

67. Watkins, G., et al., *Increased levels of SPARC (osteonectin) in human breast cancer tissues and its association with clinical outcomes.* Prostaglandins Leukot Essent Fatty Acids, 2005. **72**(4): p. 267-72.

68. Woelfle, U., et al., *Molecular signature associated with bone marrow micrometastasis in human breast cancer.* Cancer Res, 2003. **63**(18): p. 5679-84.

69. Briggs, J., et al., *Transcriptional upregulation of SPARC, in response to c-Jun overexpression, contributes to increased motility and invasion of MCF7 breast cancer cells.* Oncogene, 2002. **21**(46): p. 7077-91.

70. Campo McKnight, D.A., et al., *Roles of osteonectin in the migration of breast cancer cells into bone.* J Cell Biochem, 2006. **97**(2): p. 288-302.

71. Jacob, K., et al., *Osteonectin promotes prostate cancer cell migration and invasion: a possible mechanism for metastasis to bone.* Cancer Res, 1999. **59**(17): p. 4453-7.

72. Zajchowski, D.A., et al., *Identification of gene expression profiles that predict the aggressive behavior of breast cancer cells.* Cancer Res, 2001. **61**(13): p. 5168-78.

73. Minn, A.J., et al., *Genes that mediate breast cancer metastasis to lung.* Nature, 2005. **436**(7050): p. 518-24.

74. Sangaletti, S., et al., *Macrophage-derived SPARC bridges tumor cell-extracellular matrix interactions toward metastasis.* Cancer Res, 2008. **68**(21): p. 9050-9.

75. Sangaletti, S., et al., *Leukocyte, rather than tumor-produced SPARC, determines stroma and collagen type IV deposition in mammary carcinoma.* J Exp Med, 2003. **198**(10): p. 1475-85.

76. Siddiq, F., et al., *Increased osteonectin expression is associated with malignant transformation and tumor associated fibrosis in the lung.* Lung Cancer, 2004. **45**(2): p. 197-205.

77. Koukourakis, M.I., et al., *Enhanced expression of SPARC/osteonectin in the tumor-associated stroma of non-small cell lung cancer is correlated with markers of hypoxia/acidity and with poor prognosis of patients.* Cancer Res, 2003. **63**(17): p. 5376-80.

78. Fromigue, O., et al., *Gene expression profiling of normal human pulmonary fibroblasts following coculture with non-small-cell lung cancer cells reveals alterations related to matrix degradation, angiogenesis, cell growth and survival.* Oncogene, 2003. **22**(52): p. 8487-97.

79. Prenzel, K.L., et al., *Significant overexpression of SPARC/osteonectin mRNA in pancreatic cancer compared to cancer of the papilla of Vater.* Oncol Rep, 2006. **15**(5): p. 1397-401.

80. Ryu, B., et al., *Invasion-specific genes in malignancy: serial analysis of gene expression comparisons of primary and passaged cancers.* Cancer Res, 2001. **61**(5): p. 1833-8.

81. Guweidhi, A., et al., *Osteonectin influences growth and invasion of pancreatic cancer cells.* Ann Surg, 2005. **242**(2): p. 224-34.

82. Infante, J.R., et al., *Peritumoral fibroblast SPARC expression and patient outcome with resectable pancreatic adenocarcinoma.* J Clin Oncol, 2007. **25**(3): p. 319-25.

83. Mantoni, T.S., et al., *Stromal SPARC expression and patient survival after chemoradiation for non-resectable pancreatic adenocarcinoma.* Cancer Biol Ther, 2008. **7**(11).

84. Ledda, F., et al., *The expression of the secreted protein acidic and rich in cysteine (SPARC) is associated with the neoplastic progression of human melanoma.* J Invest Dermatol, 1997. **108**(2): p. 210-4.

85. Alonso, S.R., et al., *A high-throughput study in melanoma identifies epithelial-mesenchymal transition as a major determinant of metastasis.* Cancer Res, 2007. **67**(7): p. 3450-60.

86. Massi, D., et al., *Osteonectin expression correlates with clinical outcome in thin cutaneous malignant melanomas.* Hum Pathol, 1999. **30**(3): p. 339-44.

87. Ikuta, Y., et al., *Highly sensitive detection of melanoma at an early stage based on the increased serum secreted protein acidic and rich in cysteine and glypican-3 levels.* Clin Cancer Res, 2005. **11**(22): p. 8079-88.

88. Robert, G., et al., *SPARC represses E-cadherin and induces mesenchymal transition during melanoma development.* Cancer Res, 2006. **66**(15): p. 7516-23.

89. Smit, D.J., B.B. Gardiner, and R.A. Sturm, *Osteonectin downregulates E-cadherin, induces osteopontin and focal adhesion kinase activity stimulating an invasive melanoma phenotype.* Int J Cancer, 2007. **121**(12): p. 2653-60.

90. Ledda, M.F., et al., *Suppression of SPARC expression by antisense RNA abrogates the tumorigenicity of human melanoma cells.* Nat Med, 1997. **3**(2): p. 171-6.

91. Alvarez, M.J., et al., *Secreted protein acidic and rich in cysteine produced by human melanoma cells modulates polymorphonuclear leukocyte recruitment and antitumor cytotoxic capacity.* Cancer Res, 2005. **65**(12): p. 5123-32.

92. Prada, F., et al., *SPARC endogenous level, rather than fibroblast-produced SPARC or stroma reorganization induced by SPARC, is responsible for melanoma cell growth.* J Invest Dermatol, 2007. **127**(11): p. 2618-28.

93. Sosa, M.S., et al., *Proteomic analysis identified N-cadherin, clusterin, and HSP27 as mediators of SPARC (secreted protein, acidic and rich in cysteines) activity in melanoma cells.* Proteomics, 2007. **7**(22): p. 4123-34.

94. Kato, Y., et al., *High production of SPARC/osteonectin/BM-40 in mouse metastatic B16 melanoma cell lines.* Pathol Oncol Res, 2000. **6**(1): p. 24-6.

95. Rumpler, G., et al., *Identification of differentially expressed genes in models of melanoma progression by cDNA array analysis: SPARC, MIF and a novel cathepsin protease characterize aggressive phenotypes.* Exp Dermatol, 2003. **12**(6): p. 761-71.

96. Nimphius, W., et al., *CD34+ fibrocytes in chronic cystitis and noninvasive and invasive urothelial carcinomas of the urinary bladder.* Virchows Arch, 2007. **450**(2): p. 179-85.

97. Yamanaka, M., et al., *Analysis of the gene expression of SPARC and its prognostic value for bladder cancer.* J Urol, 2001. **166**(6): p. 2495-9.

98. Hedvat, C.V., et al., *Insights into extramedullary tumour cell growth revealed by expression profiling of human plasmacytomas and multiple myeloma.* Br J Haematol, 2003. **122**(5): p. 728-44.

99. Martinez, N., et al., *The molecular signature of mantle cell lymphoma reveals multiple signals favoring cell survival.* Cancer Res, 2003. **63**(23): p. 8226-32.

100. Dalla-Torre, C.A., et al., *Effects of THBS3, SPARC and SPP1 expression on biological behavior and survival in patients with osteosarcoma.* BMC Cancer, 2006. **6**: p. 237.

101. Fanburg-Smith, J.C., G.L. Bratthauer, and M. Miettinen, *Osteocalcin and osteonectin immunoreactivity in extraskeletal osteosarcoma: a study of 28 cases.* Hum Pathol, 1999. **30**(1): p. 32-8.

102. Schulz, A., et al., *[Bone matrix production in osteosarcoma]*. Verh Dtsch Ges Pathol, 1998. **82**: p. 144-53.

103. Rempel, S.A., S. Ge, and J.A. Gutierrez, *SPARC: a potential diagnostic marker of invasive meningiomas.* Clin Cancer Res, 1999. **5**(2): p. 237-41.

104. Kaiser, S., et al., *Transcriptional recapitulation and subversion of embryonic colon development by mouse colon tumor models and human colon cancer.* Genome Biol, 2007. **8**(7): p. R131.

105. Lussier, C., J. Sodek, and J.F. Beaulieu, *Expression of SPARC/osteonectin/BM4O in the human gut: predominance in the stroma of the remodeling distal intestine.* J Cell Biochem, 2001. **81**(3): p. 463-76.

106. Madoz-Gurpide, J., et al., *Proteomics-based validation of genomic data: applications in colorectal cancer diagnosis.* Mol Cell Proteomics, 2006. **5**(8): p. 1471-83.

107. Porte, H., et al., *Neoplastic progression of human colorectal cancer is associated with overexpression of the stromelysin-3 and BM-40/SPARC genes.* Int J Cancer, 1995. **64**(1): p. 70-5.

108. St Croix, B., et al., *Genes expressed in human tumor endothelium.* Science, 2000. **289**(5482): p. 1197-202.

109. Wewer, U.M., et al., *Osteonectin/SPARC/BM-40 in human decidua and carcinoma, tissues characterized by de novo formation of basement membrane.* Am J Pathol, 1988. **132**(2): p. 345-55.

110. Wiese, A.H., et al., *Identification of gene signatures for invasive colorectal tumor cells.* Cancer Detect Prev, 2007. **31**(4): p. 282-95.

111. Sansom, O.J., et al., *Deficiency of SPARC suppresses intestinal tumorigenesis in APCMin/+ mice.* Gut, 2007. **56**(10): p. 1410-4.

112. Volmer, M.W., et al., *Tumor suppressor Smad4 mediates downregulation of the anti-adhesive invasion-promoting matricellular protein SPARC: Landscaping activity of Smad4 as revealed by a "secretome" analysis.* Proteomics, 2004. **4**(5): p. 1324-34.

113. Brabender, J., et al., *The molecular signature of normal squamous esophageal epithelium identifies the presence of a field effect and can discriminate between patients with Barrett's esophagus and patients with Barrett's-associated adenocarcinoma.* Cancer Epidemiol Biomarkers Prev, 2005. **14**(9): p. 2113-7.

114. Che, Y., et al., *The differential expression of SPARC in esophageal squamous cell carcinoma.* Int J Mol Med, 2006. **17**(6): p. 1027-33.

115. Luo, A., et al., *Discovery of Ca2+-relevant and differentiation-associated genes downregulated in esophageal squamous cell carcinoma using cDNA microarray.* Oncogene, 2004. **23**(6): p. 1291-9.

116. Mitas, M., et al., *Accurate discrimination of Barrett's esophagus and esophageal adenocarcinoma using a quantitative three-tiered algorithm and multimarker real-time reverse transcription-PCR.* Clin Cancer Res, 2005. **11**(6): p. 2205-14.

117. Porte, H., et al., *Overexpression of stromelysin-3, BM-40/SPARC, and MET genes in human esophageal carcinoma: implications for prognosis.* Clin Cancer Res, 1998. **4**(6): p. 1375-82.

118. Wong, F.H., et al., *Combination of microarray profiling and protein-protein interaction databases delineates the minimal discriminators as a metastasis network for esophageal squamous cell carcinoma.* Int J Oncol, 2009. **34**(1): p. 117-28.

119. Xue, L.Y., et al., *Tissue microarray analysis reveals a tight correlation between protein expression pattern and progression of esophageal squamous cell carcinoma.* BMC Cancer, 2006. **6**: p. 296.

120. Yamashita, K., et al., *Clinical significance of secreted protein acidic and rich in cystein in esophageal carcinoma and its relation to carcinoma progression.* Cancer, 2003. **97**(10): p. 2412-9.

121. Chin, D., et al., *Novel markers for poor prognosis in head and neck cancer.* Int J Cancer, 2005. **113**(5): p. 789-97.

122. Choi, P., et al., *Examination of oral cancer biomarkers by tissue microarray analysis.* Arch Otolaryngol Head Neck Surg, 2008. **134**(5): p. 539-46.

123. Kato, Y., et al., *Expression of SPARC in tongue carcinoma of stage II is associated with poor prognosis: an immunohistochemical study of 86 cases.* Int J Mol Med, 2005. **16**(2): p. 263-8.

124. Gieseg, M.A., et al., *Expression profiling of human renal carcinomas with functional taxonomic analysis.* BMC Bioinformatics, 2002. **3**: p. 26.

125. Sakai, N., et al., *SPARC expression in primary human renal cell carcinoma: upregulation of SPARC in sarcomatoid renal carcinoma.* Hum Pathol, 2001. **32**(10): p. 1064-70.

126. Goldenberg, D., et al., *Analysis of differentially expressed genes in hepatocellular carcinoma using cDNA arrays.* Mol Carcinog, 2002. **33**(2): p. 113-24.

127. Lau, C.P., et al., *SPARC and Hevin expression correlate with tumour angiogenesis in hepatocellular carcinoma.* J Pathol, 2006. **210**(4): p. 459-68.

128. Le Bail, B., et al., *Osteonectin/SPARC is overexpressed in human hepatocellular carcinoma.* J Pathol, 1999. **189**(1): p. 46-52.

129. Brown, T.J., et al., *Activation of SPARC expression in reactive stroma associated with human epithelial ovarian cancer.* Gynecol Oncol, 1999. **75**(1): p. 25-33.

130. Paley, P.J., et al., *Alterations in SPARC and VEGF immunoreactivity in epithelial ovarian cancer.* Gynecol Oncol, 2000. **78**(3 Pt 1): p. 336-41.

131. Bloomston, M., et al., *Stromal osteonectin overexpression is associated with poor outcome in patients with ampullary cancer.* Ann Surg Oncol, 2007. **14**(1): p. 211-7.

132. Sato, N., et al., *SPARC/osteonectin is a frequent target for aberrant methylation in pancreatic adenocarcinoma and a mediator of tumor-stromal interactions.* Oncogene, 2003. **22**(32): p. 5021-30.

133. Best, C.J., et al., *Molecular alterations in primary prostate cancer after androgen ablation therapy.* Clin Cancer Res, 2005. **11**(19 Pt 1): p. 6823-34.

134. Lapointe, J., et al., *Gene expression profiling identifies clinically relevant subtypes of prostate cancer.* Proc Natl Acad Sci U S A, 2004. **101**(3): p. 811-6.

135. Thomas, R., et al., *Differential expression of osteonectin/SPARC during human prostate cancer progression.* Clin Cancer Res, 2000. **6**(3): p. 1140-9.

136. Chen, N., et al., *A secreted isoform of ErbB3 promotes osteonectin expression in bone and enhances the invasiveness of prostate cancer cells.* Cancer Res, 2007. **67**(14): p. 6544-8.

137. De, S., et al., *Molecular pathway for cancer metastasis to bone.* J Biol Chem, 2003. **278**(40): p. 39044-50.

138. Kuphal, S., et al., *Snail-regulated genes in malignant melanoma.* Melanoma Res, 2005. **15**(4): p. 305-13.

139. Sturm, R.A., et al., *Osteonectin/SPARC induction by ectopic beta(3) integrin in human radial growth phase primary melanoma cells.* Cancer Res, 2002. **62**(1): p. 226-32.

140. Aycock, R.L., et al., *Development of UV-induced squamous cell carcinomas is suppressed in the absence of SPARC.* J Invest Dermatol, 2004. **123**(3): p. 592-9.

141. Inoue, H., et al., *Prognostic score of gastric cancer determined by cDNA microarray.* Clin Cancer Res, 2002. **8**(11): p. 3475-9.

142. Maeng, H.Y., et al., *Osteonectin-expressing cells in human stomach cancer and their possible clinical significance.* Cancer Lett, 2002. **184**(1): p. 117-21.

143. Takeno, A., et al., *Integrative approach for differentially overexpressed genes in gastric cancer by combining large-scale gene expression profiling and network analysis.* Br J Cancer, 2008. **99**(8): p. 1307-15.

144. Wang, C.S., et al., *Overexpression of SPARC gene in human gastric carcinoma and its clinic-pathologic significance.* Br J Cancer, 2004. **91**(11): p. 1924-30.

145. Maeng, H.Y., et al., *Appearance of osteonectin-expressing fibroblastic cells in early rat stomach carcinogenesis and stomach tumors induced with N-methyl-N'-nitro-N-nitrosoguanidine.* Jpn J Cancer Res, 2002. **93**(9): p. 960-7.

146. Takano, T., et al., *Quantitative analysis of osteonectin mRNA in thyroid carcinomas.* Endocr J, 2002. **49**(4): p. 511-6.

147. Chen, Y., et al., *Identification of cervical cancer markers by cDNA and tissue microarrays.* Cancer Res, 2003. **63**(8): p. 1927-35.

148. Rodriguez-Jimenez, F.J., et al., *Overexpression of SPARC protein contrasts with its transcriptional silencing by aberrant hypermethylation of SPARC CpG-rich region in endometrial carcinoma.* Oncol Rep, 2007. **17**(6): p. 1301-7.

149. Cheetham, S., et al., *SPARC promoter hypermethylation in colorectal cancers can be reversed by 5-Aza-2'deoxycytidine to increase SPARC expression and improve therapy response.* Br J Cancer, 2008. **98**(11): p. 1810-9.

150. Yang, E., et al., *Frequent inactivation of SPARC by promoter hypermethylation in colon cancers.* Int J Cancer, 2007. **121**(3): p. 567-75.

151. Suzuki, M., et al., *Aberrant methylation of SPARC in human lung cancers.* Br J Cancer, 2005. **92**(5): p. 942-8.

152. Wang, Y., et al., *Survey of differentially methylated promoters in prostate cancer cell lines.* Neoplasia, 2005. **7**(8): p. 748-60.

153. Socha, M.J., et al., *Aberrant promoter methylation of SPARC in ovarian cancer.* Neoplasia, 2009. **11**(2): p. 126-35.

154. Hong, S.M., et al., *Multiple genes are hypermethylated in intraductal papillary mucinous neoplasms of the pancreas.* Mod Pathol, 2008. **21**(12): p. 1499-507.

155. Brune, K., et al., *Genetic and epigenetic alterations of familial pancreatic cancers.* Cancer Epidemiol Biomarkers Prev, 2008. **17**(12): p. 3536-42.

156. Sova, P., et al., *Discovery of novel methylation biomarkers in cervical carcinoma by global demethylation and microarray analysis.* Cancer Epidemiol Biomarkers Prev, 2006. **15**(1): p. 114-23.

157. Tai, I.T., et al., *Genome-wide expression analysis of therapy-resistant tumors reveals SPARC as a novel target for cancer therapy.* J Clin Invest, 2005. **115**(6): p. 1492-502.

158. Taghizadeh, F., M.J. Tang, and I.T. Tai, *Synergism between vitamin D and secreted protein acidic and rich in cysteine-induced apoptosis and growth inhibition results in increased susceptibility of therapy-resistant colorectal cancer cells to chemotherapy.* Mol Cancer Ther, 2007. **6**(1): p. 309-17.

159. Kram, A., et al., *Mapping and genome sequence analysis of chromosome 5 regions involved in bladder cancer progression.* Lab Invest, 2001. **81**(7): p. 1039-48.

160. Bullinger, L., et al., *Use of gene-expression profiling to identify prognostic subclasses in adult acute myeloid leukemia.* N Engl J Med, 2004. **350**(16): p. 1605-16.

161. DiMartino, J.F., et al., *Low or absent SPARC expression in acute myeloid leukemia with MLL rearrangements is associated with sensitivity to growth inhibition by exogenous SPARC protein.* Leukemia, 2006. **20**(3): p. 426-32.

162. Ross, M.E., et al., *Gene expression profiling of pediatric acute myelogenous leukemia.* Blood, 2004. **104**(12): p. 3679-87.

163. Chlenski, A., et al., *SPARC is a key Schwannian-derived inhibitor controlling neuroblastoma tumor angiogenesis.* Cancer Res, 2002. **62**(24): p. 7357-63.

164. Chlenski, A., et al., *Neuroblastoma angiogenesis is inhibited with a folded synthetic molecule corresponding to the epidermal growth factor-like module of the follistatin domain of SPARC.* Cancer Res, 2004. **64**(20): p. 7420-5.

165. Beck, A.H., et al., *The fibromatosis signature defines a robust stromal response in breast carcinoma.* Lab Invest, 2008. **88**(6): p. 591-601.

166. Dhanesuan, N., et al., *Doxycycline-inducible expression of SPARC/Osteonectin/BM40 in MDA-MB-231 human breast cancer cells results in growth inhibition.* Breast Cancer Res Treat, 2002. **75**(1): p. 73-85.

167. Koblinski, J.E., et al., *Endogenous osteonectin/SPARC/BM-40 expression inhibits MDA-MB-231 breast cancer cell metastasis.* Cancer Res, 2005. **65**(16): p. 7370-7.

168. Chlenski, A., et al., *SPARC enhances tumor stroma formation and prevents fibroblast activation.* Oncogene, 2007. **26**(31): p. 4513-22.

169. Chlenski, A., et al., *SPARC expression is associated with impaired tumor growth, inhibited angiogenesis and changes in the extracellular matrix.* Int J Cancer, 2006. **118**(2): p. 310-6.

170. Pan, M.R., et al., *The nonsteroidal anti-inflammatory drug NS398 reactivates SPARC expression via promoter demethylation to attenuate invasiveness of lung cancer cells.* Exp Biol Med (Maywood), 2008. **233**(4): p. 456-62.

171. Huang, D.Y., et al., *Transcription factor SOX-5 enhances nasopharyngeal carcinoma progression by down-regulating SPARC gene expression.* J Pathol, 2008. **214**(4): p. 445-55.

172. Yiu, G.K., et al., *SPARC (secreted protein acidic and rich in cysteine) induces apoptosis in ovarian cancer cells.* Am J Pathol, 2001. **159**(2): p. 609-22.

173. Bull Phelps, S.L., et al., *Secreted protein acidic and rich in cysteine as a regulator of murine ovarian cancer growth and chemosensitivity.* Am J Obstet Gynecol, 2009. **200**(2): p. 180 e1-7.

174. Mok, S.C., et al., *SPARC, an extracellular matrix protein with tumor-suppressing activity in human ovarian epithelial cells.* Oncogene, 1996. **12**(9): p. 1895-901.

175. Said, N. and K. Motamed, *Absence of host-secreted protein acidic and rich in cysteine (SPARC) augments peritoneal ovarian carcinomatosis.* Am J Pathol, 2005. **167**(6): p. 1739-52.

176. Said, N., I. Najwer, and K. Motamed, *Secreted protein acidic and rich in cysteine (SPARC) inhibits integrin-mediated adhesion and growth factor-dependent survival signaling in ovarian cancer.* Am J Pathol, 2007. **170**(3): p. 1054-63.

177. Said, N., et al., *Normalization of the ovarian cancer microenvironment by SPARC.* Mol Cancer Res, 2007. **5**(10): p. 1015-30.

178. Arnold, S., et al., *Forced expression of MMP9 rescues the loss of angiogenesis and abrogates metastasis of pancreatic tumors triggered by the absence of host SPARC.* Exp Biol Med (Maywood), 2008. **233**(7): p. 860-73.

179. Puolakkainen, P.A., et al., *Enhanced growth of pancreatic tumors in SPARC-null mice is associated with decreased deposition of extracellular matrix and reduced tumor cell apoptosis.* Mol Cancer Res, 2004. **2**(4): p. 215-24.

180. Kahn, S.L., et al., *Quantitative methylation-specific PCR for the detection of aberrant DNA methylation in liquid-based Pap tests.* Cancer, 2008. **114**(1): p. 57-64.

181. Streuli, C.H., *Integrins and cell-fate determination.* J Cell Sci, 2009. **122**(Pt 2): p. 171-7.

182. Streuli, C.H. and N. Akhtar, *Signal co-operation between integrins and other receptor systems.* Biochem J, 2009. **418**(3): p. 491-506.

183. Engbring, J.A. and H.K. Kleinman, *The basement membrane matrix in malignancy.* J Pathol, 2003. **200**(4): p. 465-70.

184. Ioachim, E., et al., *Immunohistochemical expression of extracellular matrix components tenascin, fibronectin, collagen type IV and laminin in breast cancer: their prognostic value and role in tumour invasion and progression.* Eur J Cancer, 2002. **38**(18): p. 2362-70.

185. Timar, J., et al., *Proteoglycans and tumor progression: Janus-faced molecules with contradictory functions in cancer.* Semin Cancer Biol, 2002. **12**(3): p. 173-86.

186. Berrier, A.L. and K.M. Yamada, *Cell-matrix adhesion.* J Cell Physiol, 2007. **213**(3): p. 565-73.

187. Juliano, R.L., *Signal transduction by cell adhesion receptors and the cytoskeleton: functions of integrins, cadherins, selectins, and immunoglobulin-superfamily members.* Annu Rev Pharmacol Toxicol, 2002. **42**: p. 283-323.

188. Stupack, D.G., *The biology of integrins.* Oncology (Williston Park), 2007. **21**(9 Suppl 3): p. 6-12.

189. Moser, M., et al., *The tail of integrins, talin, and kindlins.* Science, 2009. **324**(5929): p. 895-9.

190. Schultz, G.S. and A. Wysocki, *Interactions between extracellular matrix and growth factors in wound healing.* Wound Repair Regen, 2009. **17**(2): p. 153-62.

191. Norose, K., et al., *SPARC deficiency leads to early-onset cataractogenesis.* Invest Ophthalmol Vis Sci, 1998. **39**(13): p. 2674-80.

192. Gilmour, D.T., et al., *Mice deficient for the secreted glycoprotein SPARC/osteonectin/BM40 develop normally but show severe age-onset cataract formation and disruption of the lens.* Embo J, 1998. **17**(7): p. 1860-70.

193. Yan, Q., et al., *Expression of the matricellular protein SPARC in murine lens: SPARC is necessary for the structural integrity of the capsular basement membrane.* J Histochem Cytochem, 2003. **51**(4): p. 503-11.

194. Delany, A.M., et al., *Osteonectin-null mutation compromises osteoblast formation, maturation, and survival.* Endocrinology, 2003. **144**(6): p. 2588-96.

195. Bradshaw, A.D., et al., *SPARC-null mice display abnormalities in the dermis characterized by decreased collagen fibril diameter and reduced tensile strength.* J Invest Dermatol, 2003. **120**(6): p. 949-55.

196. Bradshaw, A.D., et al., *SPARC-null mice exhibit increased adiposity without significant differences in overall body weight.* Proc Natl Acad Sci U S A, 2003. **100**(10): p. 6045-50.

197. Bradshaw, A.D., M.J. Reed, and E.H. Sage, *SPARC-null mice exhibit accelerated cutaneous wound closure.* J Histochem Cytochem, 2002. **50**(1): p. 1-10.

198. Puolakkainen, P., et al., *Compromised production of extracellular matrix in mice lacking secreted protein, acidic and rich in cysteine (SPARC) leads to a reduced foreign body reaction to implanted biomaterials.* Am J Pathol, 2003. **162**(2): p. 627-35.

199. Eliceiri, B.P., *Integrin and growth factor receptor crosstalk.* Circ Res, 2001. **89**(12): p. 1104-10.

200. Porter, J.C. and N. Hogg, *Integrins take partners: cross-talk between integrins and other membrane receptors.* Trends Cell Biol, 1998. **8**(10): p. 390-6.

201. Somanath, P.R., A. Ciocea, and T.V. Byzova, *Integrin and growth factor receptor alliance in angiogenesis.* Cell Biochem Biophys, 2009. **53**(2): p. 53-64.

202. Bradshaw, A.D., et al., *Primary mesenchymal cells isolated from SPARC-null mice exhibit altered morphology and rates of proliferation.* Mol Biol Cell, 1999. **10**(5): p. 1569-79.

203. Barker, T.H., et al., *SPARC regulates extracellular matrix organization through its modulation of integrin-linked kinase activity.* J Biol Chem, 2005. **280**(43): p. 36483-93.

204. Weaver, M.S., G. Workman, and E.H. Sage, *The copper binding domain of SPARC mediates cell survival in vitro via interaction with integrin beta1 and activation of integrin-linked kinase.* J Biol Chem, 2008. **283**(33): p. 22826-37.

205. Nie, J., et al., *IFATS collection: Combinatorial peptides identify alpha5beta1 integrin as a receptor for the matricellular protein SPARC on adipose stromal cells.* Stem Cells, 2008. **26**(10): p. 2735-45.

206. Davis, G.E. and D.R. Senger, *Endothelial extracellular matrix: biosynthesis, remodeling, and functions during vascular morphogenesis and neovessel stabilization.* Circ Res, 2005. **97**(11): p. 1093-107.

207. Motamed, K., et al., *Inhibition of PDGF-stimulated and matrix-mediated proliferation of human vascular smooth muscle cells by SPARC is independent of changes in cell shape or cyclin-dependent kinase inhibitors.* J Cell Biochem, 2002. **84**(4): p. 759-71.

208. Nozaki, M., et al., *Loss of SPARC-mediated VEGFR-1 suppression after injury reveals a novel antiangiogenic activity of VEGF-A.* J Clin Invest, 2006. **116**(2): p. 422-9.

209. Kato, Y., et al., *Induction of SPARC by VEGF in human vascular endothelial cells.* Biochem Biophys Res Commun, 2001. **287**(2): p. 422-6.

210. Bradshaw, A.D., et al., *Increased fibrovascular invasion of subcutaneous polyvinyl alcohol sponges in SPARC-null mice.* Wound Repair Regen, 2001. **9**(6): p. 522-30.

211. Yunker, C.K., et al., *SPARC-induced increase in glioma matrix and decrease in vascularity are associated with reduced VEGF expression and secretion.* Int J Cancer, 2008. **122**(12): p. 2735-43.

212. Schiemann, B.J., J.R. Neil, and W.P. Schiemann, *SPARC inhibits epithelial cell proliferation in part through stimulation of the transforming growth factor-beta-signaling system.* Mol Biol Cell, 2003. **14**(10): p. 3977-88.

213. Verrecchia, F. and A. Mauviel, *Transforming growth factor-beta and fibrosis.* World J Gastroenterol, 2007. **13**(22): p. 3056-62.

214. Ford, R., et al., *Modulation of SPARC expression during butyrate-induced terminal differentiation of cultured human keratinocytes: regulation via a TGF-beta-dependent pathway.* Exp Cell Res, 1993. **206**(2): p. 261-75.

215. Reed, M.J., et al., *TGF-beta 1 induces the expression of type I collagen and SPARC, and enhances contraction of collagen gels, by fibroblasts from young and aged donors.* J Cell Physiol, 1994. **158**(1): p. 169-79.

216. Pavasant, P., et al., *The synergistic effect of TGF-beta and 1,25-dihydroxyvitamin D3 on SPARC synthesis and alkaline phosphatase activity in human pulp fibroblasts.* Arch Oral Biol, 2003. **48**(10): p. 717-22.

217. Wrana, J.L., C.M. Overall, and J. Sodek, *Regulation of the expression of a secreted acidic protein rich in cysteine (SPARC) in human fibroblasts by transforming growth factor beta. Comparison of transcriptional and post-transcriptional control with fibronectin and type I collagen.* Eur J Biochem, 1991. **197**(2): p. 519-28.

218. Bassuk, J.A., et al., *Induction of TGF-beta1 by the matricellular protein SPARC in a rat model of glomerulonephritis.* Kidney Int, 2000. **57**(1): p. 117-28.

219. Francki, A., et al., *SPARC regulates the expression of collagen type I and transforming growth factor-beta1 in mesangial cells.* J Biol Chem, 1999. **274**(45): p. 32145-52.

220. Tian, M. and W.P. Schiemann, *The TGF-beta paradox in human cancer: an update.* Future Oncol, 2009. **5**(2): p. 259-71.

CHAPTER TWO

Forced expression of MMP9 rescues the loss of angiogenesis and abrogates metastasis of pancreatic tumors triggered by the absence of host SPARC

Shanna Arnold[1#], Emilia Mira[2#], Sabeeha Muneer[1#], Grzegorz Korpanty[1], Adam W. Beck[1], Shane E. Holloway[1], Santos Mañes[2], Rolf A. Brekken*[1]

[1]Hamon Center for Therapeutic Oncology Research, Departments of Surgery and Pharmacology, University of Texas Southwestern Medical Center, Dallas, TX 75390 USA.

[2]Department of Immunology and Oncology, Centro Nacional de Biotecnología/CSIC, Universidad Autónoma de Madrid, Cantoblanco, E-28049 Madrid, Spain.

[#] These authors contributed equally.

Running header 'SPARC and MMP9 effect tumor progression'

*Corresponding Author:
Rolf A. Brekken, PhD
Hamon Center for Therapeutic Oncology Research
UT-Southwestern Medical Center
6000 Harry Hines Blvd.
Dallas, TX 75390-8593
Tel: 214 648 5151 Fax: 214 648 4940
e-mail address: rolf.brekken@utsouthwestern.edu

Supported in part by The Effie Marie Cain Scholarship in Angiogenesis Research (to RAB.), The National Pancreas Foundation (grant 47431 to RAB.), The American Cancer Society (grant 47411/56540 to RAB.), and the NIH (R01 CA118240 to RAB). SA was supported in part by a training grant from the NIH (GM007062). The Department of Immunology and Oncology was founded and is supported by the Spanish Council for Scientific Research (CSIC) and by Pfizer. This work was in part supported by the grant SAF2005-00241 from the Spanish Ministry of Science and Education (to S Mañes).

Abstract

Pancreatic adenocarcinoma is characterized by desmoplasia, local invasion, and metastasis. These features are regulated in part by MMP9 and SPARC. To explore the interaction of SPARC and MMP9 in cancer, we first established orthotopic pancreatic tumors in *SPARC-null* and *wild-type* mice with the murine pancreatic adenocarcinoma cell line, PAN02. MMP9 expression was higher in tumors from *wild-type* compared to *SPARC-null* mice. Coincident with lower MMP9 expression, tumors grown in SPARC-null mice were significantly larger, had decreased ECM deposition and reduced microvessel density compared to wild-type controls. In addition, metastasis was enhanced in the absence of host SPARC. Therefore, we next analyzed the orthotopic tumor growth of PAN02 cells transduced with MMP9 or a control empty vector. Forced expression of MMP9 by the PAN02 cells resulted in larger tumors in both *wild-type* and *SPARC-null* animals compared to empty vector controls and further diminished ECM deposition. Importantly, forced expression of MMP9 within the tumor reversed the decrease in angiogenesis and abrogated the metastatic potential displayed by control tumors grown in SPARC-null mice. Finally, contrary to the *in vivo* results, MMP9 increased cell migration *in vitro*, which was blocked by the addition of SPARC. These results suggest that SPARC and MMP9 interact to regulate many stages of tumor progression including ECM deposition, angiogenesis and metastasis.

Key words: ECM; metastasis; MMP9; pancreatic; SPARC; tumor microenvironment

Introduction

SPARC is a highly conserved multifunctional glycoprotein that belongs to the matricellular class of proteins. Matricellular proteins function as adaptors that mediate cell-extracellular matrix (ECM) interactions [1] and are expressed in tissues undergoing repair or remodeling. For example, SPARC is expressed in healing wounds, areas of bone morphogenesis, developing embryonic tissue, as well as, sites of angiogenesis [2]. Consistent with its function as a mediator of tissue remodeling, SPARC regulates the expression of proteins involved in ECM turnover and formation including collagens and matrix metalloproteinases (MMPs) [3]. SPARC can also directly affect endothelial cell behavior by regulating proliferation, cell shape and response to different angiogenic growth factors including transforming growth factor (TGF-β), fibroblast growth factor (FGF), vascular endothelial growth factor (VEGF) and platelet-derived growth factor (PDGF) [1, 4, 5].

MMPs are zinc-dependent endopeptidases that contribute to proteolytic events important for homeostasis, tissue remodeling and cancer progression [6]. The targets of MMPs have traditionally been considered structural components of the ECM, although it is now clear that these enzymes have a broader array of substrates [7]. For instance, MMP9 triggers the angiogenic switch by releasing ECM-associated VEGF, thus influencing subsequent tumor growth [8]. MMPs may also influence tumor progression by facilitating events pivotal for neovascularization and establishment of distant metastasis including proliferation, survival and migration of endothelial, tumor and stromal cells [9, 10].

SPARC expression is altered in many cancers. There is increased expression of SPARC in melanoma, glioma, colorectal, and breast carcinomas compared to their respective normal tissues [11]. In these tumors, high levels of SPARC often correlate with enhanced invasion and metastasis [11]. In contrast, increased expression of SPARC by ovarian carcinoma cells led to increased tumor cell apoptosis and correlated inversely with tumor progression *in vivo* [12, 13]. In pancreatic tumors, expression of SPARC by cancer cells is limited due to promoter hypermethylation, while infiltrating stromal cells express increased levels of SPARC [14]. Thus, the context of SPARC expression in the microenvironment is critical for understanding its influence on tumor growth and progression. Whether produced by tumor or stromal cells, SPARC protein is often found at tumor-stromal interfaces, tumor capsules, areas of desmoplasia and areas of angiogenesis and vascular remodeling [15]. Given these findings, SPARC is well-placed to participate in the host response to tumor growth.

We showed previously that ectopic tumor growth is enhanced significantly in *SPARC-null* (*SPARC*$^{-/-}$) mice compared to *wild-type* (*WT*) animals. These studies demonstrate that ECM deposition within and around the tumor is altered in the absence of host-derived SPARC and further suggest that SPARC is important in the host response to an implanted tumor [16, 17]. In this context, it has been proposed that SPARC influences ECM production, deposition and function, in part, by modulating proteases or their inhibitors. In fact, SPARC has been shown to induce the expression of MMP9 in macrophages/monocytes, a predominant source of MMP9 in the tumor microenvironment [18]. SPARC is also a substrate for MMP activity. Cleavage of SPARC between L196-L197 or L197-L198 by MMPs increases the affinity of SPARC for collagen I and IV [19,

20]. Sage et al. [21] showed that SPARC can be cleaved into at least three bioactive polypeptides by MMP3. One of the polypeptides (designated Z2) has L198 at its COOH-terminus and promoted the migration of endothelial cells, but inhibited cell proliferation *in vitro*.

To explore the function of SPARC and MMP9 in the tumor microenvironment, we established orthotopic pancreatic tumors in *WT* and *SPARC*$^{-/-}$ mice with a mouse pancreatic adenocarcinoma cell line, PAN02, which was engineered to express MMP9. This study demonstrates that forced expression of MMP9 by PAN02 cells not only enhances primary tumor growth in *WT* and *SPARC*$^{-/-}$ mice, but also rescues angiogenesis and abrogates metastasis in tumors grown in *SPARC*$^{-/-}$ mice. These results demonstrate that SPARC and MMP9 interact to influence tumorigenesis by affecting angiogenesis, ECM deposition and degradation, and metastatic progression.

Results

Orthotopic tumor growth is enhanced in the absence of host SPARC.

We showed previously that PAN02 tumors grew larger after subcutaneous injection into *SPARC*$^{-/-}$ mice compared to *WT* littermates [16]. To determine if this phenotype extended to tumors grown in the pancreas, we injected PAN02 cells underneath the capsule of the pancreas of *SPARC*$^{-/-}$ and *WT* animals. Figure 1A shows that orthotopic tumors were approximately 3-fold larger in *SPARC*$^{-/-}$ compared to *WT* mice ($p<0.01$). Tumors grown in *SPARC*$^{-/-}$ animals displayed a less robust capsule and were more invasive. Furthermore, the number of metastatic events increased in the absence of host SPARC

(data not shown). Given that MMP9 expression is linked to ECM remodeling and tumor cell metastasis, we evaluated the level of expression of MMP9 and its cell distribution by immunohistochemistry in subcutaneous and orthotopic PAN02 tumors grown in *WT* and *SPARC*$^{-/-}$ animals. The number of cells positive for MMP9 was reduced in the absence of host-derived SPARC, such that there were 53.0 +/- 14.7 and 33.8 +/- 5.0 MMP9 positive cells in orthotopic tumors grown in *WT* and *SPARC*$^{-/-}$ mice, respectively (Figure 1B, $p<0.05$). Immunofluorescence analysis of MMP9 does reveal some stromal-associated MMP9 but the majority of the staining is cell-associated. Neutrophils are known to infiltrate tumors and to express MMP9 [22]. Therefore, we evaluated the tumors for neutrophils and MMP9 (Figure 2). The level of Gr-1 positive cells was reduced in tumors grown in SPARC$^{-/-}$ animals. Image analysis of co-localization of Gr-1 and MMP9 demonstrates that the majority of MMP9 produced in PAN02 tumor microenvironment was associated with Gr-1 positive cells. We anticipate that the MMP9 detected represents newly produced protein or MMP9 in the secretory pathway. However, an alternative explanation is that the immuno-positive cells have tethered MMP9 to the cell surface via CD44 [23] or other alternative cell surface receptors.

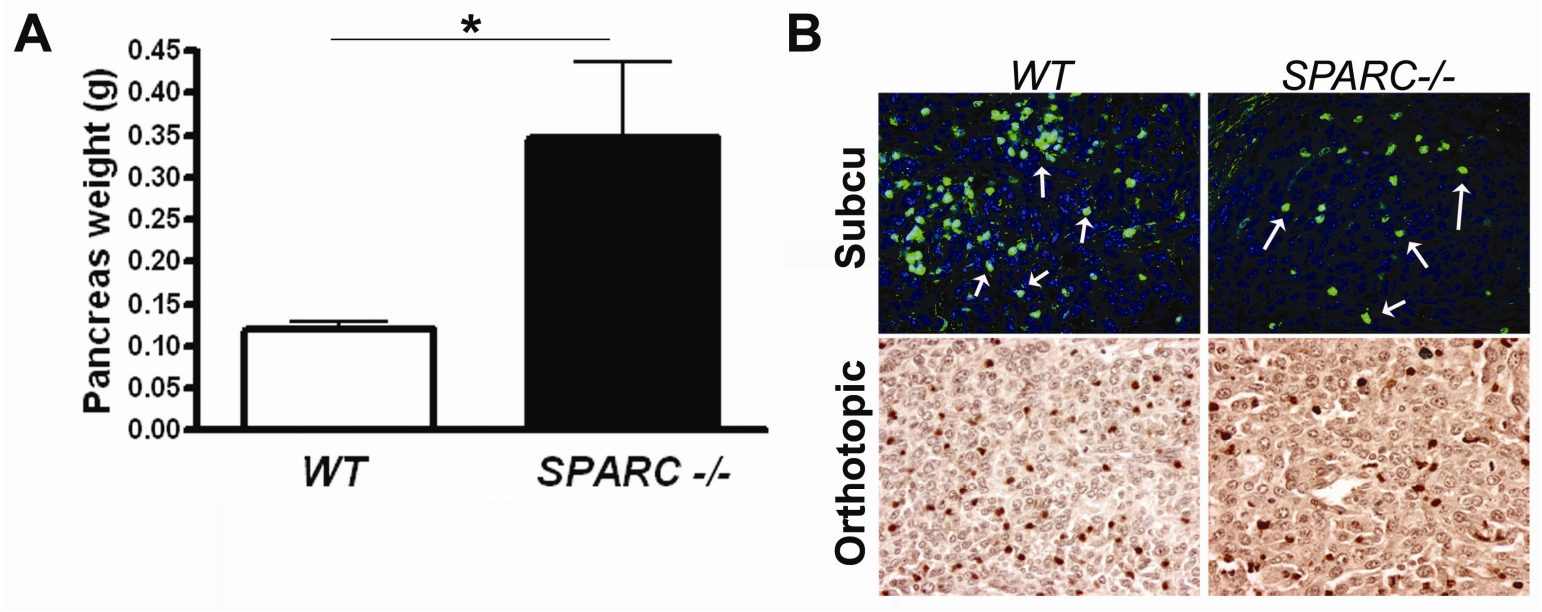

Figure 1. Pancreatic tumor growth is increased in the absence of host SPARC. A) 5 x10^5 murine pancreatic adenocarcinoma (PAN02) cells were injected orthotopically into wild-type (*WT,* n=9) and *SPARC*$^{-/-}$ (*SPARC*-/-, n=5) mice. The mice were sacrificed 28 days after tumor cell injection and the weight (g) of the entire pancreas including tumor was determined. The mean pancreas weight +/- SEM for *WT* and *SPARC*$^{-/-}$ mice are displayed. *, $p<0.01$. B) Orthotopic and subcutaneous PAN02 tumors from *WT* and *SPARC*$^{-/-}$ mice were harvested, fixed in methyl Carnoys or formalin, respectively, sectioned and evaluated for MMP9 expression by immunohistochemistry. MMP9 levels (green) in subcutaneous tumors were developed with FITC-conjugated secondary antibody and sections counterstained with DAPI to identify nuclei (blue). Arrows indicate cells positive for MMP9. MMP9 levels in orthotopic tumors were developed with a peroxidase-conjugated secondary antibody with subsequent reaction with the chromagen DAB. MMP9 positive cells were hand counted in a minimum of 10 fields/group to be 53.0 +/- 14.7 and 33.8 +/- 5.0 in *WT* and *SPARC*$^{-/-}$ mice, respectively ($p<0.05$). Total magnification is 400x.

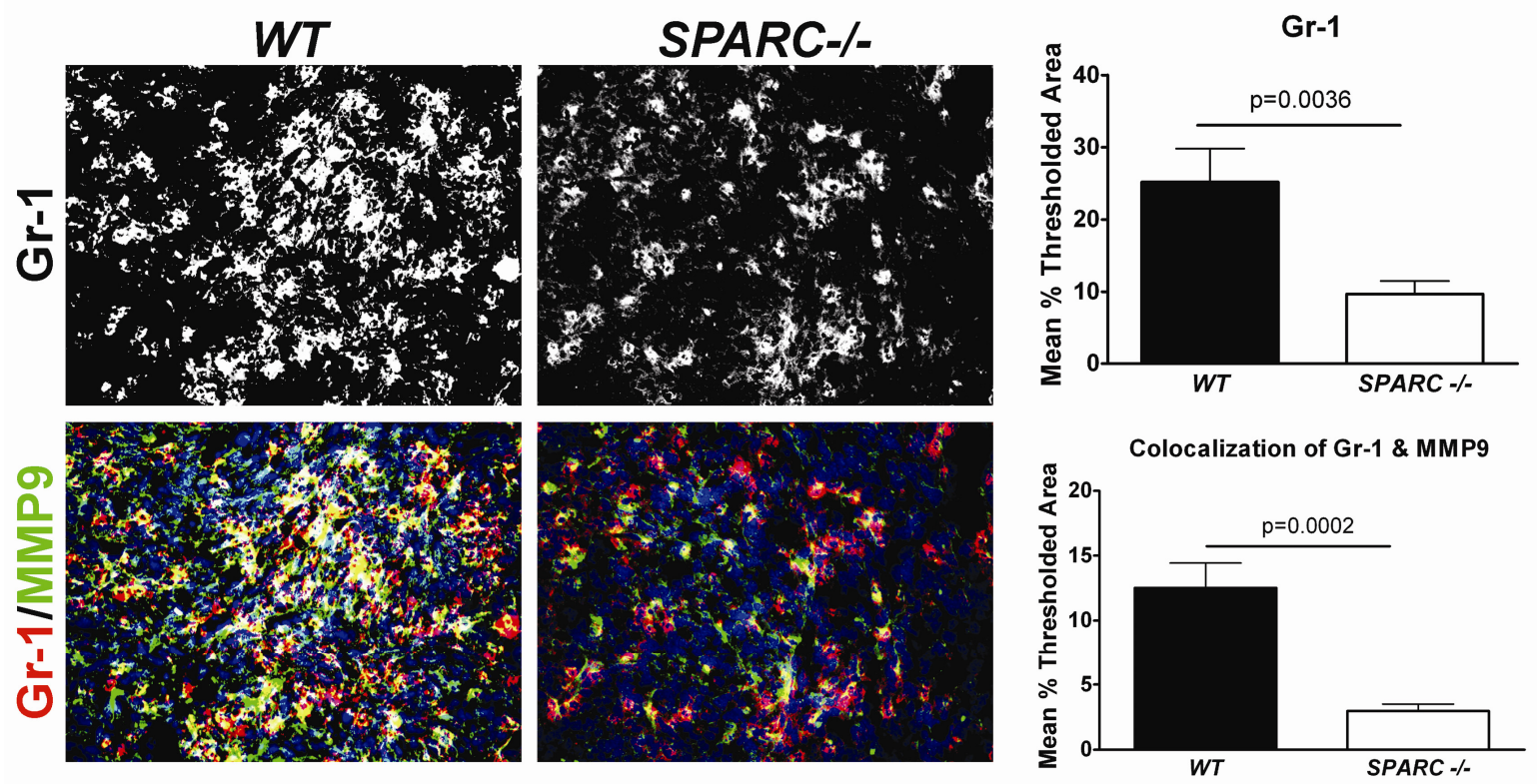

Figure 2. Neutrophils express MMP9 and their infiltration into PAN02 tumors is reduced in the absence of host SPARC. Paraffin-embedded sections of orthotopic PAN02 tumors grown in *WT* or *SPARC-/-* mice were evaluated immunohistochemically for Gr-1 (red) and MMP9 (green) and sections were counterstained with DAPI to identify nuclei. The level of Gr-1 staining and co-localization of Gr-1 with MMP9 was quantified using Metamorph software. Total magnification is 400x.

Forced MMP9 expression confers PAN02 cells with increased proteolytic activity.

To determine the effect of forced expression of MMP9 on tumor growth and if host SPARC had any effect on tumor-derived MMP9, PAN02 cells were transduced with recombinant retroviruses containing either empty vector (PRV) or native human MMP9 (MMP9). Zymographic analysis of total cell extracts from PAN02 cells transduced with MMP9 (PAN02-MMP9) detected a double gelatinolytic band corresponding to the pro and activated form of MMP9 (Figure 3A). In empty vector transduced cells (PAN02-PRV), no gelatinolytic activity was observed. As expected for a secreted protein, MMP9 was expressed abundantly in conditioned medium of PAN02-MMP9 cells (Figure 3B). In addition, cell fractionation of PAN02-MMP9 cells confirmed that MMP9 associates with both the cytosol and the cell membrane (Figure 3C). The membrane protein transferrin receptor (TfR) was used as a marker of the membrane fraction and tubulin (Tub) was used as a marker of the cytosol.

The cellular localization of MMP9 in PAN02-MMP9 cells plated on tissue culture plastic or collagen IV was determined by immunocytochemistry (Figure 3D). Consistent with the zymographic (Figure 3A, B) and biochemical (Figure 3C) analyses, PAN02-PRV cells showed no MMP9 staining, while PAN02-MMP9 cells exhibited staining distributed between internal membranes and the cytosol (Figure 3D).

We found no significant difference in the expression level of SPARC in parental and modified PAN02 cells by immunocytochemistry. However the subcellular distribution of SPARC was altered in PAN02-MMP9 cells. We found SPARC in the membrane fraction in PAN02-MMP9 but not PAN02-PRV cells by Western blot analysis

(Figure 3C). Furthermore, we observed SPARC at the tip of cell extensions more frequently in PAN02-MMP9 compared to PAN02-PRV cells (Figure 3E). To analyze *in vitro* proteolytic activity of cells expressing MMP9, we performed *in situ* zymography with DQ-gelatin. Incubation of PAN02-PRV or PAN02-MMP9 cells with DQ-gelatin for 1hr resulted in a similar punctate staining (Figure 3F). However, longer incubation with the substrate, especially at 22hrs, revealed that PAN02-MMP9 cells display significantly greater gelatinolytic activity compared to PAN02-PRV cells, possibly as a result of increased MMP9 expression (Figure 3G).

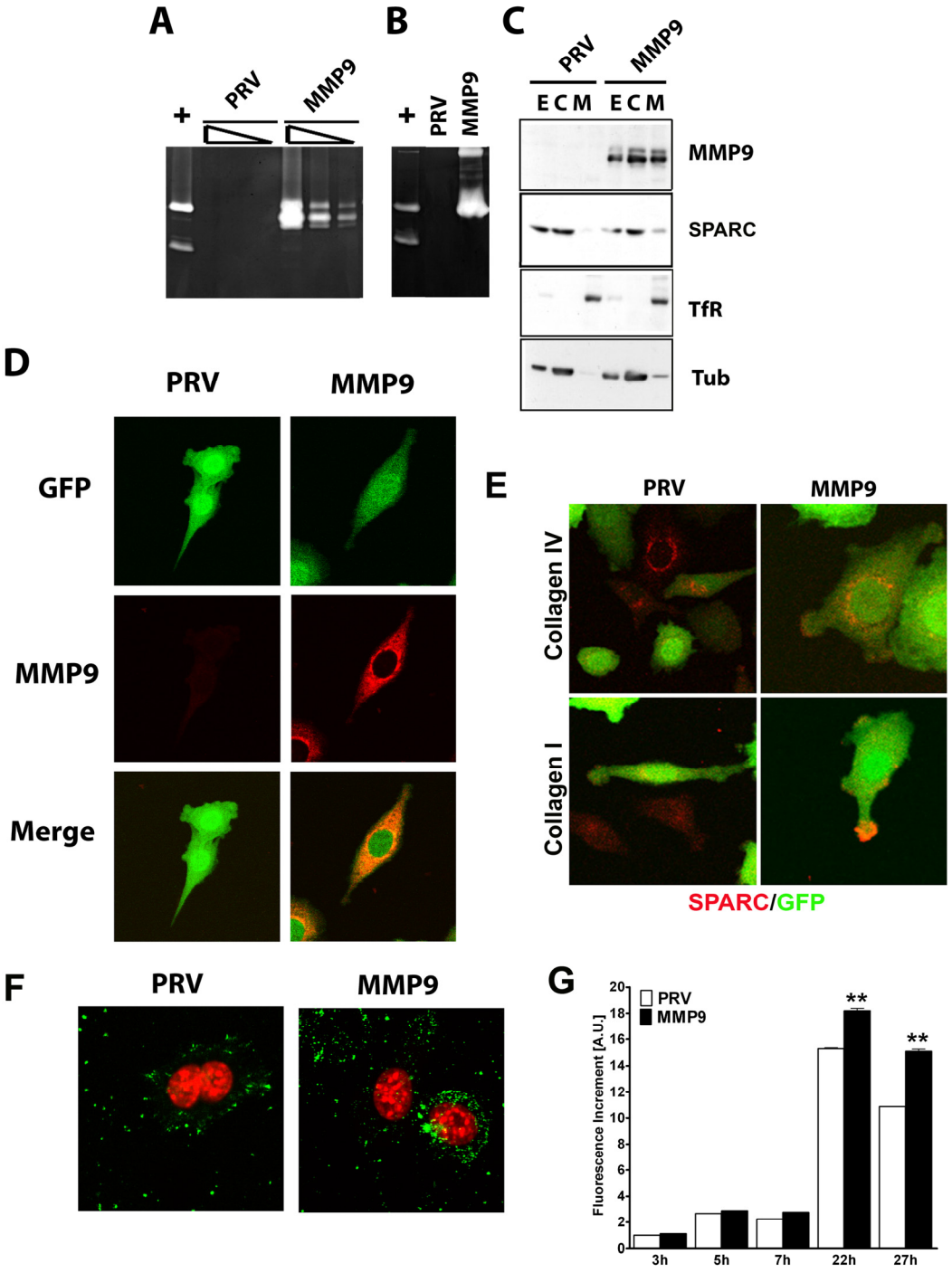

Figure 3. Characterization of MMP9 and SPARC expression in PAN02-PRV and PAN02-MMP9 cells. A) Gelatinolytic activity in total cell extracts of PAN02-PRV (PRV) and PAN02-MMP9 (MMP). Three serial dilutions of RIPA extracts corresponding

to 5, 1, and 0.2 μg of protein were loaded on an 8% gelatin-containing SDS gels. B) Gelatinolytic activity in conditioned medium from the same cells as in (A) after 24 h of serum depletion. In panel A and B HT1080 conditioned media (+) was loaded as a positive control of gelatinolytic activity and shows MMP9 and MMP2 bands. C) Membrane and cytosolic fractions were obtained from total cell lysates. 25 μg of total extracts (E) and cytosolic (C) fraction and 1/6 of the membrane fraction (M) were analyzed on a 10% SDS gel. Western blot analysis of MMP9 and SPARC was performed; anti-TfR (membrane marker) and anti-tubulin (cytosolic marker) were used as controls for fractionation. D) Confocal microscopy of MMP9 (red) in PAN02 cells, cells transduced with the indicated construct are positive for GFP (green). E) PAN02-PRV (PRV) and PAN02-MMP9 (MMP) cells plated on either collagen I or collagen IV slides were analyzed for SPARC (red) expression by immunocytochemistry. Cells transduced with the indicated construct are positive for GFP (green). F) PAN02-PRV (PRV) and PAN02-MMP9 (MMP) cells were analyzed for gelatinase activity (green) by incubating with DQ-gelatin and subsequent confocal microscopy. To-Pro3 cell tracker (red) was used to localize nuclei. G) Quantification of gelatinase activity in PAN02-PRV (PRV) and PAN02-MMP9 (MMP9). Cells were incubated with DQ-gelatin for the indicated time and the fluorescence increment was represented. Values are normalized to PAN02-PRV cells after 3h of incubation (** $p<0.01$, Students t test). These experiments were performed by our collaborators in the Department of Immunology and Oncology, Centro Nacional de Biotecnología/CSIC, Universidad Autónoma de Madrid, Cantoblanco, E-28049 Madrid, Spain.

Host SPARC contributes to MMP9-mediated effects on tumor growth.

To recapitulate the events of pancreatic cancer progression, we used an orthotopic pancreatic cancer model where PAN02-PRV and PAN02-MMP9 cells were injected directly into the tail of the pancreas of age-matched *WT* and *SPARC*$^{-/-}$ mice (n=6/group) in two independent experiments. One hundred percent of the mice in each genotype developed primary pancreatic tumors with a reproducible pattern of growth. Figure 4A shows that PAN02-PRV tumors were larger in *SPARC*$^{-/-}$ mice compared to *WT* counterparts, which is consistent with previous results [16, 17]. Tumors initiated with PAN02-MMP9 cells were significantly larger in both genotypes compared to PAN02-PRV tumors (*WT* mice, $p<0.01$; *SPARC*$^{-/-}$ mice, $p<0.001$). Tumors grown in the absence of host SPARC were more invasive such that the tumor margin was more difficult to identify grossly and there was a higher frequency of involvement of local organs (e.g., spleen, stomach, intestine, peritoneal wall). The invasive character of tumors grown in *SPARC*$^{-/-}$ animals was confirmed by analysis of H&E stained tumor tissue. Overall, these results demonstrate that tumor cell MMP9 and host SPARC both contribute to promotion or control of tumor growth, respectively. It is also evident that the absence of host SPARC and increased MMP9 expression is additive in terms of promoting tumor size.

Consistent with previous studies, the deposition of collagen as shown by Masson's trichrome (Figure 4B) and immunohistochemistry (data not shown) was reduced in and around pancreatic tumors grown in *SPARC*$^{-/-}$ mice. There were, however, notable differences between PAN02-PRV and PAN02-MMP9 tumors. PAN02-MMP9 tumors displayed less collagen staining than PAN02-PRV tumors in *WT* and *SPARC*$^{-/-}$

animals. The Masson's trichrome staining was consistent with the local invasiveness and gross appearance of the tumors upon necropsy.

We evaluated the level of MMP activity in tumors from a subset of each group of animals (Figure 4C) and found that there was a significant increase in the level of enzyme activity in PAN02-MMP9 compared to PAN02-PRV tumors. However, the presence or absence of host SPARC did not alter the level of enzyme activity detected by zymography of tumor lysates.

We also evaluated the growth of the cells *in vitro* (Figure 5A) and *in vivo* (Figure 5B). Under normal *in vitro* growth conditions PAN02-MMP9 cells proliferated more rapidly than control transfected PAN02-PRV cells (Figure 5A). To evaluate *in vivo* growth characteristics we quantified the number of proliferating and apoptotic cells in tumors grown in *WT* and *SPARC*$^{-/-}$ mice by detecting nuclei positive for phosphorylated histone H3 (phospho-H3) or terminal deoxynucleotidyl transferase mediated dUTP nick-end-labeling (TUNEL), respectively. We found that the overall balance of proliferating and apoptotic cells was very similar regardless of MMP9 status or genotype (Figure 5B). These data support the idea that the proliferation and death of PAN02 cells is not the principal reason for an increase in tumor size in the absence of SPARC or in the presence of elevated levels of MMP9.

In summary, tumor growth was controlled least in tumors that were either grown in the absence of SPARC or produced and secreted MMP9. Furthermore, MMP9 expression and the absence of SPARC were additive in terms of tumor size. Overall, these *in vivo* tumor growth assays demonstrate that MMP9 and SPARC have the capacity to impact primary tumor size, local invasion and tumor survival.

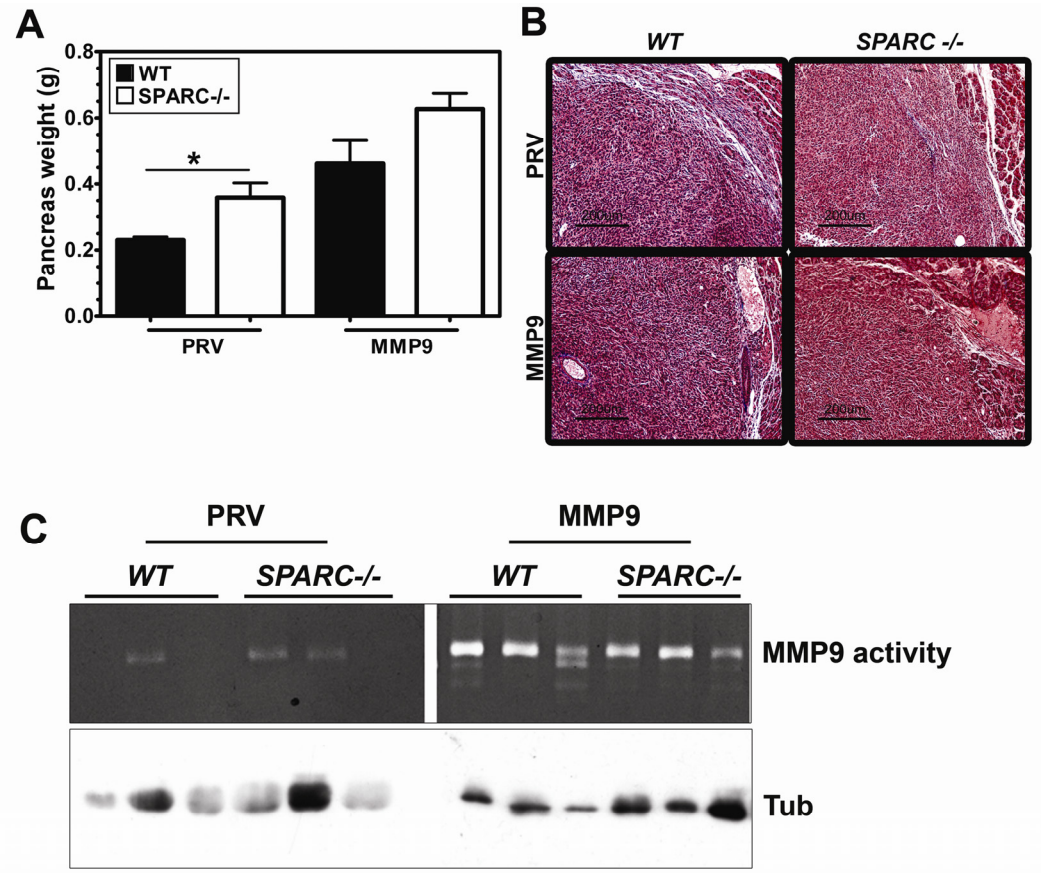

Figure 4. Forced expression of MMP9 or the absence of host SPARC increases PAN02 tumor growth. A) PAN02-PRV (PRV) and PAN02-MMP9 (MMP9) cells (5 x 10^5) were implanted orthotopically in the pancreas of age- and sex-matched *SPARC*$^{-/-}$ and *WT* mice (n= 6/group). After 6 weeks, the entire pancreas including tumor was weighed (g). A comparison of mean +/- SD pancreas weight is shown (* $p<0.05$, Student´s t test). One way ANOVA with Tukey's multiple comparison test revealed significant differences across tumor groups as well. PAN02-PRV tumors in *WT* mice were significantly smaller than PAN02-MMP9 tumors grown in *WT* mice ($p<0.01$) or *SPARC*$^{-/-}$ mice ($p<0.001$) while PAN02-PRV tumors in *SPARC*$^{-/-}$ mice were significantly different from PAN02-MMP9 in *SPARC*$^{-/-}$ mice ($p<0.001$). B) Masson's trichrome staining of paraffin-embedded tumors revealed decreased collagen fibers (blue) in tumors grown in *SPARC*$^{-/-}$ mice compared with those in *WT* mice. Forced expression of MMP9 resulted in an even further reduction in collagen deposition in response to tumor growth. C) Tumor extracts from PAN02-PRV (PRV) and PAN02-MMP9 (MMP9) grown in *WT* and *SPARC* -/- mice were analyzed by gelatin zymography. The bands corresponding to MMP9 are indicated. Western blot analysis of tubulin in equivalent amount of extracts was performed as a loading control. The experiment in panel C was performed by our collaborators in the Department of Immunology and Oncology, Centro Nacional de Biotecnología/CSIC, Universidad Autónoma de Madrid, Cantoblanco, E-28049 Madrid, Spain.

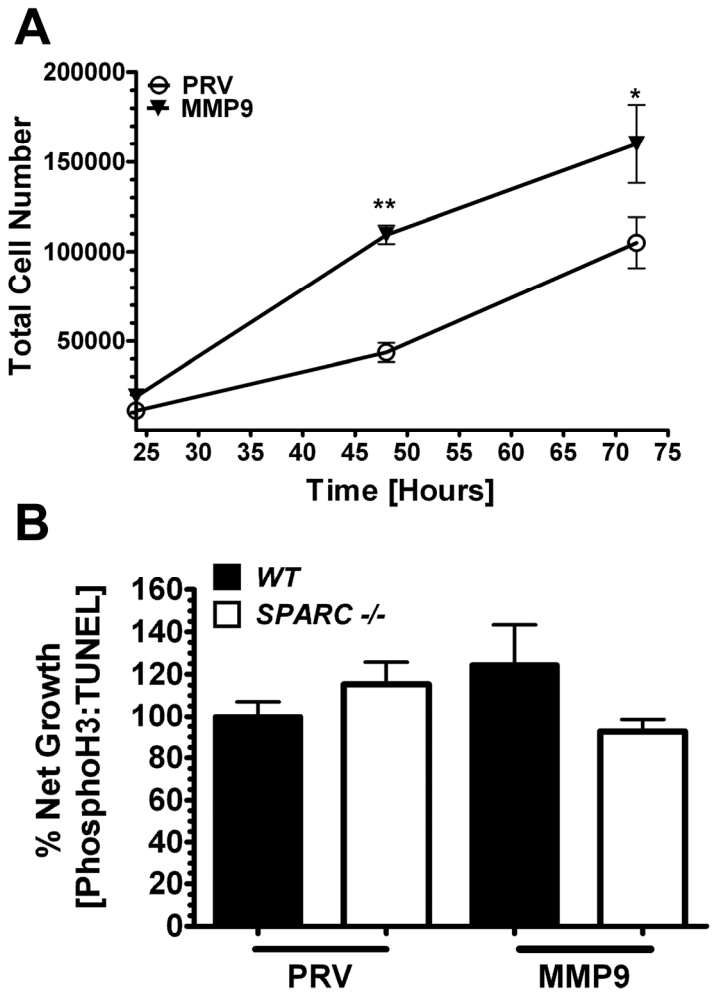

Figure 5. PAN02 proliferation and apoptosis *in vitro* and *in vivo*. A) *In vitro* proliferation of PAN02-PRV (PRV) and PAN02-MMP9 (MMP9) cells at 24, 48 and 72 hrs after seeding in DMEM containing 5% FBS. (*, $p<0.05$; **, $p<0.01$; two-way ANOVA with Bonferroni post-test) B) Net growth of tumors from PAN02-PRV (PRV) and PAN02-MMP9 (MMP9) cells grown in *WT* and *SPARC -/-* mice. Proliferating and apoptotic cells in tumor sections were counted by detecting nuclei positive for phosphorylated histone H3 (PhosphoH3) or terminal deoxynucleotidyl transferase mediated dUTP nick-end-labeling (TUNEL), respectively. The ratio of PhosphoH3 to TUNEL positive cells (% Net Growth) was calculated and normalized to PAN02-PRV (PRV) cells from *WT* mice. There was no significant difference between any groups (one-way ANOVA with Tukey's multiple comparison test)

Angiogenesis profile.

We examined the number and morphology of blood vessels in tumors by immunohistochemical identification of endothelial cells (MECA-32) and vascular basement membrane (collagen IV). For all of the analyses, we used Metamorph software to perform integrated morphometric analysis (IMA) of immunofluorescence images. Figure 6A shows an example of an image that has been rendered for morphometric analysis. The highlighted structures (green) are blood vessels that fulfill blood vessel specific parameters based on shape and size. In addition to improving accuracy, this method of analysis allows the measurement of pixel-based number, perimeter and area of antibody-bound blood vessels.

IMA analysis shows that PAN02-PRV tumors grown in *SPARC*$^{-/-}$ mice had significantly fewer MECA-32 positive vessels per high power field (hpf) compared to PAN02-PRV tumors grown in *WT* mice (Figure 6B) but there was no change in blood vessel size (Figure 6C). Unlike the PAN02-PRV tumors, the number of MECA-32 positive vessels/hpf was similar in PAN02-MMP9 tumors grown in *WT* and *SPARC*$^{-/-}$ mice (Figure 6B). Furthermore, the number of MECA-32 positive blood vessels was almost identical in PAN02-PRV and PAN02-MMP9 tumors grown in *WT* mice. Interestingly, MECA-32 positive blood vessels were significantly larger in PAN02-MMP9 tumors grown in *SPARC*$^{-/-}$ vs *WT* mice (Figure 6C). This is due to a decrease in the mean area/blood vessel in PAN02-MMP9 tumors grown in *WT* mice and is also reflected in the mean perimeter of the vessels (data not shown).

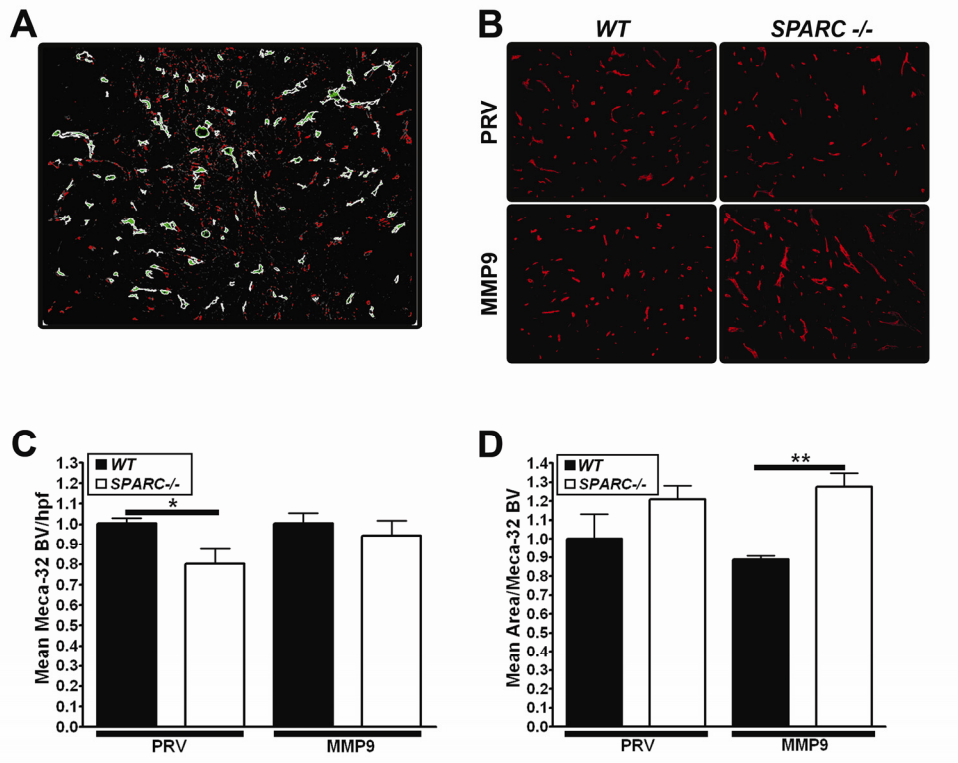

Figure 6. Analysis of angiogenesis in PAN02 tumors grown in *SPARC*$^{-/-}$ and *WT* mice. The number and size of blood vessels in tumors from PAN02-PRV (PRV) and PAN02-MMP9 (MMP9) cells were analyzed by immunohistochemistry of paraffin-embedded sections of tumors grown in *WT* or *SPARC*$^{-/-}$ mice. A) An example of integrated morphometric analysis (IMA) of immunofluorescence reactivity using MetaMorph software on Meca32 staining. An intensity and size threshold was set and maintained for every tumor section analyzed. Examples of objects meeting the size and intensity restrictions of blood vessels are shown in light green staining. B) MECA-32 immunofluorescence C) Mean blood vessel number/hpf and D) mean area/blood vessel were determined by IMA. C, D) Vascular parameters were normalized to PAN02-PRV tumors grown in *WT* mice to ease comparison between groups (*, $p<0.05$; **, $p<0.01$; one-way ANOVA with Tukey's multiple comparison test).

Collagen IV is a primary constituent of vascular basement membranes and a prominent substrate for MMP9. Figure 7 displays chromagen (DAB) immunohistochemistry for collagen IV in each tumor type. Immunohistochemical detection of collagen IV and IMA of fluorescent images in PAN02-PRV tumors showed a decrease in the number and size of collagen IV-positive blood vessels in tumors grown in *SPARC*$^{-/-}$ animals (Figure 7B, C).

The number of collagen IV-positive blood vessels decreased significantly in *WT* animals when PAN02 cells expressed MMP9 (Figure 7B). Interestingly, there was an increase, although not statistically significant, in the number of collagen IV-positive blood vessels in PAN02-MMP9 tumors grown in *SPARC*$^{-/-}$ animals (Figure 7B). Furthermore, the mean area/blood vessel as determined by collagen IV reactivity increased in PAN02-MMP9 compared to PAN02-PRV tumors grown in *SPARC*$^{-/-}$ mice (Figure 7C). Thus, forced expression of MMP9 by PAN02 tumor cells resulted in a decrease in the number of collagen IV-positive blood vessels in *WT* animals but an increase in the number (MECA-32 and collagen IV) and size (collagen IV) of blood vessels grown in the absence of SPARC.

Furthermore, collagen IV was almost exclusively found associated with the vascular basement membrane in PAN02-MMP9 tumors (Figure 7A and data not shown). In summary, analysis of the effect of host SPARC and MMP9 on vasculature in orthotopic pancreatic tumors demonstrates that MMP9 expression can rescue the lack of host-derived SPARC with respect to the number and size of blood vessels.

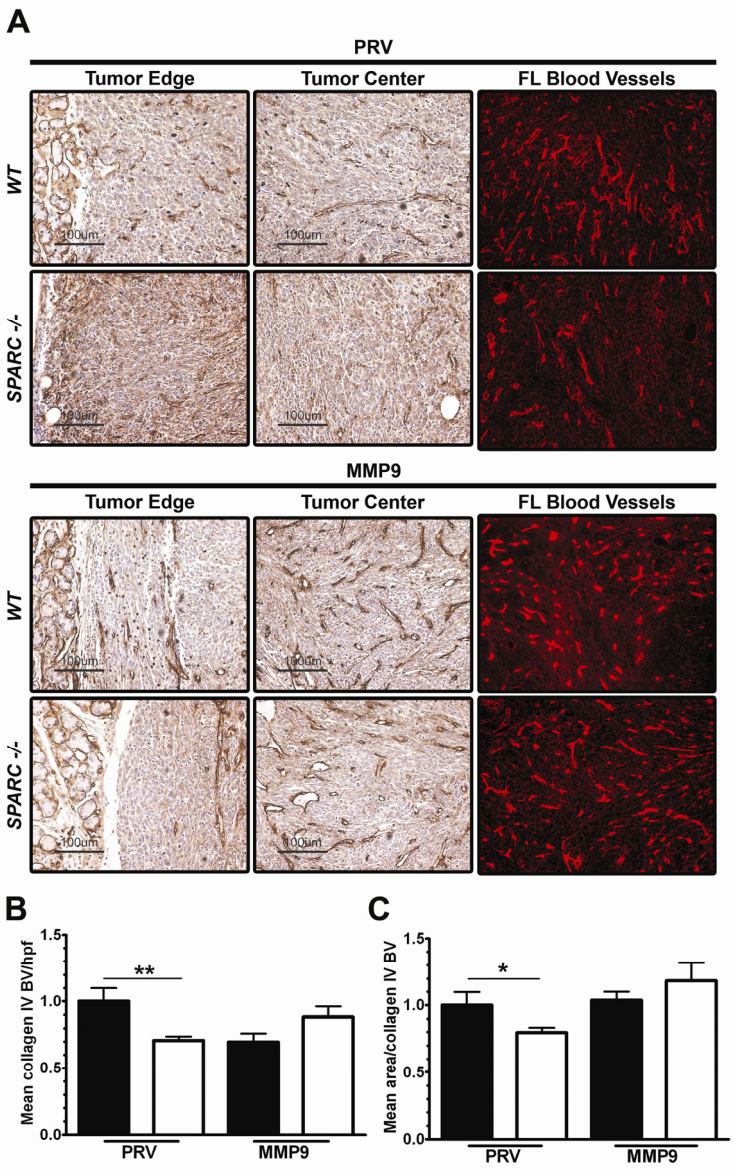

Figure 7. Collagen IV deposition in vascular basement membranes is altered by tumor cell expression of MMP9. A) The level and localization of collagen IV was determined immunohistochemically in PAN02-PRV (PRV) and PAN02-MMP9 (MMP9) tumors grown in *WT* and *SPARC*$^{-/-}$ mice. Collagen IV Immunofluorescent staining was evaluated by integrated morphometric analysis (IMA) for B) Mean blood vessel number/hpf and C) mean area/blood vessel. Total magnification of the fluorescent images is 200x. Vascular parameters were normalized to PAN02-PRV tumors grown in *WT* mice to ease comparison between groups (*, $p<0.05$; **, $p<0.01$; one-way ANOVA with Tukey's multiple comparison test).

Host SPARC is a dominant factor in tumor cell migration and metastasis.

Both SPARC and MMP9 have been shown to have effects on cell migration *in vitro* and *in vivo*. To better understand how each protein might effect cell migration of PAN02 cells, we first evaluated the migration of PAN02-PRV and PAN02-MMP9 cells in the presence and absence of SPARC in an *in vitro* cell migration assay. Forced expression of MMP9 conferred significantly increased cell migration in a transwell assay (Figure 8A). However, the addition of SPARC decreased cell migration by greater than 80% in each cell type (Figure 8A).

To better understand the function of MMP9 in PAN02 cell invasion we tested whether forced expression of MMP9 provides PAN02 cells with a selective advantage for metastasis. PAN02 cells were incubated on the top of a chick embryo chorioallantoic membrane (CAM) and intravasation was assessed by collection of the distal CAM followed by mouse specific PCR [24, 25]. Surprisingly, PAN02-MMP9 cells showed no increased intravasation compared to parental PAN02-PRV cells (Figure 8B). These results are in contrast to the *in vitro* migration assay (Figure 8A) and suggest that constitutive MMP9 activity alone does not confer greater metastatic capacity for these cells.

To validate these results, the incidence and total metastatic events was determined after orthotopic implantation of the tumor cells into *WT* and *SPARC*$^{-/-}$ mice (Table 1). The absence of host-derived SPARC increased the incidence of lymphatic metastasis but not the overall incidence of metastasis of PAN02-PRV tumors (Table 1). However, the total metastatic events were higher in *SPARC*$^{-/-}$ mice compared to their *WT*

counterparts (Table 1). Furthermore, there was an increase in tumor-related complications including bloody ascites and bowel obstructions in *SPARC*$^{-/-}$ mice bearing PAN02-PRV tumors. We anticipated that forced expression of MMP9 by PAN02 cells would result in increased tumor cell invasion and metastasis in *WT* and *SPARC*$^{-/-}$ mice. However, PAN02-MMP9 tumors showed a decrease in total number of metastatic events in *WT* and *SPARC*$^{-/-}$ animals compared to PAN02-PRV tumors. Although the PAN02-MMP9 tumors were large and locally invasive, distant metastases were limited.

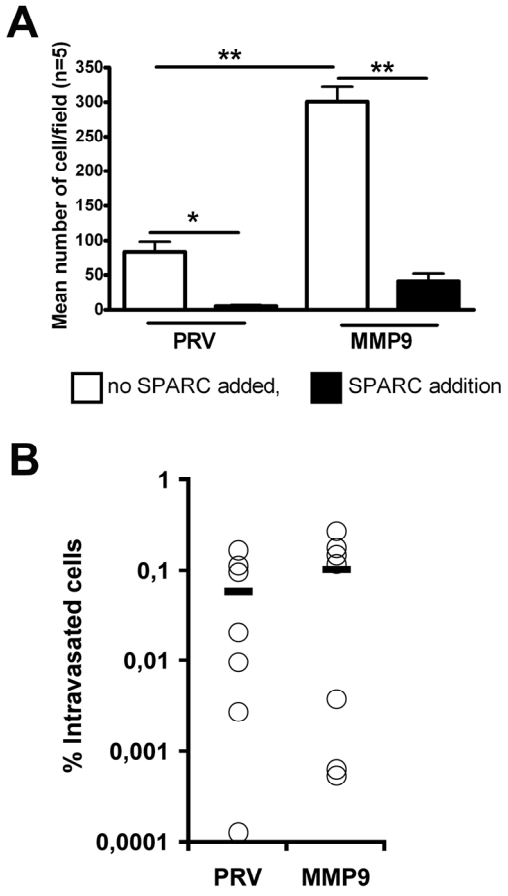

Figure 8. MMP9 expression confers increased PAN02 cell migration *in vitro* but not *in vivo*. A) PAN02-PRV (PRV) and PAN02-MMP9 (MMP9) cells in serum-free media were added to the top of an uncoated transwell insert. Serum-free media was added to the chamber below the insert. After 18 hours the inserts were removed, fixed, stained with hematoxylin, and the number of cells that migrated across the insert were counted. The mean +/- SEM number of cells/field (n=5/condition) is displayed. Addition of rSPARC (10 μg/ml) to the wells significantly decreased the number of cells that migrated (*, $p<0.05$; **, $p<0.01$). B) Cell invasion was evaluated by quantitative PCR of mouse DNA purified from CAM inoculated with PAN02 cells. Data represent the percentage of intravasated mouse cells in each sample. Mean value for PAN02-PRV and PAN02-MMP9 cells were 0.059 and 0.104 respectively. No significant differences in mean values were found (Mann-Whitney test). Panel B was performed by our collaborators in the Department of Immunology and Oncology, Centro Nacional de Biotecnología/CSIC, Universidad Autónoma de Madrid, Cantoblanco, E-28049 Madrid, Spain.

Table 1. Host SPARC regulates metastasis

		Metastatic Incidence (%)						Metastatic Events				
Genotype	**Cell Type**	**n=**	**Lymph**	**Peritoneal**	**Liver**	**Other**	**Total**	**Lymph**	**Peritoneal**	**Liver**	**Other**	**Total**
WT	PRV	6	16.7	66.7	16.7	0	66.7	1	10	1	0	12
SPARC $^{-/-}$	PRV	6	66.7	83.3	0	33.3	83.3	14	34 $^{at, bt}$	0	1	49 $^{at, bt}$
WT	MMP9	5	20.0	60.0	0	20.0	80.0	1	4	0	1	6
SPARC $^{-/-}$	MMP9	6	33.3	16.7	0	0	50.0	5	4	0	0	9

The influence of host SPARC and tumor-derived MMP9 on metastasis rate was evaluated after orthotopic implantation of pancreatic PAN02 tumors in *WT* and *SPARC*$^{-/-}$ mice. The total metastatic events and metastatic incidence in specific target organs was determined in one experiment at the time of sacrifice by visual inspection of each organ with a dissection scope under illumination with blue light to excite GFP in the tumor cells (n=number of animals in each group). Metastatic incidence is displayed as the percentage (%) of animals/group with a metastatic lesion in the target organ. The incidence of metastasis was compared between treatment groups were using a Tukey-type multiple comparison test for proportions (42). Statistical significance was set at 5%. Metastatic events are displayed as the total number of metastatic lesion in the target organ for the group. The number of metastatic events per mouse per organ was compared to median events per organ for the sample population using a Tukey-type multiple comparison test for medians (42). Trends ($p<0.10$) detected are indicated by ^{at}, vs. WT MMP9; ^{bt}, vs. SPARC MMP9.

Discussion

Pancreatic adenocarcinoma is the fourth leading cause of cancer-related death in the Western industrialized world, owing to rapid primary tumor growth and ensuing metastasis [26] (http://seer.cancer.gov). The metastatic cascade is dependent upon angiogenesis and cell migration, two processes that are regulated acutely by the local microenvironment [27-29]. Therefore, understanding the interaction of pancreatic tumor cells with stromal components is critical to developing improved therapeutic options for patients. We sought to determine if two proteins linked to the desmoplastic response of pancreatic cancer interact at a functional level in the progression of this disease. SPARC is a matricellular protein implicated in tumor growth [11] with an *in vivo* function in the desmoplastic response, characteristic of pancreatic cancer. MMP9 on the other hand is associated with ECM turnover and cell migration through the ECM.

Our results show for the first time that orthotopic pancreatic tumors grow larger and more aggressively in the absence of host SPARC. Furthermore, forced expression of MMP9 by tumor cells increases tumor size but does not increase metastasis in *WT* and *SPARC-/-* animals. We also identified that SPARC regulates MMP9 expression *in vivo* and that SPARC and MMP9 both impact ECM deposition and angiogenesis in the tumor microenvironment. We found that, in general, tumor size correlated inversely with collagen deposition and that the lack of SPARC or the increased expression of MMP9 resulted in reduced collagen.

The expression of SPARC in tumor tissue from patients with pancreatic cancer has been shown to correlate with a worse prognosis [30]. In particular, patients whose

tumor had fibroblasts that expressed SPARC by immunohistochemistry had a median survival of 15 months whereas patients whose tumor stroma did not express SPARC had a median survival of 30 months. The authors conclude that, after controlling for other prognostic factors, the relative hazard for patients with stromal expression of SPARC was 1.89 [30]. These studies support the idea that SPARC contributes to the progression of pancreatic cancer in humans, which is contrary to our results in SPARC-deficient animals. The reason(s) underlying this difference is unclear but might be due to the fact that the ECM of tumors from *SPARC*$^{-/-}$ animals is likely quite different from the ECM of human tumors from patients that have low or hard to detect SPARC protein. It is possible that defects inherent to the ECM of tumors grown in *SPARC*$^{-/-}$ mice are not replicated effectively by low or absent SPARC expression by stromal cells present in human tumors.

There are conflicting reports on whether SPARC is a substrate for MMP9. Sasaki et al. [31] found that MMP9 could cleave SPARC while Sage et al. [21] found that MMP3 but not MMP9 was the relevant MMP that mediated cleavage of SPARC. We did not determine if there was an increase in SPARC cleavage in PAN02-MMP9 tumors. It is possible however, to evaluate if SPARC is cleaved at L197 or L196 using neo-epitope specific antibodies [20], these studies are now in progress. Our results are however, consistent with previous studies [32-34] that have demonstrated that SPARC can increase the expression of MMPs.

Metastasis is the leading cause of death in pancreatic cancer patients. We provide evidence here that metastatic events occur more frequently in *SPARC*$^{-/-}$ versus *WT* animals. Since the initial steps in the metastatic cascade occur in the context of the ECM,

we hypothesize that the compromised ECM formed in the absence of host SPARC favors invasion and metastasis. SPARC expression by pancreatic tumors cells has been implicated in tumor cell migration *in vitro* and as a possible factor contributing to metastasis *in vivo* [35]. Our results suggest that an ECM formed in the absence of host SPARC can also facilitate metastasis. It is important to note that PAN02 cells produce SPARC. Therefore, we cannot exclude the possibility that tumor cell-derived SPARC contributes to metastatic spread in *WT* or *SPARC*$^{-/-}$ animals.

MMP9 expression is frequently associated with metastasis and is thought to facilitate tumor cell invasion [29]. However, results from this study supported by previous compelling reports suggest that the underlying mechanisms and the function of MMP9 in metastasis are more complex [36-38]. Our study demonstrates that orthotopic implantation of tumor cells forced to express MMP9 results in a decrease in metastatic burden compared to parental PAN02 tumor cells. Altogether, these results are in striking contrast to our own *in vitro* cell migration data and the generally perceived function of MMP9 as a promoter of metastasis but consistent with, Deryugina et al. [38] who showed that down-regulation of MMP9 in HT1080 cells resulted in increased intravasation and metastasis in the CAM.

These findings highlight the complex nature of MMP9 activity in the tumor microenvironment and might be partly explained by the paradigm that excess MMP9 expression inhibits tumor progression by generating endothelial cell inhibitors from both ECM and non-ECM sources, such as angiostatin and tumstatin [36, 39]. Thus, the outcome of MMP activity in the tumor microenvironment may be dependent on a variety of factors including ECM deposition, the presence of other proteases and cytokines, the

time, level, and site of MMP production, and the level and activity of adaptor proteins such as SPARC.

Materials and Methods

Tissue Culture.

The murine pancreatic adenocarcinoma cell line (PAN02) was purchased from the Developmental Therapeutics Program, Division of Cancer Treatment and Diagnosis, National Cancer Institute (Frederick, MD), and grown in Dulbecco's Modified Eagles Medium (DMEM; Invitrogen, Carlsbad, CA) supplemented with L-glutamine (2 mM), penicillin G (100 units/ml), streptomycin sulfate (100 µg/ml), and 5% fetal bovine serum (Life Technologies, Grand Island, NY). The PAN02 cell line was tested (Impact III PCR profiles; MU Research Animal Diagnostic Laboratory, Columbia, MO) and was found to be pathogen-free.

Recombinant MMP9 Chimeras and Cell Transduction.

MMP9 was subcloned into the bicistronic plasmid pRV-IRES-GFP to obtain a recombinant retrovirus that was used to transduce PAN02 cells [40]. Green fluorescent protein (GFP)-expressing cells were selected by fluorescence-activated cell sorting.

Cell Fractionation.

Transduced cells were disrupted with a 30-gauge needle in 50 mM Tris, pH 7.5 in the presence of protease inhibitors. After centrifugation at 800 x g (10 min, 4oC) to remove

nuclei, membrane and cytosolic fractions were obtained by centrifugation at 166,000 x g (1 h, 4oC). To verify the purity of the cell fractions, normalized protein amounts from each fraction were analyzed with anti-transferrin receptor (TfR; Zymed, San Francisco, CA) and anti-tubulin (Sigma, St. Louis, MO) by western blot. An anti-MMP9 polyclonal antibody (Calbiochem, San Diego, CA) and anti-SPARC antibody (R&D Systems, Minneapolis, MN) were employed to detect exogenous MMP9 and endogenous SPARC expression by Western blot analysis.

Immunocytochemistry.

Transduced PAN02 cells were plated on chamber slides (BD Biosciences, San Diego, CA) coated with collagen I or IV. Cells were fixed with 3.7% paraformaldehyde (15 min on ice) and afterwards incubated (1 h, 4oC) with a rabbit anti-MMP9 polyclonal antibody (Calbiochem) or mouse anti-SPARC monoclonal antibody (303) [41] followed by Cy3-labeled anti-rabbit or anti-mouse antibody respectively (Jackson ImmunoResearch, West Grove, PA; 1 h; 4oC). Slides were mounted with Vectashield (Vector Laboratories, Burlingame, CA) and analyzed by confocal laser microscopy (Leica).

MMP9 Activity Assay.

MMP9 activity was analyzed in cell extracts, serum samples and tumor extracts by gelatin zymography as described [42]. For in situ zymography, cells plated on collagen I were incubated with 40 μg/ml of FITC-gelatin (DQ-Gelatin, Molecular Probes, Eugene, OR) at 37oC. After 1 h of incubation, cells were washed with PBS, fixed with 1% paraformaldehyde, incubated for 10 min at room temperature with To-Pro3 (Invitrogen)

and analyzed by confocal laser microscopy. MMP9 activity of PAN02 cells over time was quantified by measuring the fluorescence released by cleavage of DQ-gelatin in multi-well format. Cells were incubated with 100 μg/ml of FITC-gelatin in 50 mM Tris, pH 7.4, 150 mM NaCl, 5 mM CaCl2 and 0.2 mM NaN3 for the indicated time (3, 5, 7, 22, or 27 hrs) at 37oC. Values represent the fluorescence increment after background subtraction.

Orthotopic Tumor Model.

SPARC-/- mice were generated as described previously [43]. The mice were housed in a pathogen-free facility and experiments were conducted under a protocol approved by the Institutional Animal Care and Use Committee of UT Southwestern Medical Center (Dallas, TX). For injections, PAN02 cells either expressing MMP9 or the empty vector were harvested from subconfluent cultures (>90% viable), washed once in serum-free medium and resuspended in Hank's balanced salt solution (HBSS). Orthotopic tumor cell injection was carried out as described previously [44]. Briefly, the mice were anesthetized with isoflurane and an incision was made in the left abdomen to expose the spleen and attached pancreas. Tumor cells (5x105 in 50 μl) were injected into the tail of the pancreas. Post-injection, mice were monitored for weight, signs of discomfort or morbidity and tumor size. Mice were euthanized thirty-five days after tumor cell injection and visually screened for extent of macroscopic tumor burden. The liver, entire gastrointestinal tract, lungs, mesentery, and other internal organs were visually inspected for the presence of surface metastases. Enlarged lymph nodes were counted and a subset

was surveyed by H&E histology to confirm tumor burden. The entire pancreas, containing the tumor, was harvested and weighed. Half of the tissue was snap-frozen in liquid nitrogen while the other half was fixed in methyl Carnoys, paraffin-embedded, sectioned and stained with H&E or Masson's trichrome (Molecular Histopathology Laboratory at UT Southwestern Medical Center, Dallas, TX). Two independent experiments with 6 mice/ group were performed.

Immunohistochemistry.

Tissue sections were deparaffinized in a series of xylene and ethanol washes, then rehydrated in PBSt (0.2% Tween-20). Primary antibodies used were rabbit anti-collagen I (LF67, provided by Dr. Larry Fisher, NIH/NIDCR Matrix Biology Unit) [45, 46], rabbit anti-collagen type IV (BD Biosciences), rabbit anti-phosphorylated histone H3 (phospho-H3, Upstate Biotechnology, Inc., Lake Placid, NY), rat anti-mouse Gr-1 (clone RB6-8C5, Biolegend, San Diego, CA), rabbit anti full length MMP9 (Millipore, Billerica, MA), and rat anti-mouse endothelial cell, MECA-32 (Developmental Studies Hybridoma Bank, University of Iowa, Iowa City, IA) [47]. For sections developed with diaminobenzidine (DAB) (Research Genetics, Huntsville, AL), endogenous peroxidases were blocked by incubating the samples in a 3% H2O2 /methanol solution. Sections were then washed in PBSt and blocked in 20% AquaBlock (East Coast Biologics, Inc., North Berwick, ME). Incubation with primary antibodies was performed overnight at 40C. Sections were washed in PBSt and incubated with peroxidase-conjugated secondary antibody for 1 h at room temperature. Lastly, sections were washed in PBSt, incubated with stable DAB for

5-20 minutes, counterstained with Meyer's Hematoxylin solution for 3 min and mounted in Permount (Fisher Scientific, Pittsburgh, PA). Alternatively, for fluorescence detection, following primary antibody incubation, sections were incubated for 1 h with fluorophore-conjugated (FITC or Cy3) secondary antibodies (Jackson Immunoresearch), washed in PBSt, and mounted with ProLong Gold antifade reagent with DAPI (Invitrogen).

Tissue sections were analyzed with a Nikon Eclipse E600 microscope (Nikon, Lewisville, TX). DAB images were captured with a Nikon Digital Dx1200me camera using Act1 software (Universal Imaging Corporation, Downington, PA) while fluorescence images were captured with a Photometric Coolsnap HQ camera and MetaMorph software (Universal Imaging Corporation). Phospho-H3 and TUNEL staining were quantified by manually counting the number of positive cells in five random 400X fields per tumor section. MECA-32 and collagen IV staining were processed, analyzed and quantified using MetaMorph software. Fluorescent images were captured under identical conditions (exposure time, high and low limits, and scaling). Images were thresholded to exclude background signal from secondary antibody alone. Mean blood vessel counts, blood vessel area and blood vessel perimeter were measured using MetaMorph's "Integrated Morphometry Analysis" (IMA).

In Vitro Proliferation Assay.

For the in vitro proliferation assay, PAN02 cells were plated at 27,000 cells per well in triplicate in a 24-well plate in DMEM containing 5% FBS. Cells were incubated at 37oC and counted at 24, 48 and 72 hrs after seeding. The total number of viable cells was determined by trypan blue exclusion and hand-counting cell density on a hemacytometer.

Migration Assay. The in vitro migration assays were performed using 8 μm transwell inserts formatted for 24 well tissue culture plates (Falcon). Wells were filled with 500 μl of serum-free DMEM +/- 10 μg rhSPARC. PAN02 cells (20,000 cells/well) were seeded onto the upper chamber of each transwell in serum-free DMEM. Cells were incubated at 37oC. After 24 h, cells were removed from the upper chamber and those cells that had migrated to the lower side of the membrane were fixed in 100% cold methanol and stained with hematoxylin (Sigma). The membranes were then cut from the transwell and mounted in crystal mount (Biomeda Corp. Foster City, CA). Cells were counted in five 100x fields on each membrane.

Intravasation Assay.

For intravasation assays, PAN02 cells (1 x 106) were inoculated into chorioallantoic membranes (CAM) of 9-day-old chick embryos [25, 38]. After 48 hrs incubation, CAMs were removed and total DNA isolated. The estimated percentage of intravasated cells was calculated by amplifying mouse B1 repeats in a quantitative real-time PCR [25]. Data represents the estimated percentage of intravasated cells in CAM samples compared with a standard curve made with known concentrations of mouse DNA.

Statistical Analyses.

Statistical analyses were performed using GraphPad Prism (GraphPad Software, San Diego, CA) with assistance from The Center for Biostatistics and Clinical Sciences (UT-Southwestern Medical Center, Dallas, TX). Analyses include Mann-Whitney test, Kruskal-Wallis with Dunn multiple comparison results, Student's t test, or one way

ANOVA with Tukey's multiple comparison test [48] where appropriate. Significance ($p<0.05$) was determined with 95% confidence.

Acknowledgements

We thank present and former members of the Brekken Laboratory of advice and suggestions. The hybridoma MECA-32, developed by Dr. Eugene C. Butcher, was obtained from the Developmental Studies Hybridoma Bank developed under the auspices of NICHD and maintained by The University of Iowa, Department of Biological Sciences (Iowa City, IA 52242). This study was supported in part by grants from The National Pancreas Foundation, The American Cancer Society, and the NIH (to RAB) as well as the Spanish Ministry of Science and Education (to S Mañes). RAB is the Effie Marie Cain Scholar in Angiogenesis Research.

References

1. Brekken, R.A. and E.H. Sage, *SPARC, a matricellular protein: at the crossroads of cell-matrix communication.* Matrix Biol, 2001. **19**(8): p. 816-27.

2. Bornstein, P., *Cell-matrix interactions: the view from the outside.* Methods Cell Biol, 2002. **69**: p. 7-11.

3. Lane, T.F. and E.H. Sage, *The biology of SPARC, a protein that modulates cell-matrix interactions.* Faseb J, 1994. **8**(2): p. 163-73.

4. Liaw, L. and H.C. Crawford, *Functions of the extracellular matrix and matrix degrading proteases during tumor progression.* Braz J Med Biol Res, 1999. **32**(7): p. 805-12.

5. Motamed, K. and E.H. Sage, *Regulation of vascular morphogenesis by the matricellular protein SPARC.* Kidney Int, 1997. **51**(5): p. 1383-7.

6. Forget, M.A., R.R. Desrosiers, and R. Beliveau, *Physiological roles of matrix metalloproteinases: implications for tumor growth and metastasis.* Can J Physiol Pharmacol, 1999. **77**(7): p. 465-80.

7. Himelstein, B.P., et al., *Metalloproteinases in tumor progression: the contribution of MMP-9.* Invasion Metastasis, 1994. **14**(1-6): p. 246-58.

8. Bergers, G., et al., *Matrix metalloproteinase-9 triggers the angiogenic switch during carcinogenesis.* Nat Cell Biol, 2000. **2**(10): p. 737-44.

9. Lynch, C.C. and L.M. Matrisian, *Matrix metalloproteinases in tumor-host cell communication.* Differentiation, 2002. **70**(9-10): p. 561-73.

10. Chantrain, C.F., et al., *Stromal matrix metalloproteinase-9 regulates the vascular architecture in neuroblastoma by promoting pericyte recruitment.* Cancer Res, 2004. **64**(5): p. 1675-86.

11. Framson, P.E. and E.H. Sage, *SPARC and tumor growth: where the seed meets the soil?* J Cell Biochem, 2004. **92**(4): p. 679-90.

12. Mok, S.C., et al., *SPARC, an extracellular matrix protein with tumor-suppressing activity in human ovarian epithelial cells.* Oncogene, 1996. **12**(9): p. 1895-901.

13. Brown, T.J., et al., *Activation of SPARC expression in reactive stroma associated with human epithelial ovarian cancer.* Gynecol Oncol, 1999. **75**(1): p. 25-33.

14. Sato, N., et al., *SPARC/osteonectin is a frequent target for aberrant methylation in pancreatic adenocarcinoma and a mediator of tumor-stromal interactions.* Oncogene, 2003. **22**(32): p. 5021-30.

15. Koukourakis, M.I., et al., *Enhanced expression of SPARC/osteonectin in the tumor-associated stroma of non-small cell lung cancer is correlated with markers of hypoxia/acidity and with poor prognosis of patients.* Cancer Res, 2003. **63**(17): p. 5376-80.

16. Puolakkainen, P.A., et al., *Enhanced growth of pancreatic tumors in SPARC-null mice is associated with decreased deposition of extracellular matrix and reduced tumor cell apoptosis.* Mol Cancer Res, 2004. **2**(4): p. 215-24.

17. Brekken, R.A., et al., *Enhanced growth of tumors in SPARC null mice is associated with changes in the ECM.* J Clin Invest, 2003. **111**(4): p. 487-95.

18. Chen, J.J., et al., *Tumor-associated macrophages: the double-edged sword in cancer progression.* J Clin Oncol, 2005. **23**(5): p. 953-64.

19. Sasaki, T., et al., *Crystal structure and mapping by site-directed mutagenesis of the collagen-binding epitope of an activated form of BM- 40/SPARC/osteonectin.* Embo J, 1998. **17**(6): p. 1625-34.

20. Sasaki, T., N. Miosge, and R. Timpl, *Immunochemical and tissue analysis of protease generated neoepitopes of BM-40 (osteonectin, SPARC) which are correlated to a higher affinity binding to collagens.* Matrix Biol, 1999. **18**(5): p. 499-508.

21. Sage, E.H., et al., *Cleavage of the matricellular protein SPARC by matrix metalloproteinase 3 produces polypeptides that influence angiogenesis.* J Biol Chem, 2003. **278**(39): p. 37849-57.

22. Nozawa, H., C. Chiu, and D. Hanahan, *Infiltrating neutrophils mediate the initial angiogenic switch in a mouse model of multistage carcinogenesis.* Proc Natl Acad Sci U S A, 2006. **103**(33): p. 12493-8.

23. van Hinsbergh, V.W., M.A. Engelse, and P.H. Quax, *Pericellular proteases in angiogenesis and vasculogenesis.* Arterioscler Thromb Vasc Biol, 2006. **26**(4): p. 716-28.

24. Kim, J., et al., *Requirement for specific proteases in cancer cell intravasation as revealed by a novel semiquantitative PCR-based assay.* Cell, 1998. **94**(3): p. 353-62.

25. Mira, E., et al., *Quantitative determination of tumor cell intravasation in a real-time polymerase chain reaction-based assay.* Clin Exp Metastasis, 2002. **19**(4): p. 313-8.

26. Li, D., et al., *Pancreatic cancer.* Lancet, 2004. **363**(9414): p. 1049-57.

27. Bogenrieder, T. and M. Herlyn, *Axis of evil: molecular mechanisms of cancer metastasis.* Oncogene, 2003. **22**(42): p. 6524-36.

28. Raghunand, N., R.A. Gatenby, and R.J. Gillies, *Microenvironmental and cellular consequences of altered blood flow in tumours.* Br J Radiol, 2003. **76 Spec No 1**: p. S11-22.

29. Ludwig, T., *Local proteolytic activity in tumor cell invasion and metastasis.* Bioessays, 2005. **27**(11): p. 1181-91.

30. Infante, J.R., et al., *Peritumoral fibroblast SPARC expression and patient outcome with resectable pancreatic adenocarcinoma.* J Clin Oncol, 2007. **25**(3): p. 319-25.

31. Sasaki, T., et al., *Limited cleavage of extracellular matrix protein BM-40 by matrix metalloproteinases increases its affinity for collagens.* J Biol Chem, 1997. **272**(14): p. 9237-43.

32. McClung, H.M., et al., *SPARC upregulates MT1-MMP expression, MMP-2 activation, and the secretion and cleavage of galectin-3 in U87MG glioma cells.* Neurosci Lett, 2007. **419**(2): p. 172-7.

33. Gilles, C., et al., *SPARC/osteonectin induces matrix metalloproteinase 2 activation in human breast cancer cell lines.* Cancer Res, 1998. **58**(23): p. 5529-36.

34. Fujita, T., et al., *SPARC stimulates the synthesis of OPG/OCIF, MMP-2 and DNA in human periodontal ligament cells.* J Oral Pathol Med, 2002. **31**(6): p. 345-52.

35. Guweidhi, A., et al., *Osteonectin influences growth and invasion of pancreatic cancer cells.* Ann Surg, 2005. **242**(2): p. 224-34.

36. Pozzi, A., W.F. LeVine, and H.A. Gardner, *Low plasma levels of matrix metalloproteinase 9 permit increased tumor angiogenesis.* Oncogene, 2002. **21**(2): p. 272-81.

37. Chen, X., et al., *Increased plasma MMP9 in integrin alpha1-null mice enhances lung metastasis of colon carcinoma cells.* Int J Cancer, 2005. **116**(1): p. 52-61.

38. Deryugina, E.I., et al., *Unexpected effect of matrix metalloproteinase down-regulation on vascular intravasation and metastasis of human fibrosarcoma cells selected in vivo for high rates of dissemination.* Cancer Res, 2005. **65**(23): p. 10959-69.

39. Hamano, Y., et al., *Physiological levels of tumstatin, a fragment of collagen IV [alpha]3 chain, are generated by MMP-9 proteolysis and suppress angiogenesis via [alpha]V[beta]3 integrin.* Cancer Cell, 2003. **3**(6): p. 589-601.

40. Mira, E., et al., *A role for chemokine receptor transactivation in growth factor signaling.* EMBO Rep, 2001. **2**(2): p. 151-6.

41. Sweetwyne, M.T., et al., *Functional analysis of the matricellular protein SPARC with novel monoclonal antibodies.* J Histochem Cytochem, 2004. **52**(6): p. 723-33.

42. Quesada, A.R., et al., *Evaluation of fluorometric and zymographic methods as activity assays for stromelysins and gelatinases.* Clin Exp Metastasis, 1997. **15**(1): p. 26-32.

43. Norose, K., et al., *SPARC deficiency leads to early-onset cataractogenesis.* Invest Ophthalmol Vis Sci, 1998. **39**(13): p. 2674-80.

44. Bruns, C.J., et al., *In vivo selection and characterization of metastatic variants from human pancreatic adenocarcinoma by using orthotopic implantation in nude mice.* Neoplasia, 1999. **1**(1): p. 50-62.

45. Bernstein, E.F., et al., *Long-term sun exposure alters the collagen of the papillary dermis. Comparison of sun-protected and photoaged skin by northern analysis, immunohistochemical staining, and confocal laser scanning microscopy.* J Am Acad Dermatol, 1996. **34**(2 Pt 1): p. 209-18.

46. Bernstein, E.F., et al., *Differential expression of the versican and decorin genes in photoaged and sun-protected skin. Comparison by immunohistochemical and northern analyses.* Lab Invest, 1995. **72**(6): p. 662-9.

47. Hallmann, R., et al., *Novel mouse endothelial cell surface marker is suppressed during differentiation of the blood brain barrier.* Dev Dyn, 1995. **202**(4): p. 325-32.

48. Zar, J.H., *Biostatistical Analysis*. Fourth ed. 1999.

CHAPTER THREE

Lack of Host SPARC Enhances Vascular Function and Tumor Spread in an Orthotopic Murine Model of Pancreatic Carcinoma

Shanna A. Arnold[1], Lee B. Rivera[1], Andrew F. Miller[1], Juliet G. Carbon[1], Sean P. Dineen[1], Yang Xie[2], Diego H. Castrillon[3], E. Helene Sage[4], Pauli Puolakkainen[5,6], Amy D. Bradshaw[7] and Rolf A. Brekken[1*]

[1]Hamon Center for Therapeutic Oncology Research, Departments of Surgery and Pharmacology, University of Texas Southwestern Medical Center, Dallas, TX 75390 USA
[2]Center for Biostatistics and Clinical Sciences, University of Texas Southwestern Medical Center, Dallas, TX 75390 USA
[3]Department of Pathology, University of Texas Southwestern Medical Center, Dallas, TX 75390 USA
[4]Hope Heart Program, Benaroya Research Institute at Virginia Mason, Seattle, WA 98101 USA [5]Department of Surgery, Helsinki University Central Hospital, Turku, Finland
[6]Department of Surgery, Turku University Central Hospital, Helsinki, Finland
[7]Department of Medicine, Medical University of South Carolina, Charleston, SC 29412.

*Corresponding author:
Rolf A. Brekken, PhD
Hamon Center for Therapeutic Oncology Research
UT-Southwestern Medical Center
6000 Harry Hines Blvd.
Dallas, TX 75390-8593
Tel: 214 648 5151 Fax: 214 648 4940
e-mail: rolf.brekken@utsouthwestern.edu

Running header 'Lack of host SPARC enhances tumor spread'

Supported in part by The Effie Marie Cain Scholarship in Angiogenesis Research (to RAB) and the NIH (R01CA118240 to RAB & R01GM40711 to EHS). SA was supported in part by a training grant from the NIH (GM007062). DC was supported by the NIH/NCRR grant (K26RR024196). PP was supported by Helsinki and Turku University Central Hospital Research grants (EVO) and a grant from Sigrid Juselius Foundation.

Abstract

Utilizing subcutaneous tumor models, we previously validated SPARC as a key component of the stromal response, where it regulated tumor size, angiogenesis and extracellular matrix deposition. In the present study, we demonstrate that pancreatic tumors grown orthotopically in *Sparc-null* (*Sparc*$^{-/-}$) mice are more metastatic than tumors grown in *wild-type* (*Sparc*$^{+/+}$) littermates. Tumors grown in *Sparc*$^{-/-}$ mice display reduced deposition of fibrillar collagens I and III, basement membrane collagen IV and the collagen-associated proteoglycan decorin. In addition, microvessel density and pericyte recruitment are reduced in tumors grown in the absence of host SPARC. However, tumors from *Sparc*$^{-/-}$ mice display increased permeability and perfusion and a subsequent decrease in hypoxia. Finally, we found that tumors grown in the absence of host SPARC exhibit an increase in alternatively activated macrophages. These results suggest that increased tumor burden in the absence of host SPARC is a consequence of reduced collagen deposition, disrupted vascular basement membrane, enhanced vascular function and an immune-tolerant, pro-metastatic microenvironment.

Key words: alternatively activated macrophage; angiogenesis; extracellular matrix; matricellular; osteonectin; pancreatic cancer; SPARC; vascular permeability

Introduction

Pancreatic cancer is the fourth leading cause of cancer-related death in the United States and little improvement has been seen over the last twenty years in the 5-yr survival rate, which remains at 5% (SEER). Historically, studies have focused on cell-autonomous behavior or the molecular biology of cancer cells. However, focus is shifting to the interaction of cancer cells with their microenvironment. In particular, desmoplasia or stromal response is prominent in pancreatic adenocarcinoma [1]. Cross-talk between malignant epithelial cells and the stromal compartment can promote extracellular matrix (ECM) remodeling, angiogenesis, immune cell recruitment and metastasis [2-5].

Matricellular proteins are a functional family of extracellular proteins involved in the regulation of ECM deposition and remodeling. Although primarily non-structural, they define and contribute to the structural integrity and composition of the ECM. A dominant feature of matricellular proteins is the capacity to influence ECM assembly and turn-over, a function typified by their expression at sites of tissue remodeling and increased synthesis during wound-healing [6, 7]. In addition, by functioning as adaptors between the ECM and the cell surface, matricellular proteins can direct cell fate, survival, adhesion and motility [6-8].

SPARC (secreted protein acidic and rich in cysteine), also known as osteonectin and BM-40, is a multifunctional glycoprotein that exemplifies the matricellular class of proteins [9]. SPARC expression is limited post-development to tissues with high ECM turnover, such as bone and gut [10]. Moreover, increased production of SPARC has been shown in wound-healing, at sites of angiogenesis and during tumor progression [10-14]. Mice lacking SPARC exhibit early cataractogenesis, lax skin, progressive osteopenia and

a characteristic curly tail reminiscent of ECM defects [9]. Indeed, collagen deposition and fiber assembly was found to be altered in the lens capsule and dermis of *Sparc-null* (*Sparc*$^{-/-}$) mice [15, 16]. Furthermore, SPARC binds directly to fibrillar collagens I, III and V, and to basement membrane collagen IV [17-19]. These data support the claim that SPARC functions as a mediator of tissue remodeling. *In vitro*, SPARC has been shown to induce cell rounding, or a semi-adhesive state, by disrupting focal adhesions [17, 20]. SPARC regulates the interaction of ECM structural proteins with cell surface receptors such as integrins. In fact, SPARC was recently reported to bind integrin beta 1 [21, 22]. SPARC also interacts with or indirectly regulates a variety of growth factors including fibroblast growth factor (FGF), vascular endothelial growth factor (VEGF), platelet-derived growth factor and transforming growth factor β [23-26].

By directing ECM deposition, cell-ECM interactions and growth factor signaling, SPARC would be predicted to regulate several aspects of tumorigenesis including angiogenesis, migration, proliferation and survival. Not surprisingly, many cancers exhibit altered SPARC expression. Several cancers including glioma, melanoma, tongue and oral, head and neck, esophageal and breast show increased levels of SPARC relative to that of their respective normal tissue that positively correlates with invasion and metastasis [9, 27-30]. Conversely, loss of SPARC in colorectal cancer is correlated with a worse prognosis [31, 32]. In this regard, SPARC also functions as a tumor suppressor in ovarian carcinoma [33]. Loss of SPARC expression due to promoter hypermethylation has been reported in pancreatic, cervical, colorectal and prostate cancers [31, 32, 34-38]. In pancreatic cancer, paradoxical compartmentalization of SPARC expression is observed; whereby, 52% of tumors display strong SPARC expression in the tumor-

associated stroma, but lack SPARC expression in the malignant epithelial cells [39]. This contradictory compartmentalized expression pattern of SPARC is also seen in lung and endometrial cancers [40, 41]. Moreover, positive stromal SPARC expression is associated with decreased survival of patients with pancreatic ductal adenocarcinoma, regardless of tumor-derived SPARC production [39]. Therefore, the effect of SPARC on tumor growth and metastasis is both tumor-type dependent and context dependent. In other words, the source or location of SPARC in the tumor microenvironment contributes to the complexity of how SPARC influences tumor progression.

We have demonstrated previously that growth of subcutaneous tumors is augmented significantly in the absence of host-derived SPARC [42, 43]. Furthermore, tumors grown in *Sparc*$^{-/-}$ animals exhibit a diminished deposition of ECM compared to those grown in *wild-type* (*Sparc*$^{+/+}$) counterparts [42, 43]. These findings indicate that SPARC governs stromal response to tumorigenesis and thereby regulates tumor progression. In the current study, to further assess the function of stromal-derived SPARC in pancreatic tumor growth and metastasis, we have utilized an orthotopic model of pancreatic cancer in which the murine pancreatic adenocarcinoma cell line, PAN02, is injected directly into the pancreas of *Sparc*$^{+/+}$ and *Sparc*$^{-/-}$ mice. We now report that *Sparc*$^{-/-}$ mice exhibited a significant increase in metastasis compared to *Sparc*$^{+/+}$ controls. In addition, tumors grown in the absence of host-derived SPARC showed a marked reduction in the deposition of fibrillar collagens I and III, basement membrane collagen IV and the collagen-associated proteoglycan decorin. Surprisingly, although the tumors grown in *Sparc*$^{-/-}$ mice were more invasive, they displayed a significant decrease in microvessel density (MVD) and pericyte recruitment. Alterations in the vascular

basement membrane led to enhanced vascular permeability and perfusion, as well as, a subsequent decrease in hypoxia in tumors established in the absence of host-derived SPARC. Finally, we found that tumors grown in *Sparc*$^{-/-}$ mice demonstrated increased fibroblast recruitment and increased activation of alternatively activated (M2) macrophages. These results validate the function of stromal-derived SPARC in angiogenesis, metastasis and immune response during tumor development.

Results

Tumors are More Invasive and Metastatic in the Absence of Host SPARC.

We characterized the function of stromal-derived SPARC in tumor growth and metastasis by utilizing an orthotopic model of pancreatic cancer. Tumors were established by injecting the murine pancreatic adenocarcinoma cell line, PAN02, directly into the pancreas of *wild-type* (*Sparc*$^{+/+}$) and *Sparc*$^{-/-}$ mice. Previously, we showed that both subcutaneous and orthotopic PAN02 tumors grew larger in *Sparc*$^{-/-}$ mice compared to *Sparc*$^{+/+}$ controls [43, 44]. In the preceding orthotopic PAN02 study, animals were sacrificed at an endpoint pre-determined to have solid tumor growth and regardless of animal morbidity (~4 weeks). In the current study, orthotopic tumors were allowed to grow for an extended time, until a majority of the mice appeared moribund to permit the study of metastatic progression and expansion of secondary tumors (6-8 weeks). The results revealed that, although final primary tumor weight at this later time point was not significantly different (data not shown), tumors grown in *Sparc*$^{-/-}$ mice were more locally invasive than those in *Sparc*$^{+/+}$ counterparts (Figure 1A,B). In *Sparc*$^{+/+}$ mice, tumors were solid with well-defined, encapsulated borders and preserved significant residual

pancreas (Figure 1A, 5X). However, tumors grown in the absence of host SPARC were malleable with little encapsulation and revealed sparse pancreatic tissue (Figure 1A, 5X). Tumors grown in *Sparc*$^{-/-}$ mice had more irregular margins than those grown in *Sparc*$^{+/+}$ mice and were characterized by invasive finger-like projections into adjacent structures leading to greater tissue destruction and enhanced local invasion (Figure 1A,B 100X).

In *Sparc*$^{+/+}$ and *Sparc*$^{-/-}$ mice, PAN02 tumors invaded adjacent tissues such as the spleen, adipose, abdominal muscle, intestine and stomach (Figure 1C, spleen, muscle, adipose). Orthotopic PAN02 tumors also exhibited macroscopic metastasis to peritoneal organs including the liver, mesenteric lymph nodes, peritoneal wall and diaphragm (Figure 1C, liver). Therefore, we counted both adjacent tissue invasion and distant organ dissemination as metastatic events. Although *Sparc*$^{+/+}$ and *Sparc*$^{-/-}$ mice had similar metastatic incidence, total tumor burden was increased significantly in *Sparc*$^{-/-}$ mice (Table 1, $p<0.0001$). Most striking was the increase in metastasis to the liver, where *Sparc*$^{-/-}$ mice displayed ten times the number of events as *Sparc*$^{+/+}$ counterparts (Table 1, $p<0.0001$). Accelerated tumor progression in the absence of host SPARC was highlighted by a survival study that revealed that *Sparc*$^{-/-}$ mice bearing orthotopic PAN02 tumors had significantly reduced survival compared to *Sparc*$^{+/+}$ controls with a median survival of 28 days versus 36 days, respectively (Figure 1D, $p<0.018$). These data indicated that tumors were more invasive and metastatic in the absence of host SPARC. However, acceleration of tumor progression was not due to changes in proliferation or apoptosis of PAN02 cells [44]. Therefore, we aimed to characterize angiogenesis and the composition of the ECM in PAN02 tumors to delineate a mechanism by which the absence of host SPARC augments invasion and metastasis.

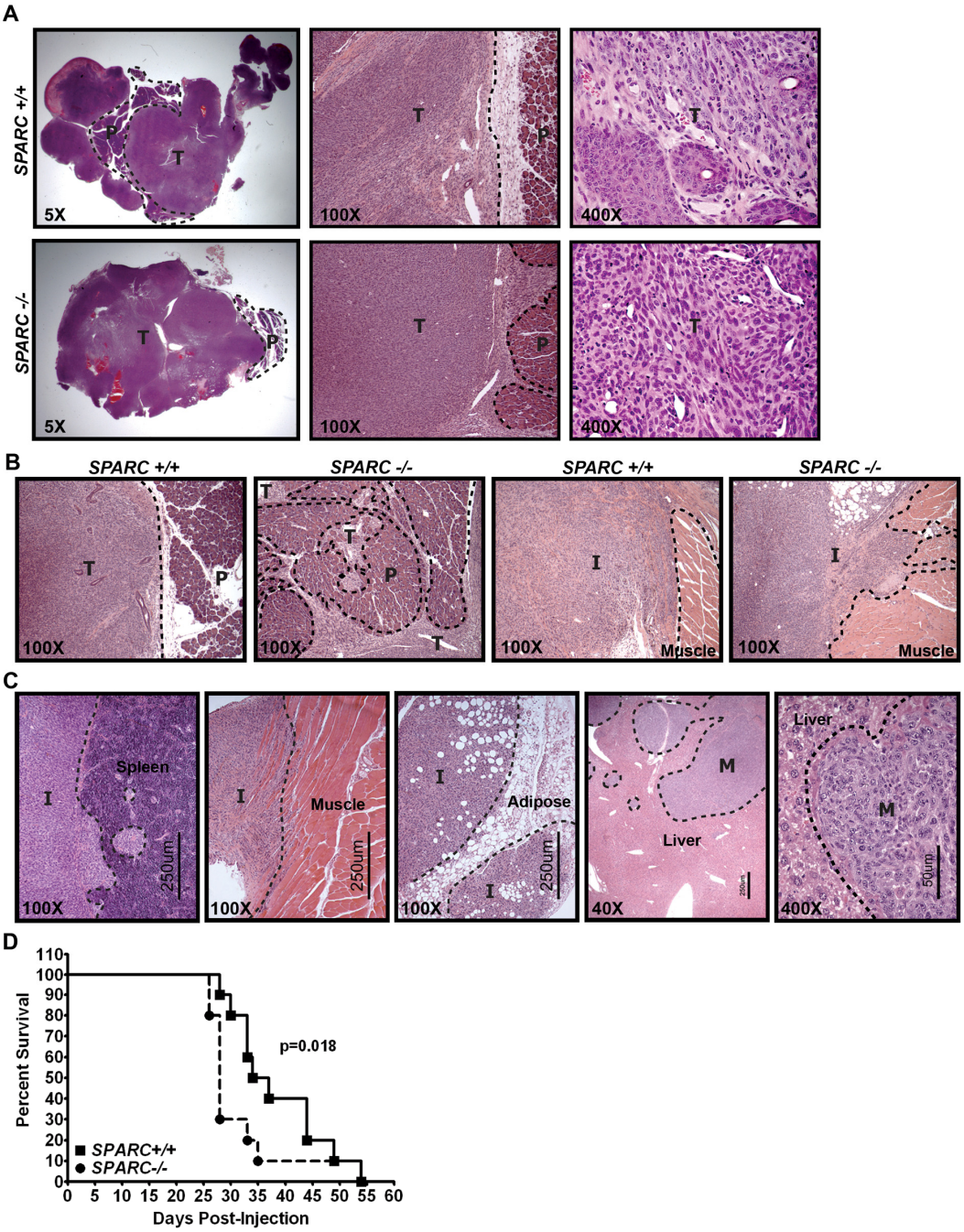

Figure 1. Orthotopic Tumor Local Invasion and Metastasis. 1x10^6 PAN02 cells were injected into the tail of the pancreas of *Sparc*$^{+/+}$ and *Sparc*$^{-/-}$ mice. Tumors were allowed to grow for 6-8 weeks. (A-C) H&E stained tissue sections reveal the invasive nature of

tumor growth in *Sparc*$^{-/-}$ mice. Dotted lines demarcate normal pancreas (P) and adjacent tissue from primary tumor (T), invasive lesions (I) or metastatic lesions (M). Total magnification and/or scale bars (50 and 250 μm) are shown. (A) Low (5X) magnification images of primary tumor sections show residual pancreas, medium (100X) magnification images show the primary tumor border, and high (400X) magnification images show tumor cell morphology in *Sparc*$^{+/+}$ compared to *Sparc*$^{-/-}$ mice. (B) Images reveal the finger-like invasion of tumors grown in the absence of host SPARC at both the primary pancreatic site (P) and into adjacent tissue (muscle) in direct contrast to the well-defined borders of tumors grown in *Sparc*$^{+/+}$ controls. (C) Images display PAN02 local invasion into the spleen, abdominal muscle and visceral fat (adipose), as well as, metastasis (M) to the liver. (D) Survival curve of *Sparc*$^{+/+}$ and *Sparc*$^{-/-}$ mice challenged with orthotopic PAN02 tumors. (n=10/group; p=0.018; Gehan-Breslow-Wilcoxon Test).

Table 1. Metastatic Incidence and Events

Metastatic Incidence							
Genotype	**n=**	**Lymph**	**Spleen**	**Perit.**	**Liver**	**Other**	**Total**
***SPARC* +/+**	52	1 (2%)	13 (25%)	13 (25%)	4 (8%)	25 (48%)	37 (71%)
***SPARC* -/-**	49	8 (16%)	17 (35%)	19 (39%)	6 (12%)	29 (59%)	39 (80%)
p-value		**0.034**	**0.186**	**0.139**	**0.448**	**0.264**	**0.328**
Metastatic Events							
Genotype	**n=**	**Lymph**	**Spleen**	**Perit.**	**Liver**	**Other**	**Total**
***SPARC* +/+**	52	1	37	17	4	145	204
***SPARC* -/-**	49	24	48	33	40	183	326
p-value		**0.0015**	**0.0816**	**0.0155**	**<0.0001**	**0.0086**	**<0.0001**

Metastatic incidences were recorded as the number of mice bearing metastasis in each organ. Metastatic incidence rates (%) were calculated by dividing the metastatic incidence by the total number of mice in the group. Statistical analyses of the metastatic incidence rates compared *Sparc*$^{+/+}$ to *Sparc*$^{-/-}$ groups by the logistic regression model, assuming a binomial distribution. Metastatic events were recorded as the total number of individual metastases in each organ. Statistical analyses of metastatic events were calculated with a Poisson regression model, assuming a Poisson distribution. Metastatic events in different organs were treated as independent.

Angiogenesis is Diminished in Tumors Grown in Sparc-null Mice.

We analyzed microvessel density (MVD) and endothelial cell-pericyte association by immunohistochemistry. Quantifying MVD with three vascular markers confirmed that tumors grown in *Sparc*$^{-/-}$ mice displayed decreased angiogenesis relative to tumors grown in *Sparc*$^{+/+}$ controls (Figure 2A-C). Meca-32, a panvascular marker, showed a significant reduction in the number of blood vessels per field in tumors collected from *Sparc*$^{-/-}$ mice compared to *Sparc*$^{+/+}$ littermates (Figure 2A, $p<0.05$). Immunohistochemistry for the detection of endomucin also revealed a significant reduction in MVD in tumors grown in the absence of host SPARC, as measured by percent thresholded area (Figure 2C, $p<0.05$). Endomucin is a sialomucin that is expressed by proliferating endothelial cells, especially those stimulated by tumor conditioned media, and is found constitutively on venous and capillary, but not arterial endothelium [45, 46]. Finally, CD31 (Pecam-1) staining showed reduced vascularity in tumors grown in *Sparc*$^{-/-}$ mice compared to *Sparc*$^{+/+}$ controls, although the difference did not reach statistical significance (Figure 2B).

In addition to angiogenesis, we also characterized the extent of pericyte association of blood vessels within the tumors. We colocalized the aforementioned vascular markers with markers of smooth muscle cells/ pericytes (Figure 2A&B). Quantification of Meca-32 colocalized with smooth muscle actin (SMA) demonstrated that blood vessel maturity is compromised in tumors grown in *Sparc*$^{-/-}$ mice relative to *Sparc*$^{+/+}$ counterparts (Figure 2A, $p<0.01$). In addition, colocalization of CD31 with NG2 chondroitin sulfate validated that tumors grown in the absence of host SPARC exhibit reduced pericyte recruitment (Figure 2B, $p<0.05$).

Finally, the decrease in MVD and pericyte recruitment in tumors grown in *Sparc*$^{-/-}$ mice is not a result of decreased levels of vascular endothelial growth factor receptor 2 (VEGFR2), nor to a deficiency in vascular endothelial growth factor signaling (Figure 2D). The amount of VEGFR2 on vascular endothelium was assessed by immunohistochemistry with the rat monoclonal antibody RAFL-2 [47]. Surprisingly, quantification of RAFL-2 revealed that tumors grown in the absence of host SPARC have significantly increased levels of VEGFR2 (Figure 2D, $p<0.001$). Therefore, in the absence of host-derived SPARC, tumor vascular endothelium showed elevated expression of VEGFR2; however this did not correspond to increased MVD. In addition, staining with an antibody that specifically recognizes VEGF bound to a cognate receptor (Gv39M) indicated that the reduction in angiogenesis in *Sparc*$^{-/-}$ mice during tumorigenesis was not caused by a loss of VEGF binding to its receptors (Figure 2D) [48]. This is displayed as both total Gv39M (VEGF:VEGFR) staining and the ratio of activated vasculature, Gv39M colocalized to RAFL-2, to total vasculature, total RAFL-2 (Figure 2D, Active/Total). In either case, there was no difference in the amount of activated VEGFR2 on the vasculature of tumors grown in *Sparc*$^{-/-}$ compared to *Sparc*$^{+/+}$ mice.

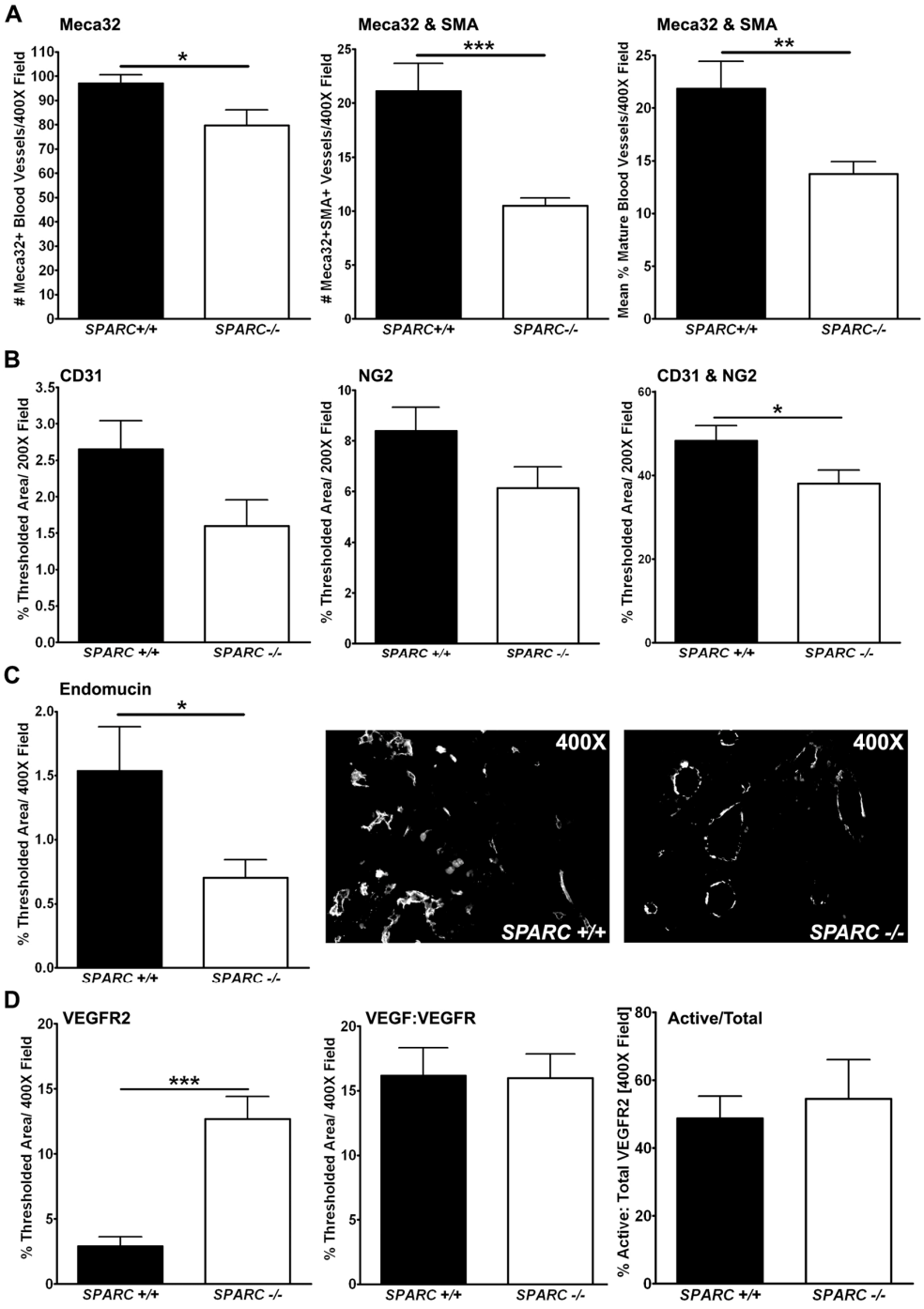

Figure 2. Tumor Microvessel Density and Maturity.
Fluorescence immunohistochemistry was utilized to quantify microvessel density, pericyte association, and blood vessel activation in PAN02 orthotopic tumors grown in *Sparc*$^{+/+}$ and *Sparc*$^{-/-}$ mice (A-D). (A) The number of MECA-32 positive vessels and the

number of MECA-32 and SMA colocalized vessels was quantified in Methyl Carnoy's fixed tumor sections stained with rat anti-mouse endothelial cell MECA-32 [49] and rabbit anti-SMA. Percent mature vessels were calculated as the number of MECA-32 & SMA colocalized vessels divided by the total number of MECA-32 positive vessels in each image. (B) Percent thresholded area was quantified for CD31, NG2 and CD31/NG2 colocalization in frozen tumor sections stained with rat anti-mouse CD31 and rabbit anti-NG2. (C) Quantification of rat anti-endomucin, another blood vessel marker, was used to confirm microvessel density in Methyl Carnoy's fixed tumor sections. Representative images of endomucin staining in tumors from *Sparc*$^{+/+}$ and *Sparc*$^{-/-}$ mice are shown. (D) The levels of VEGFR2 and VEGF:VEGF Receptor complex were quantified in frozen tumor sections stained with rat anti-VEGFR2 (RAFL-2) [47] and biotinylated mouse anti-VEGF:VEGFR complex (Gv39M) [48]. Total VEGFR2 and activated VEGF receptor staining (VEGF:VEGFR) was quantified as percent thresholded area in an entire field. The amount of activated vasculature (Active:Total) was calculated by dividing the colocalized area of RAFL-2 and Gv39M by the total RAFL-2 area and recorded as a percent. Total magnification is indicated. (* $p<0.05$, ** $p<0.01$, *** $p<0.001$; Student's t test).

Vascular Basement Membrane is Disrupted in Tumors Grown in the Absence of Host SPARC.

Utilizing transmission electron microscopy (TEM), we examined the vascular basement membranes in organs from tumor-bearing *Sparc*$^{+/+}$ and *Sparc*$^{-/-}$ mice. The tumor vasculature in *Sparc*$^{-/-}$ mice appeared altered compared to *Sparc*$^{+/+}$ controls (Figure 3A). There was a noticeable reduction in the density of the vascular basement membrane in tumors grown in the absence of host SPARC (Figure 3A, arrows). Possibly due to the lack of sufficient basement membrane, the endothelial cell layer was discontinuous and somewhat separated from the underlying tissue (Figure 3A, arrowheads). The liver vasculature was also disrupted in tumor-bearing *Sparc*$^{-/-}$ mice relative to *Sparc*$^{+/+}$ littermates (Figure 3B). The hepatic endothelial cells were detached from the underlying hepatocytes (Figure 3B, arrows) and endothelial cell junctions appeared as gaps rather than as fenestrations (Figure 3B, arrowheads). However, these vascular differences in tumor-bearing mice did not extend to the blood-brain barrier. Endothelial cell layers in the brain of *Sparc*$^{+/+}$ and *Sparc*$^{-/-}$ mice were continuous and closely associated with an underlying dense vascular basement membrane (Figure 3C, arrows).

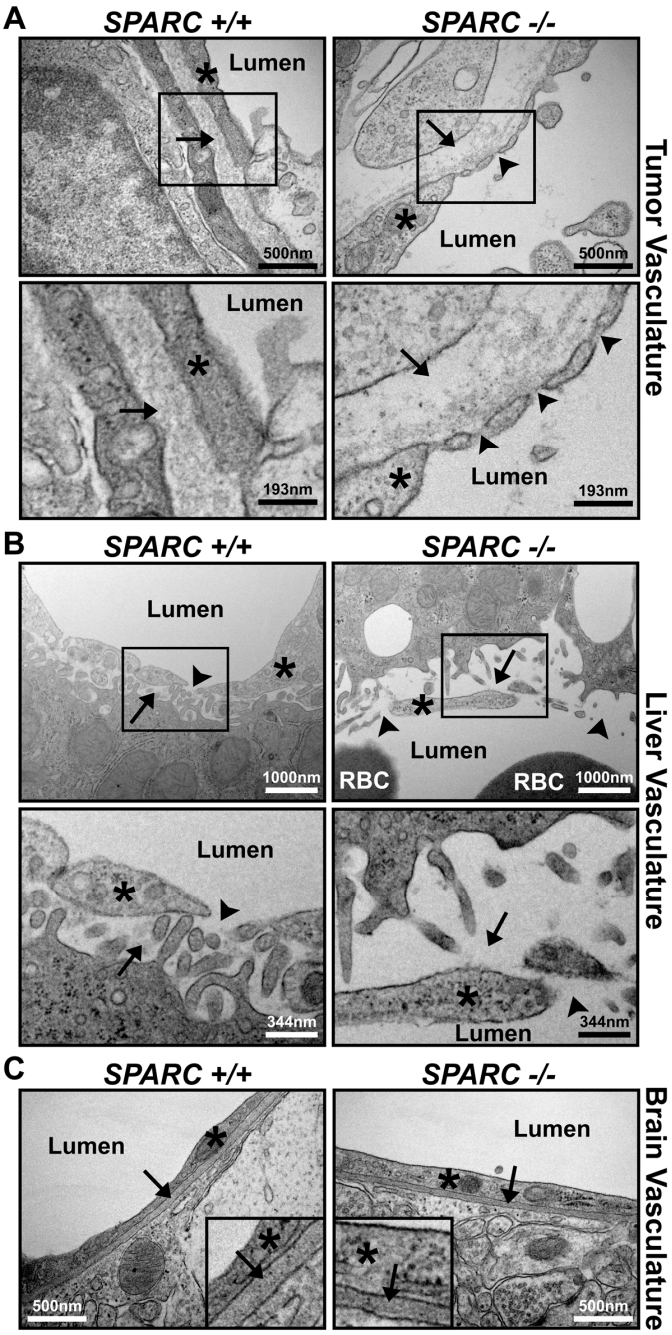

Figure 3. Microvessel Structure in Organs from Tumor-Bearing *Sparc*$^{+/+}$ and *Sparc*$^{-/-}$ Mice. TEM images of blood vessels within the tumor (A), liver (B) and brain (C) of *Sparc*$^{+/+}$ and *Sparc*$^{-/-}$ animals bearing orthotopic PAN02 tumors. Red blood cells (RBC) and blood vessel lumens are labeled. (A) Note the reduction of ECM deposition under (arrows) and gaps between (arrowheads) endothelial cells (*) in tumors from *Sparc*$^{-/-}$ mice compared to *Sparc*$^{+/+}$ animals. The lower panels are magnified regions taken from the upper panels as indicated. (B) Note differences in how the sinusoidal endothelial cells (*) associate with the underlying hepatocytes (arrows) and each other (arrowheads) in the liver of tumor-bearing *Sparc*$^{-/-}$ mice compared to SPARC+/+ counterparts. The lower panels are magnified regions taken from the upper panels as indicated. (C) Tumor-bearing *Sparc*$^{-/-}$ mice present a normal blood-brain barrier and endothelial cell (*) attachment to the vascular basement membrane (arrows). Insets are regions enlarged approximately four-fold to aid in the visualization of the vascular basement membrane within the brain.

Vascular Function is Enhanced During Tumor Progression in Sparc-null Mice.

We surmised that vascular function would be altered as a result of the disruptions in the vascular basement membrane in tumors grown in the absence of host SPARC. To test this hypothesis, we measured functional parameters such as permeability, perfusion and hypoxia. The amount of Evans Blue Dye (EBD) entering the tumors after intravenous injection was quantified by fluorescence microscopy and found to be increased significantly in tumors grown in *Sparc*$^{-/-}$ mice (Figure 4A, $p<0.05$, red). Next, we quantified the perfusion and permeability of fluorescently labeled dextrans (Figure 4B). Permeability of fluorescein isothiocyanate (FITC)-labeled dextran ($2x10^6$ kDa) in tumors grown in *Sparc*$^{-/-}$ mice was increased significantly (Figure 4B, $p<0.001$, green). In addition, there was a greater than four-fold increase in the perfusion of the smaller molecular weight rhodamine-dextran (10,000 kDa) in tumors grown in *Sparc*$^{-/-}$ relative to *Sparc*$^{+/+}$ mice (Figure 4B, $p<0.01$, red). Concomitant with the increase in permeability and perfusion, the degree of hypoxia within the tumors was found to be decreased significantly in *Sparc*$^{-/-}$ mice relative to *Sparc*$^{+/+}$ counterparts (Figure 4C, $p<0.05$, green).

Consistent with alterations in the vascular basement membrane, tumor-bearing *Sparc*$^{-/-}$ mice also displayed enhanced liver permeability and perfusion relative to *Sparc*$^{+/+}$ mice as measured by EBD ($p<0.05$), FITC-dextran ($p<0.001$) and rhodamine-dextran ($p<0.001$) (Figure 4D). It is important to note that there was a trend towards increased EBD permeability in the pancreas and liver of non-tumor bearing *Sparc*$^{-/-}$ mice (Supplemental Figure S1A). However, by TEM, the vasculature appeared comparable between the two non-tumor bearing groups (Supplemental Figure S1B). It appears as

though the vasculature of *Sparc*$^{-/-}$ animals is more compliant or sensitive to perturbation; thereby, vascular permeability is exaggerated when challenged by the tumor. Therefore, it is possible that the compromised vascular basement membrane in tumor-bearing *Sparc*$^{-/-}$ mice not only contributes to primary tumor growth and survival, but also to enhanced metastasis, especially to the liver.

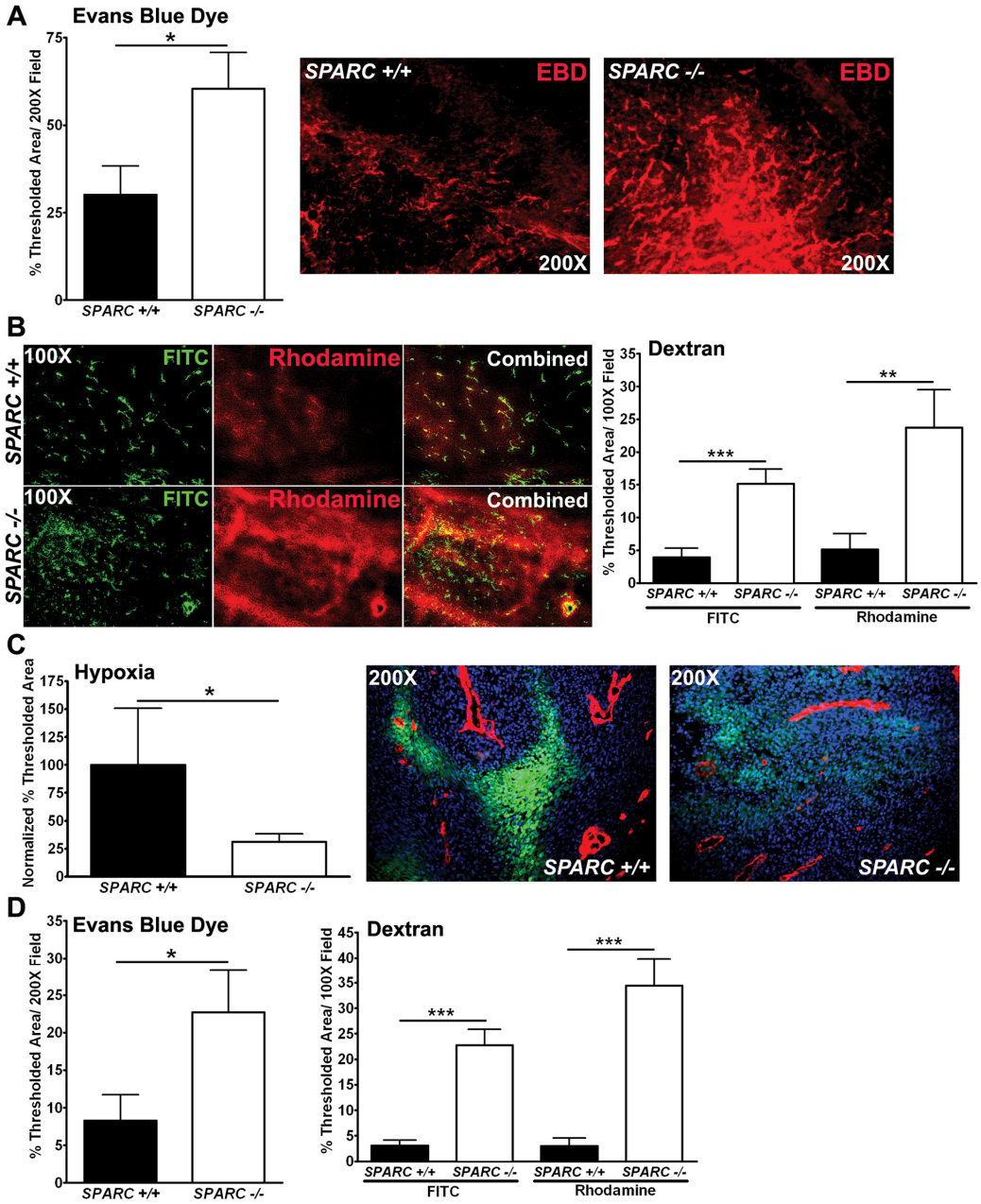

Figure 4. Permeability, Perfusion and Vascular Function. Mice bearing orthotopic PAN02 tumors were injected intravenously with Evans Blue Dye (A), fluorescent dextrans (B) or a hypoxia marker (Hypoxyprobe™-1; Chemicon) (C). Tissue was snap frozen, sectioned (10 μm) and analyzed by fluorescence microscopy. (A) Quantification of Evans Blue Dye permeability within tumors was recorded as percent thresholded area.

Representative images of Evans Blue Dye fluorescence (red) in tumors grown in *Sparc*$^{+/+}$ and *Sparc*$^{-/-}$ mice. (B) FITC-Dextran (2 million MW) (Green) and Rhodamine-Dextran (10,000 MW) (Red) permeability in tumors. Percent thresholded area was quantified. (C) The amount of hypoxia within tumors was quantified using an antibody directed against an adduct that forms when Hypoxyprobe™-1 enters hypoxic tissue, FITC-conjugated mouse anti-pimonidazole (Chemicon). Percent thresholded area was quantified and two separate experiments were combined by normalization to data from *Sparc*$^{+/+}$ mice. Images display hypoxia (green) near the vasculature (red) stained with antibody rat anti-mouse endothelial cell (Meca-32) within tumors. Nuclei are marked with DAPI (blue). (D) Liver permeability was also affected by the lack of host SPARC as measured by both Evans Blue Dye and the fluorescent dextrans. Total magnification is indicated. (* $p<0.05$, ** $p<0.01$, *** $p<0.001$; Student's t test).

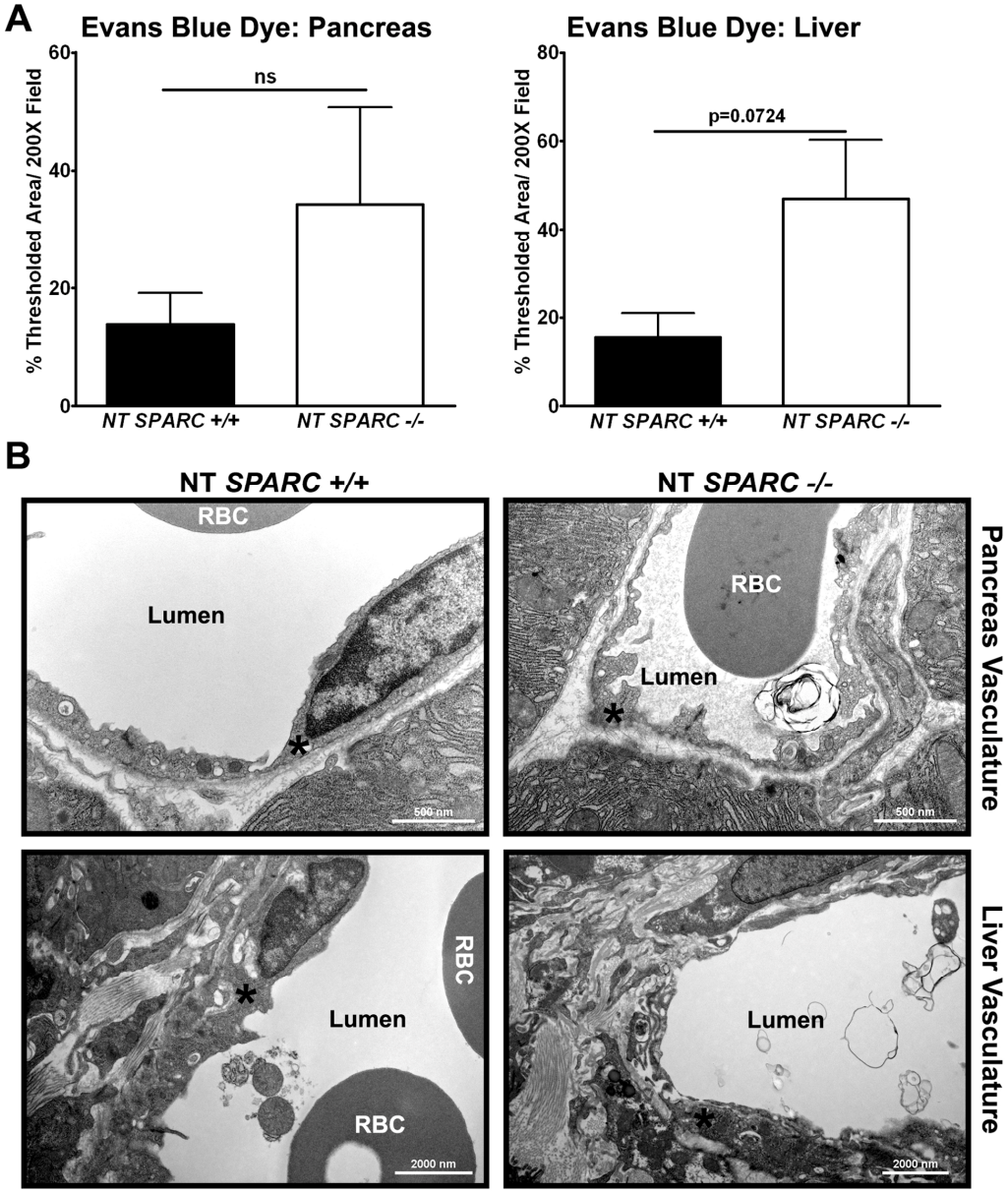

Figure S1. Non-Tumor Bearing Vasculature. (A) Non-tumor bearing *Sparc*$^{+/+}$ (NT SPARC+/+) and *Sparc*$^{-/-}$ (NT SPARC-/-) mice were injected intravenously with Evans Blue Dye (EBD) and fluorescence quantification of EBD permeability within the pancreas and liver was recorded as percent thresholded area. (B) TEM images of blood vessels within the pancreas and liver of non-tumor bearing *Sparc*$^{+/+}$ and *Sparc*$^{-/-}$ mice. Red blood cells (RBC), blood vessel lumens and endothelial cells (*) are marked. (ns, no significance; Student's t test).

Collagen Deposition and Fibrillogenesis are Decreased in Tumors Grown in the Absence of Host SPARC.

Previous studies have shown the importance of stromal SPARC for collagen deposition and fibrillogenesis in subcutaneous tumors [42, 43]. We wanted to validate this observation in the orthotopic model of pancreatic cancer. We first utilized immunohistochemistry to stain for collagen I (Figure 5A). Staining with antibodies LF-67 and 46425 showed no significant change in the overall expression of collagen I (α1) or collagen I (α2) within the tumors when percent thresholded area was quantified (data not shown). However, the pattern of staining was different in tumors grown in *Sparc*$^{-/-}$ versus *Sparc*$^{+/+}$ animals. Most of the collagen I in the tumors of *Sparc*$^{-/-}$ mice was cell-associated and not organized into collagen fibrils (unpublished observations). Alternatively, collagen I in *Sparc*$^{+/+}$ mice was found organized into large tracks of aligned fibrils with minimal cell association (Figure 5A). Therefore, when looking specifically at tracks of fibrillar collagen I, it became apparent that tumors grown in the absence of host SPARC showed a decrease in collagen fibrillogenesis, especially at the tumor border (Figure 5A). Images in Figure 5A display typical collagen I fiber tracks found in tumors grown in *Sparc*$^{-/-}$ mice relative to *Sparc*$^{+/+}$ counterparts and do not represent total collagen production. Notice that in the absence of host SPARC, fibrillar collagen I tracks were sparser and had significantly less organization.

Staining with Masson's trichrome, which reacts with all fibrillar collagens (blue), confirmed that tumors grown in *Sparc*$^{-/-}$ mice displayed a significant reduction in fibril-associated collagen (Figure 5C, center $p<0.05$, edge $p<0.001$). This was most apparent at the tumor edge where there was a greater than four-fold decrease in collagen deposition

in tumors grown in *Sparc*$^{-/-}$ mice compared to *Sparc*$^{+/+}$ controls (Figure 5C, 1.4% vs. 6.4%, arrowheads and graph). The size or maturity of collagen fibers in tumors from *Sparc*$^{+/+}$ and *Sparc*$^{-/-}$ mice was assessed with picrosirius red, a dye that stains and enhances the birefringence of fibrillar collagens (Figure 5B). Under polarized light, mature or larger fibers appear orange and red, whereas smaller, less mature fibers appear yellow and green. Tumors grown in *Sparc*$^{-/-}$ mice had fewer collagen fibers by picrosirius red staining than tumors grown in *Sparc*$^{+/+}$ counterparts. Furthermore, the collagen fibers were smaller and less mature, as depicted by the yellow and green staining compared to the red and orange staining in the control tumors (Figure 5B).

Not only are the fibrillar collagens affected, but tumors grown in *Sparc*$^{-/-}$ mice also displayed a significant reduction in the deposition of the basement membrane-associated collagen IV compared to *Sparc*$^{+/+}$ counterparts (Figure 5D, $p<0.05$). The decrease in collagen deposition and fibrillogenesis in the tumors of *Sparc*$^{-/-}$ mice was not a result of changes in collagen production or secretion because we found no significant difference in the levels of hydroxyproline in tumor lysates, a posttranslational modification that occurs almost exclusively on all collagens (Figure 5E). Therefore, the absence of stromal-derived SPARC does not diminish the expression or secretion of collagen, rather SPARC is indispensible for proper collagen maturation and fibrillogenesis during malignant progression, a role consistent with its participation in collagen deposition and fibrillogenesis during development and wound-healing.

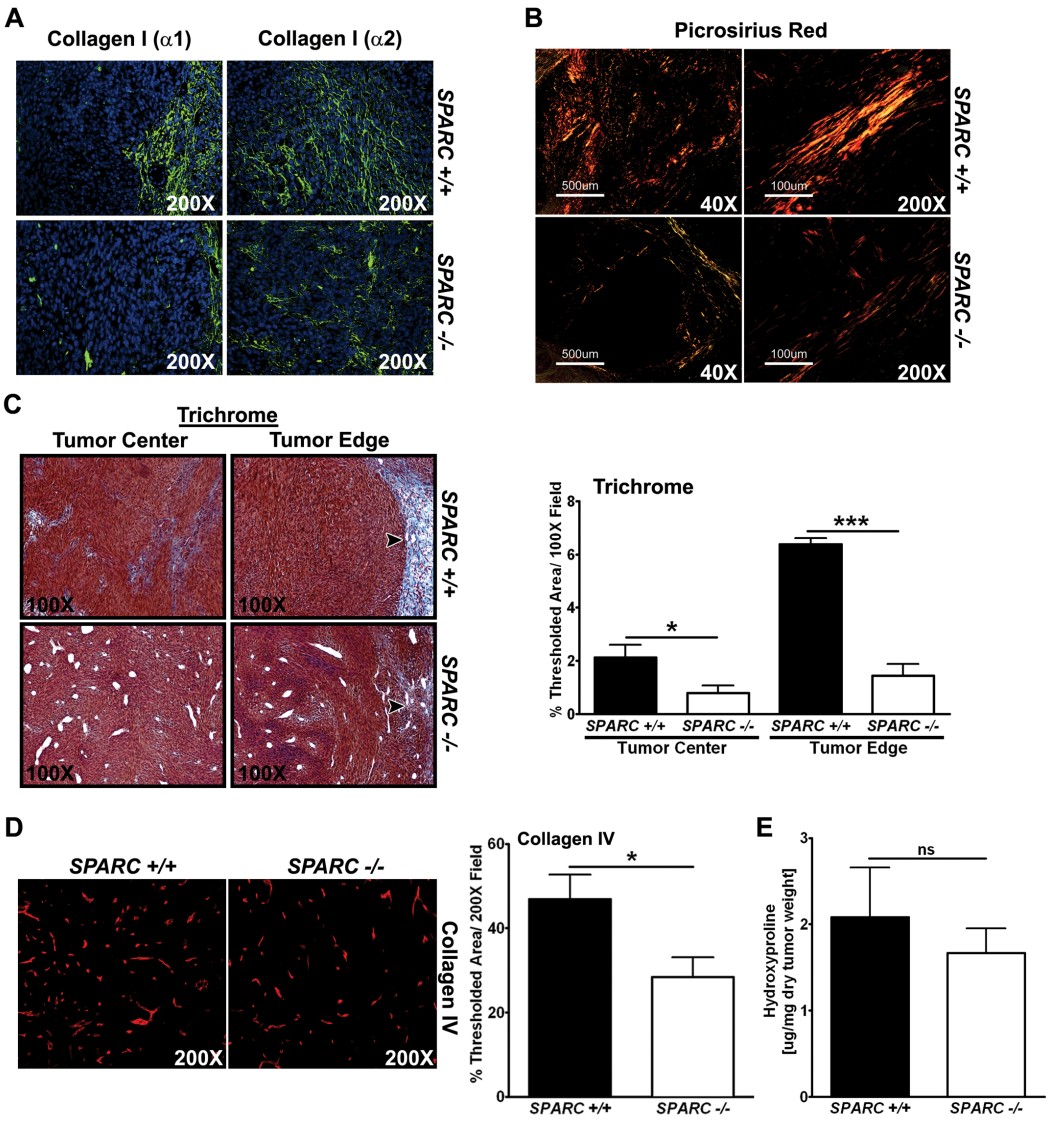

Figure 5. Collagen Deposition and Maturation in PAN02 Orthotopic Tumors. The amount of collagen production, deposition and maturation was assessed in orthotopic tumors from *Sparc*$^{-/-}$ and *Sparc*$^{+/+}$ mice. (A) Immunohistochemistry was performed on tumors with antibodies rabbit anti-collagen I (a1) (LF-67) [50, 51] and rabbit anti-collagen I (a2) (46425, green). Nuclei are stained with DAPI (blue). (B) Picrosirius Red staining reveals the maturity of the fibrillar collagen within tumors. *Sparc*$^{-/-}$ mice show less mature and/or smaller collagen fibrils (yellow & orange) compared to tumors grown in *Sparc*$^{+/+}$ mice, which display more mature and/or larger collagen fibrils (orange & red) under polarized light. (C) Masson's Trichrome staining shows the amount of fibrillar collagen (blue) deposited in and around tumors. Arrowheads point to the collagen capsule

at the tumor border. Collagen deposition at the tumor edge and center was quantified on trichrome stained tissue and was recorded as percent thresholded area. (D) IHC with antibody rabbit anti-collagen type IV (red) and quantification of percent thresholded area. (E) The amount of collagen produced and secreted within tumors was quantified by hydroxyproline analysis. Total magnification is indicated. (ns, not significant, * $p<0.05$, *** $p<0.001$; Student's t test).

Noncollagenous ECM Deposition in Tumors Grown in Sparc-null Mice.

We demonstrated that absence of host SPARC during tumor progression leads to a reduction in collagen deposition and fibrillogenesis. However, it is not clear if lack of stromal-derived SPARC contributes to alterations in the deposition of noncollagenous ECM proteins during tumorigenesis. Decorin, a small leucine-rich proteoglycan, binds fibrillar collagens and is a vital player in collagen fibrillogenesis [52]. The quantity of decorin in orthotopic tumors was assessed by immunohistochemistry and found to be substantially decreased in *Sparc*$^{-/-}$ mice compared to *Sparc*$^{+/+}$ littermates (Figure 6A). Because collagen fibers serve, in part, as a storage compartment for decorin, the reduction in collagen deposition in *Sparc*$^{-/-}$ mice might lead to a concomitant loss of decorin retention in tumors.

Fibronectin and laminin are both noncollagenous glycoproteins that have been shown to promote cell adhesion and migration, particularly in tumors [53-56]. Fibronectin is also a provisional matrix that is laid down during wound healing and augmented during tumor formation. We found no remarkable difference in the amount of fibronectin deposited within (Figure 6B, inset) or encapsulating the tumor (Figure 6B). However, it was surprising that the tumor capsule in *Sparc*$^{-/-}$ mice is pronounced when assessed by fibronectin staining, but indiscernible by collagen staining (Figure 5C vs. 6B).

Laminin is a constituent of mature basement membrane and enhances tumor cell motility and invasion [57, 58]. By immunohistochemistry, there was no significant difference in laminin deposition within the tumors (Figure 6C, tumor center). However,

the level of laminin staining was noticeably increased at the tumor border in *Sparc*$^{-/-}$ relative to *Sparc*$^{+/+}$ mice (Figure 6C, tumor edge). Increased laminin surrounding the tumors in *Sparc*$^{-/-}$ mice might be a compensatory reaction to the reduction in collagen deposition. Collectively these data indicate that SPARC is involved predominantly in collagen synthesis and fibrillogenesis. In addition, the similar levels of fibronectin and increased accumulation of laminin, both proven stimulators of tumor cell invasion, leads to the proposal that these alternative matrices might contribute to the accelerated tumor growth in *Sparc*$^{-/-}$ mice**.**

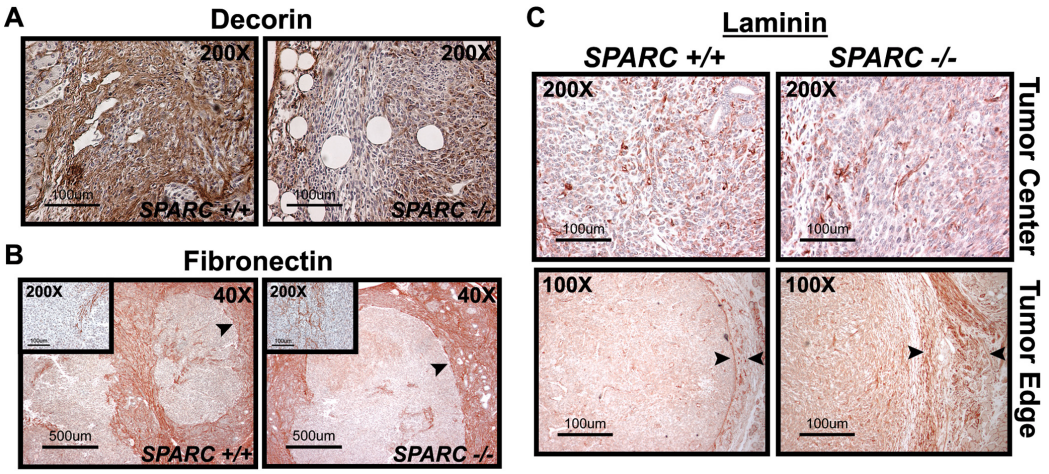

Figure 6. ECM Deposition and Composition in PAN02 Orthotopic Tumors. Immunohistochemistry for decorin (A), fibronectin (B) and laminin (C) was performed on Methyl Carnoy's fixed, paraffin-embedded tumor sections. (A) IHC with antibody goat anti-mouse decorin (brown). (B) IHC with antibody rabbit anti-fibronectin (red). Insets are higher magnification images of the tumor center. (C) IHC with antibody rabbit anti-laminin (red). Images show the tumor center and edge. Total magnification is indicated. Arrowheads specify the tumor capsule in (B) and (C).

Tumors Grown in the Absence of Host SPARC have Alterations in Infiltration of Host Cells.

The stromal compartment is an important component of the ECM and is capable of influencing tumor growth and metastasis. It consists of endothelial cells, pericytes, fibroblasts and immune cells. Fibroblasts are a rich source for ECM secretion and deposition. Consequently, we assessed fibroblast infiltration into orthotopic PAN02 tumors to determine if the diminished collagen deposition and fibrillogenesis in the absence of host SPARC is due to a deficiency in fibroblast recruitment and/or activation. Staining for smooth muscle actin (SMA), a marker of activated mesenchymal cells, and a pan reticular fibroblast marker (fibroblast) confirmed that tumors grown in *Sparc*$^{-/-}$ mice did not have a deficit in fibroblast recruitment or activation relative to *Sparc*$^{+/+}$ mice (Figure 7A). In fact, by anti-SMA immunoreactivity, there was a significant increase in activated fibroblasts infiltrating tumors grown in *Sparc*$^{-/-}$ mice compared to *Sparc*$^{+/+}$ littermates (Figure 7A, $p<0.05$). Thus, fibroblasts are recruited and activated in the absence of SPARC but are unable to elicit a proper fibrotic response.

A cell population previously shown to be involved in angiogenesis and tumor progression is the neutrophil [59]. Therefore, we stained tumor sections for myeloperoxidase (MPO), a marker of granulocytes, to assess neutrophil infiltration into orthotopic tumors. The number of MPO^{+} cells within tumors grown in *Sparc*$^{-/-}$ mice compared to *Sparc*$^{+/+}$ controls was similar (Figure 7B, red). These results introduce the possibility that monocytic cell populations other than neutrophils might be contributing to the accelerated metastasis in the absence of host-derived SPARC.

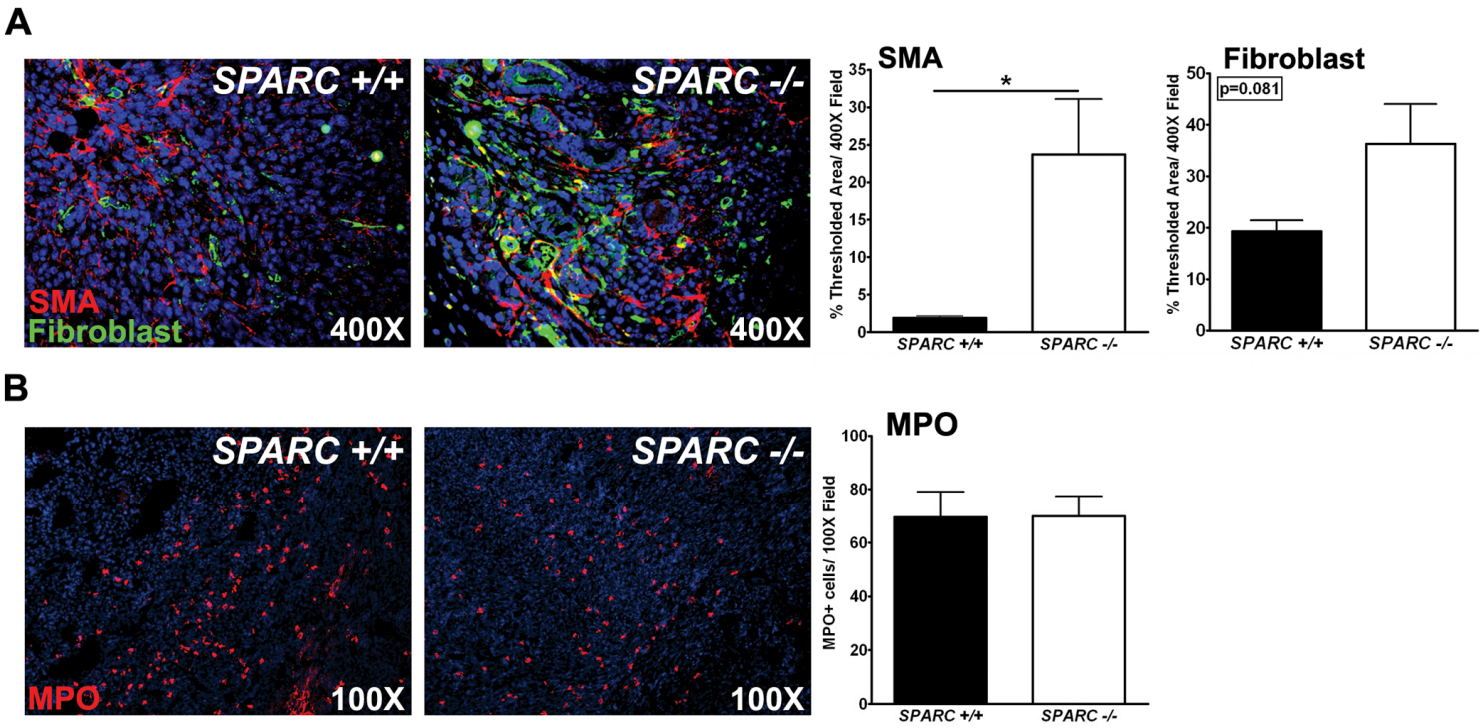

Figure 7. Host-Cell Infiltration in PAN02 Orthotopic Tumors. Fluorescence immunohistochemistry was performed to evaluate stromal response in tumors grown in *Sparc*$^{+/+}$ and *Sparc*$^{-/-}$ mice (A-C). (A) Methyl Carnoy's fixed tumors were stained with antibodies rabbit anti smooth muscle actin (SMA, red) and rat anti pan reticular fibroblast marker (fibroblast, green) and percent thresholded area quantified. (B) Snap frozen tumors were stained with antibody rabbit anti myeloperoxidase (MPO, red) and number of MPO+ cells per field quantified. Total magnification is indicated. Nuclei are stained with DAPI (blue). (* $p<0.05$, ** $p<0.01$; Student's t test).

Macrophage Recruitment and Activation of the M2 Phenotype is Increased in Tumors Grown in Sparc-null Mice.

Tumor associated macrophages have been implicated in tumor progression, metastasis, angiogenesis and immunosuppression [60]. In a previous study that focused on subcutaneous tumor growth of PAN02 in the absence of host SPARC, we found that macrophage distribution was altered, such that, tumors grown in *Sparc*$^{+/+}$ mice displayed a concentrated macrophage population at the tumor border, which was diminished in tumors grown in *Sparc*$^{-/-}$ mice [43]. However, it was noted that macrophages were evenly distributed throughout the tumors grown in the absence of host SPARC. Therefore, we sought to quantify and define the macrophage population in our orthotopic PAN02 model by fluorescence immunohistochemistry. Total macrophage infiltration was determined by staining for F4/80, a general macrophage marker, and found to be significantly increased in tumors grown in *Sparc*$^{-/-}$ mice compared to *Sparc*$^{+/+}$ littermates (Figure 8A, $p<0.01$). Staining for an activated macrophage marker, Mac-3, also displayed augmented macrophage infiltration and activation in the absence of host SPARC (Figure 8A, $p<0.001$). To further define the macrophage population within these tumors, immunohistochemistry was performed against markers shown to delineate classically-activated, immunostimulatory macrophages (M1) from alternatively-activated, immunosuppressive macrophages (M2) [59, 61]. Colocalization of CD11b (green) with iNOS (red) revealed that tumors grown in *Sparc*$^{-/-}$ mice exhibit similar activation of M1 macrophages relative to *Sparc*$^{+/+}$ mice (Figure 8B). Conversely, M2 macrophage activation is significantly enhanced in tumors grown in the absence of host SPARC, as measured by the colocalization of macrophage mannose receptor (MMR, green) with

CD163 (red) (Figure 8C, $p<0.001$). Therefore, the absence of host-derived SPARC increases macrophage recruitment/activation and polarizes the macrophage population within tumors towards an M2 phenotype. This suggests that the microenvironment in tumors grown in *Sparc*$^{-/-}$ mice is immunosuppressive and, thus, pro-tumorigenic and metastatic.

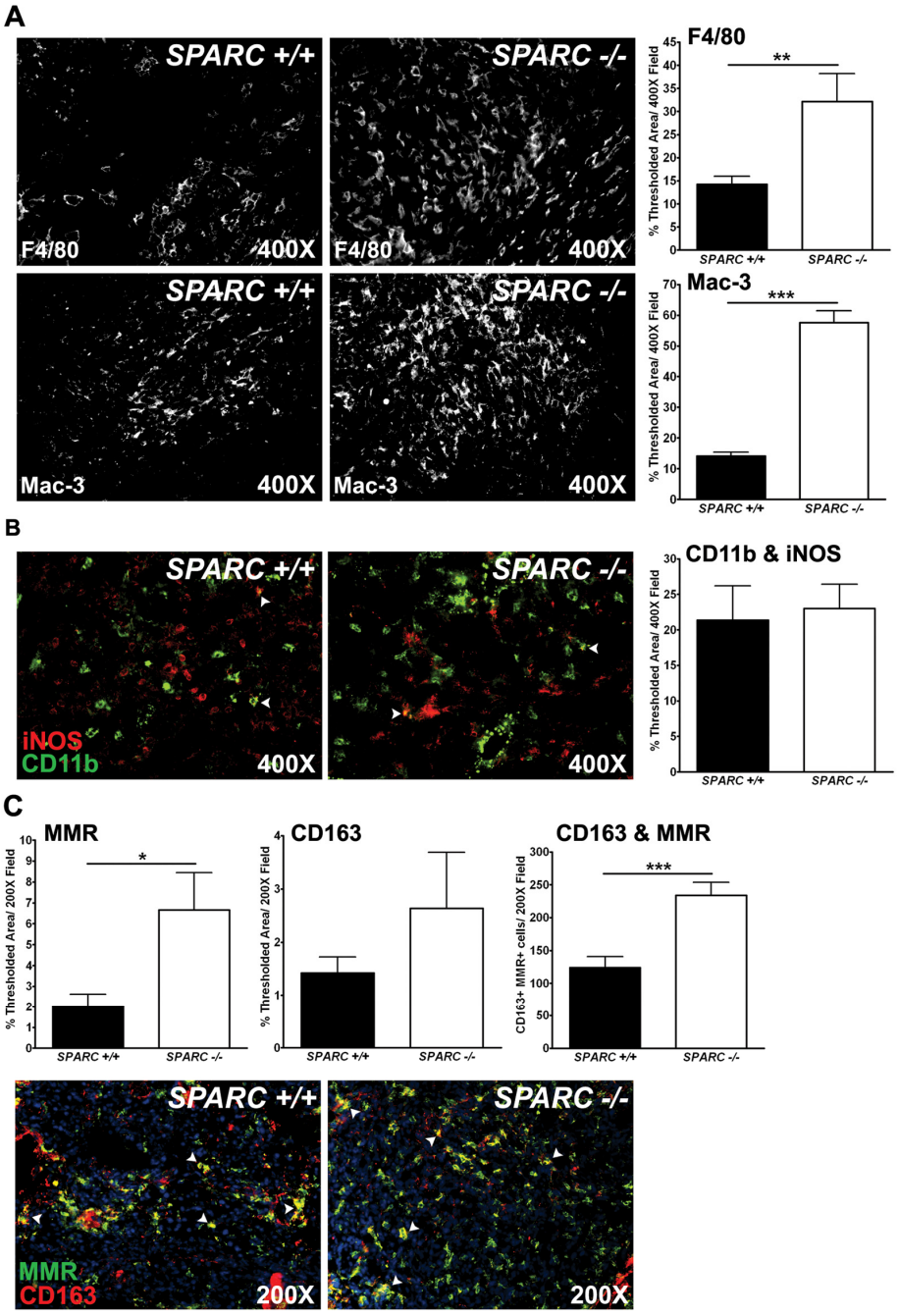

Figure 8. Macrophage Recruitment and Activation in PAN02 Orthotopic Tumors. Fluorescence immunohistochemistry was utilized to assess macrophage recruitment and activation in tumors grown in *Sparc*$^{+/+}$ and *Sparc*$^{-/-}$ mice (A-C). (A) Methyl Carnoy's fixed tumors were stained with antibody rat anti F4/80 or antibody rat anti Mac-3 and

percent thresholded area quantified. (B) Snap frozen tumors were stained with antibodies rat anti CD11b (green) and rabbit anti iNOS (red). The percent thresholded area of CD11b colocalized with iNOS was quantified. (C) Snap frozen tumors were stained with antibodies rat anti mannose receptor (MMR, green) and rabbit anti CD163 (red). The percent thresholded area of MMR alone, CD163 alone and colocalization was quantified. Nuclei are stained with DAPI (blue). Total magnification is indicated. (* $p<0.05$, ** $p<0.01$, *** $p<0.001$; Student's t test).

Discussion

At first glance, it is counterintuitive to imagine how tumor growth and metastasis can be augmented in *Sparc*$^{-/-}$ animals in the face of reduced angiogenesis and pericyte recruitment. However, due to the importance of SPARC for appropriate ECM deposition and collagen fibrillogenesis, we speculated that the absence of SPARC could weaken the vascular basement membrane and alter the tumor microenvironment such that the tumors were able to overcome this diminution in angiogenesis. Indeed, we found that the vascular basement membrane was disrupted and vascular function was enhanced in tumors grown in *Sparc*$^{-/-}$ mice compared to controls. Ultimately, enhanced vascular function in the absence of host SPARC is most likely a consequence of a combination of factors including decreased pericyte recruitment, a deficient vascular basement membrane, reduced microvessel density and/or altered chemokine and growth factor signaling.

Alterations in the ECM as well as enhanced vascular function could account for the accelerated tumor progression and metastasis in *Sparc*$^{-/-}$ mice. Structural and functional abnormalities of the tumor vasculature have been attributed to decreases in pericyte coverage and stabilization [62, 63]. Consistent with these observations, tumors grown in *Sparc*$^{-/-}$ mice display a reduction in pericyte recruitment and a concomitant alteration in vascular structure and function. Furthermore, it has been shown that the integrity of the vasculature is vital to the control of metastasis [64, 65]. In our orthotopic model of pancreatic cancer, the enhancement of metastatic progression and burden in the absence of host SPARC might be a result of hematological tumor cell dissemination augmented by the loss of pericyte coverage and the concomitant disruption of the

vascular basement membrane. In tumor-bearing *Sparc*$^{-/-}$ mice, the endothelial cell layer is compromised, not only in the primary tumor, but also at metastatic sites such as the liver. These changes could facilitate intravasation and the extravasation of tumor cells. In addition, the enhanced vascular permeability and perfusion in tumor-bearing *Sparc*$^{-/-}$ mice are expected to contribute to tumor progression by, presumably, improving the delivery of oxygen and nutrients.

Tumors grown in *Sparc*$^{-/-}$ mice also exhibit deficits in collagen fibrillogenesis and alterations in non-collagenous ECM protein deposition. The ECM is not just a passive bystander. In addition to providing structural support, the ECM influences cell adhesion, migration, differentiation, proliferation and survival by binding to and signaling through adhesion receptors such as integrins [66]. Several studies have shown that the ECM contributes substantially to tumor progression and metastasis [67-69]. Our studies further highlight the importance of proper deposition and organization of ECM in the control of pancreatic tumor cell dissemination.

The immune cell compartment of the tumor microenvironment participates in tumor progression. The balance between immunostimulatory and immunosuppressive cell recruitment and activation is a critical factor in the fate of malignant lesions. Tumor associated macrophages can elicit opposing effects [59, 61]. Classically-activated macrophages (M1) are important for tumor clearance by releasing inflammatory cytokines that stimulate the adaptive immune response. On the other hand, alternatively-activated macrophages (M2) are associated with tumor angiogenesis, immunosuppression and metastasis [59, 61]. It is the M2 macrophage that contributes to immune tolerance by

subverting adaptive immune responses. Furthermore, an increased number of M2 macrophages correlates with a poor prognosis in several human cancers [70]. In our murine model of pancreatic carcinoma, macrophage recruitment and polarization to the M2 phenotype is augmented in the absence of host-derived SPARC. This provides another explanation for accelerated tumor progression and enhanced metastasis in *Sparc*$^{-/-}$ mice.

A study of human pancreatic adenocarcinoma has shown that increased SPARC expression by the tumor stroma correlates with decreased patient survival [39]. Nevertheless, correlation does not always translate to causation. Indeed, Sato et al. found that SPARC expression is increased in fibroblasts isolated from human pancreatic tumors compared to noncancerous tissue and that exposure of the noncancerous-derived fibroblasts to human pancreatic cancer cells upregulated their expression of SPARC [38]. However, this same group, as well as others, demonstrated that exogenous administration of SPARC inhibits the proliferation of human pancreatic cell lines [38, 71]. Therefore, we suspect that SPARC expression is a read-out for how responsive the stroma is to the tumor microenvironment and may even be a protective mechanism by which the stroma attempts to control aggressive tumor growth. In other words, stromal SPARC expression may correlate with a worse prognosis simply because it is upregulated in response to and acts as an indicator of invasive disease. Similar to SPARC, transforming growth factor-β (TGFβ) isoforms have been shown to be increased in pancreatic cancer, to correlate with increased invasion and decreased survival in late-stage disease, and to have paradoxical effects on pancreatic tumor progression [72, 73]. Moreover, TGFβ isoforms activate

pancreatic stellate cells and increase SPARC expression to induce a desmoplastic response characteristic of pancreatic ductal adenocarcinoma [12, 74, 75]. Although epithelial-derived, PAN02 cells display mesenchymal characteristics *in vitro* and *in vivo*. A common occurrence in metastatic progression of pancreatic carcinoma is epithelial-to-mesenchymal transition (EMT). Therefore, orthotopic PAN02 tumors model late stage, invasive pancreatic cancer. Interestingly, TGFβ functions as a tumor promoter in late-stage pancreatic adenocarcinoma by stimulating EMT and invasion. Therefore, the effect of SPARC on malignant progression may depend on TGFβ and other growth factor signaling events. Indeed, preliminary data from our laboratory suggests that TGFβ contributes substantially to the phenotypic alterations observed during tumor progression and metastasis in the absence of host SPARC.

Although one predicts from studies of SPARC expression in human pancreatic cancer that loss of SPARC expression from stromal cells would diminish tumor growth and metastasis, in the present model, absence of stromal-derived SPARC accelerates tumor progression. Our study indicates that this is due to alterations in the ECM and vascular basement membrane which enhance vascular function, specifically, in the tumor microenvironment and at metastatic sites. While this aspect of the model may not precisely mimic human disease, it does raise concerns related to the use of SPARC as a therapeutic target. A recent review featured SPARC as a protumorigenic, prometastatic protein and proposed that it should be inhibited as a means of tumor therapy [12]. What our data suggest is that inhibiting SPARC could have unforeseen consequences on the vasculature and tumor microenvironment which could result in altered therapeutic response and increased metastasis. In other words, targeting SPARC might enhance drug

delivery but also pose an increased risk for metastatic dissemination. In addition, several labs have shown that SPARC expression by tumor cells in human pancreatic adenocarcinoma is a prognostic indicator of better outcome, which is in direct opposition to how SPARC expression by the stromal compartment correlates with survival [38, 76, 77]. However, these studies are consistent with the aforementioned data and show that SPARC inhibits pancreatic tumor cell proliferation [38, 71]. These examples highlight the necessity for studies aimed at clarifying what and how distinct cell populations are effected by the loss of SPARC in the tumor microenvironment.

We propose that the function of SPARC in malignant progression is not trivial and is dependent on a variety of factors such as the epithelial/mesenchymal state or stage of the tumor, integrin expression and surface localization, ECM composition, chemokine/growth factor profiles and bioavailability, and immune modulation. Our study emphasizes the complexity of SPARC function during tumorigenesis and underscores the necessity for comprehensive studies in the pursuit of a SPARC mechanism(s).

Materials and Methods

Tissue Culture

The murine pancreatic adenocarcinoma cell line (PAN02, also known as Panc02) was purchased from the Developmental Therapeutics Program, Division of Cancer Treatment and Diagnosis, National Cancer Institute (Frederick, MD), and grown in high glucose Dulbecco's Modified Eagles Medium (DMEM + GlutaMAX™-1, Invitrogen, Carlsbad, CA) supplemented with 5% fetal bovine serum (FBS, Life Technologies, Grand Island,

NY). The PAN02 cell line was tested (Impact III PCR profiles; MU Research Animal Diagnostic Laboratory, Columbia, MO) and was found to be pathogen-free.

Orthotopic Tumor Model

B6;129S-*Sparc*^{tm1Hwe} mice were generated as described previously [78] and backcrossed into C57BL/6J a minimum of 10 generations. The mice were housed in a pathogen-free facility and experiments were conducted under a protocol approved by the Institutional Animal Care and Use Committee of UT Southwestern Medical Center (Dallas, TX). All experiments were performed with *Sparc-null* (*Sparc*$^{-/-}$) and *wild-type* (*Sparc*$^{+/+}$) littermates. For injections, confluent cultures of PAN02 cells (>90% viable) were trypsinized, pelleted in DMEM 5% FBS, washed twice in phosphate buffered saline (PBS) and resuspended in 0.9% sterile saline (Sigma, St. Louis, MO). Tumor cells ($1x10^6$) were injected directly into the tail of the pancreas to establish orthotopic tumors as previously described [44, 79]. The mice were evaluated for changes in body weight and signs of discomfort or morbidity, while bulk tumor growth was monitored through abdominal palpation. Mice were euthanized six to eight weeks after tumor cell injection, when the majority of mice showed signs of morbidity, and visually screened for locally invasive and metastatic lesions. The liver, heart, lung, kidney, brain, spleen and pancreas, including the tumor, were removed and weighed. Metastasis was assessed macroscopically by visual examination. Suspected metastases were fixed, stained with H&E and verified as metastatic lesions histologically. Therefore, only visible macroscopic metastatic and locally invasive lesions were counted towards metastatic

incidence and burden. Five independent experiments were performed. For the survival study, individual mice were monitored daily and were euthanized when they displayed signs of tumor-associated morbidity such as excessive weight gain or loss, ascites, lethargy and/or distress.

Immunohistochemistry

Fixed Tissue: Tissues were fixed in either Methyl Carnoy's solution (60% methanol, 30% chloroform, 10% glacial acetic acid) or 10% formalin and sent to the Molecular Histopathology Laboratory at UT Southwestern Medical Center (Dallas, TX) for paraffin-embedding and sectioning. The Molecular Histopathology Laboratory also performed staining with hematoxylin & eosin, Masson's trichrome or picrosirius red according to standard protocols. Tissue sections were deparaffinized and rehydrated in PBS containing 0.2% Tween-20 (PBSt) prior to staining.

Frozen Tissue: Tissues were snap-frozen in liquid nitrogen, embedded in optimal cutting temperature compound (OCT) (Tissue-Tek®), cut into 10 μm thick sections, air-dried overnight, fixed for 2 minutes in acetone and washed in PBSt prior to staining.

Chromagen Detection: For sections developed with either diaminobenzidine (DAB) (Research Genetics, Huntsville, AL) or 3-amino-9-ethylcarbazole (AEC) (Sigma), endogenous peroxidases were blocked by incubating the samples in a 3% H2O2 /methanol solution. Sections were then blocked in 20% AquaBlock (East Coast Biologics, Inc., North Berwick, ME), incubated with primary antibody overnight at 40C, then incubated with peroxidase-conjugated secondary antibody (Jackson Immunoresearch, West Grove, PA) (1:500) for 1 hour at room temperature. Lastly,

sections were developed with DAB or AEC for 5-20 minutes and counterstained with Meyer's Hematoxylin solution for 3-5 minutes. DAB developed slides were mounted in Permount (Fisher Scientific, Pittsburgh, PA), whereas AEC-treated sections were mounted in Crystal Mount (Biomeda Corporation, Foster City, CA) and dried 1 hour at 600C.

Fluorescence Detection: Deparaffinized and rehydrated sections were blocked in 20% AquaBlock (East Coast Biologics), incubated with primary antibody overnight at 40C, incubated with fluorophore-conjugated (FITC or Cy3) secondary antibody (Jackson Immunoresearch) (1:500) for 1 hour at room temperature and mounted with ProLong Gold Antifade Reagent with DAPI (Invitrogen).

Antibody Specifics: Primary antibodies used for IHC are listed in Supplemental Table S1 [47-51]. Antigen retrieval was performed, as indicated, by either boiling in citrate buffer (Lab Vision/Thermo Scientific, Fremont, CA) in a pressure cooker for 20 minutes or by digesting with 20 μg/ml proteinase K for 5 minutes at room temperature. Biotinylated Gv39M staining required blocking with Avidin-Biotin Block (Cell Marque, Rocklin, CA) according to the manufacturer's protocol.

Supplemental Table S1. Primary Antibodies and Applications

Antigen	Antibody Clone or Catalog # (Ref)	Species	Source	Frozen	Methyl Carnoy's	Formalin	Retrieval Citrate	Retrieval PK Digest	DAB	AEC	FL
CD11b	M1/70	Rat	AbD Serotec, Raleigh, NC	√							√
CD163	M-96	Rabbit	Santa Cruz Biotechnology Inc., Santa Cruz, CA	√							√
CD31	ab28364	Rabbit	Abcam Inc., Cambridge, MA	√							√
Collagen I (a1), C-terminal telopeptide	LF-67 (1,2)	Rabbit	Dr. Larry Fisher, NIH/NIDCR Matrix Biology Unit			√	√				√
Collagen I (a2)	46425	Rabbit	Developed in House			√	√				√
Collagen IV	AB756P	Rabbit	Chemicon International Inc., Temecula, CA		√						√
Decorin	AF1060	Goat	R&D Systems, Minneapolis, MN		√				√		
Endomucin	V.7C7	Rat	Santa Cruz Biotechnology Inc., Santa Cruz, CA		√						√
F4/80	Cl:A3-1	Rat	AbD Serotec, Raleigh, NC		√			√			√
Fibronectin	DP3060	Rabbit	Acris Antibodies, Hiddenhausen, Germany		√					√	
iNOS	NB120-15323	Rabbit	Novus Biologicals, Littleton, CO	√							√
Laminin	AHP420	Rabbit	AbD Serotec, Raleigh, NC		√					√	
Mac-3	M3/84	Rat	PharMingen/BD Biosciences, San Jose, CA		√		√				√
Mannose Receptor (MMR) (CD206)	MR5D3	Rat	Biolegend, San Diego, CA	√							√
Myeloperoxidase (MPO)	HP9048	Rabbit	Hycult Biotechnology, Uden, Netherlands	√							√
NG2 chondroitin sulfate proteoglycan	AB5320	Rabbit	Chemicon International Inc., Temecula, CA	√							√
Pan Endothelial Cell Marker	Meca-32 (*3*)	Rat	Developmental Studies Hybridoma Bank, University of Iowa, Iowa City, IA		√						√
Pan Reticular Fibroblast Marker	ER-TR7	Rat	Biogenesis Ltd, Poole, UK		√		√				√
Smooth Muscle Actin (SMA)	RB-9010	Rabbit	Lab Vision, Fremont, CA		√						√
VEGFR2	RAFL-2 (*4*)	Rat	Dr. P. Thorpe, UT Southwestern Medical Center, Dallas, TX	√							√
VEGF:VEGFR Complex	Gv39M-Biotinylated (*5*)	Mouse	Purified in House	√							√

Primary antibodies used for immunohistochemistry, tissue fixation methods, retrieval protocols and detection procedures are listed. Antigen retrieval was performed, as indicated, by either boiling in citrate buffer for 20 minutes in a pressure cooker (Retrieval Citrate) or by digesting with 20 µg/ml proteinase K for 5 minutes at room temperature (Retrieval PK Digest). (DAB) diaminobenzidine detection, (AEC) 3-amino-9-ethylcarbazole detection and (FL) fluorescence detection. 1,2 (Bernstein et al., 1996; Bernstein et al., 1995); 3 (Hallmann et al., 1995); 4 (Brekken et al., 1998); 5 (Ran et al., 2003).

Imaging and Quantification

Tissue sections were analyzed with a Nikon Eclipse E600 microscope (Nikon, Lewisville, TX). Color images were captured with a Nikon Digital Dx1200me camera and Act1 software (Universal Imaging Corporation, Downington, PA). Collagen deposition in Masson's trichrome stained tissue was performed with NIS Elements AR 2.30 software (Nikon) by thresholding images for the characteristic blue hue associated with fibrillar collagens. Sections stained with picrosirius red were visualized under polarized light. Fluorescence images were captured with a Photometric Coolsnap HQ camera and NIS Elements. Fluorescent images were captured randomly throughout the entire tumor, including the center and border, and under identical conditions including magnification and exposure time to allow quantification of signal intensities, object counts and percent thresholded area with NIS Elements AR 2.30 software (Nikon). Images were thresholded to exclude background signal from secondary antibody alone. An average of ten images per tumor and a minimum of three tumors per group were used for each target.

Transmission Electron Microscopy (TEM)

Mice were anesthetized with isoflurane and perfused with 20 ml of TEM buffer (4% paraformaldehyde and 1% glutaraldehyde in 0.1M cacodylate buffer). The organs were collected, weighed and placed in TEM buffer at 4^0C. The tissues were processed for TEM by the Molecular and Cellular Imaging Facility (MCIF) at UT Southwestern Medical Center (Dallas, TX). Images were taken with the FEI Tecnai G2 Spirit Biotwin (FEI Co., Hillsboro, OR) housed in the MCIF.

Evans Blue Dye (EBD) Permeability

Prior to sacrifice, mice were injected intravenously (tail vein) with 5 mg/ml Evans Blue Dye (EBD) (Sigma) in 0.9% sterile saline at a dose of 30 mg/kg. The EBD was allowed to circulate 30 minutes before the mice were anesthetized with isoflurane and perfused with sterile PBS at a constant rate for 8 minutes. Organs were removed, weighed, snap frozen, embedded in OCT and cut into 10 μm thick sections. EBD permeability was visualized under fluorescence microscopy with excitation and emission wavelengths of 580 nm (green) and 680 nm (red), respectively. Images were taken for both the EBD (red channel) and the autofluorescence (green channel). A minimum of six random pictures were taken of each tissue with an average of three animals per group used to quantify EBD permeability. Using NIS-Elements software, images were corrected for background autofluorescence on a pixel by pixel basis as described previously [80]. Briefly, the red autofluorescence of images from injected mice was calculated by multiplying the green autofluorescence image by the mean ratio of red to green autofluorescence intensity of uninjected control tissue (ratio=0.37). The resulting image was subtracted from the corresponding red image to yield the autofluorescence-corrected EBD permeability. Corrected images were then thresholded and the percent thresholded area recorded.

Fluorescent Dextran Permeability

Prior to sacrifice, mice were injected intravenously (tail vein) with a mixture of fluorescein isothiocyanate-conjugated dextran (FITC-Dextran) (25 mg/ml) ($2x10^6$mw; D7137; Molecular Probes/Invitrogen, Eugene, OR) and rhodamine B-conjugated dextran

(Rhodamine-Dextran) (12.5 mg/ml) ($1x10^4$mw; D1824; Molecular Probes) in 0.9% sterile saline at a dose of 200 µl/mouse. The fluorescent dextrans were allowed to circulate 10 minutes before the mice were anesthetized with isoflurane. Organs were removed, weighed, snap frozen, embedded in OCT and cut into 10 µm thick sections. FITC-dextran and Rhodamine-dextran permeability were assessed by fluorescence microscopy. A minimum of six random photographs was taken of each tissue, with an average of three animals per group. Results were recorded as mean percent thresholded area.

Tumor Hypoxia Analysis

Prior to sacrifice, mice were injected intravenously (tail vein) with 60 mg/kg of Hypoxyprobe™-1 (HP2-100; Chemicon, Temecula, CA) that had been resuspended at a concentration of 30 mg/ml in 0.9% sterile saline. The solution was allowed to circulate 90 minutes before the mice were anesthetized with isoflurane. Organs were removed, weighed, snap-frozen, embedded in OCT and cut into 10 µm thick sections. Next, the sections were fixed, blocked and stained with the primary antibodies rat anti-mouse endothelial cell (Meca-32) and FITC-conjugated mouse anti-pimonidazole (Chemicon), followed by Cy3-conjugated donkey anti-rat secondary IgG (Jackson Immunoresearch). A minimum of six random photographs was taken of each tissue and an average of three animals per group was used to quantify hypoxia.

Hydroxyproline Analysis

Mice were anesthetized with isoflurane and organs were removed and weighed as described before. Organs were then snap frozen, lyophilized, weighed (dry weight), pulverized and subjected to complete acid hydrolysis with 6 N HCl for 18 hours at 120°C. Each sample was then neutralized to pH7 with 4N NaOH. One ml of Chloramine T was added to 2 ml volumes of collagen sample and incubated at room temperature for 20 minutes. One ml of Ehrlich's Reagent (60% perchloric acid, 15 ml 1-propanol, 3.75 g p-dimethyl-amino-benzaldehyde in 25 ml) was added and samples were incubated at 60°C for 20 minutes. Absorbance at 558 λ was read on a spectrophotometer. Collagen was quantified as μg hydroxyproline per mg dry weight of starting material.

Statistical Analyses

Metastatic incidence rates, the number of mice with metastasis divided by the total number of mice in the group, were compared between *Sparc*$^{+/+}$ and *Sparc*$^{-/-}$ groups by logistic regression model, assuming a binomial distribution. Metastatic event rates, the number of metastatic events divided by the total number of mice, were compared between *Sparc*$^{+/+}$ and *Sparc*$^{-/-}$ groups by Poisson regression model, assuming a Poisson distribution. We assume metastatic events in different organs were independent. Both Logistic regression and Poisson regression were implanted in R software (R Development Core Team; http://www.R-project.org) [81]. Unpaired Student's t test of immunohistochemistry quantification was carried out in GraphPad Prism (GraphPad Software, San Diego, A) where a p-value less than 0.05 was considered significant. The survival curves were analyzed in GraphPad Prism with the Gehan-Breslow-Wilcoxon test.

Acknowledgements

We gratefully acknowledge Dr. Tom Wight and members of the Brekken laboratory for helpful discussion, the Molecular and Cellular Imaging Facility at UT-Southwestern for assistance with TEM, Dr. Shane E. Holloway for assistance with surgical implantation of tumor cells and Dr. Larry Fisher for providing anti-collagen I antibody LF-67. The hybridoma MECA-32, developed by Dr. Eugene C. Butcher, was obtained from the Developmental Studies Hybridoma Bank developed under the auspices of NICHD and maintained by The University of Iowa (Iowa City, IA 52242). This study was supported in part by The Effie Marie Cain Scholarship in Angiogenesis Research (RAB) and the NIH (R01CA118240 to RAB & R01GM40711 to EHS). SA was supported by the NIH training grant (GM007062). DC was supported by the NIH/NCRR grant (K26RR024196). PP was supported by Helsinki and Turku University Central Hospital Research grants (EVO) and a grant from Sigrid Juselius Foundation.

Competing Interests Statement

The authors declare no competing interests.

Author Contributions

SAA contributed to the design and execution of all experiments, performed the data analysis and wrote the manuscript. LBR assisted with animal studies. AFM contributed to the initial design and optimization of the permeability and perfusion studies. JGC assisted

in the maintenance of the animal colony and contributed to the animal studies. SPD performed surgical implantation of tumor cells and assisted in animal studies. DC reviewed the pathology of tumor/tissue sections. YX performed the statistical analysis on the metastatic incidence and events. EHS provided reagents, contributed to interpretation of results and aided in the drafting of the manuscript. PP performed the tumor studies, contributed to interpretation of results and aided in the drafting of the manuscript. ADB performed hydroxyproline analysis, contributed to interpretation of results and aided in the drafting of the manuscript. RAB oversaw the design, execution, and interpretation of the experiments and writing of the manuscript.

References

1. Korc, M., *Pancreatic cancer-associated stroma production.* Am J Surg, 2007. **194**(4 Suppl): p. S84-6.

2. Desmouliere, A., C. Guyot, and G. Gabbiani, *The stroma reaction myofibroblast: a key player in the control of tumor cell behavior.* Int J Dev Biol, 2004. **48**(5-6): p. 509-17.

3. Zalatnai, A., *Molecular aspects of stromal-parenchymal interactions in malignant neoplasms.* Curr Mol Med, 2006. **6**(6): p. 685-93.

4. Wernert, N., *The multiple roles of tumour stroma.* Virchows Arch, 1997. **430**(6): p. 433-43.

5. Liotta, L.A. and E.C. Kohn, *The microenvironment of the tumour-host interface.* Nature, 2001. **411**(6835): p. 375-9.

6. Bornstein, P., *Thrombospondins as matricellular modulators of cell function.* J Clin Invest, 2001. **107**(8): p. 929-34.

7. Bornstein, P. and E.H. Sage, *Matricellular proteins: extracellular modulators of cell function.* Curr Opin Cell Biol, 2002. **14**(5): p. 608-16.

8. Brekken, R.A. and E.H. Sage, *SPARC, a matricellular protein: at the crossroads of cell-matrix communication.* Matrix Biol, 2001. **19**(8): p. 816-27.

9. Framson, P.E. and E.H. Sage, *SPARC and tumor growth: where the seed meets the soil?* J Cell Biochem, 2004. **92**(4): p. 679-90.

10. Bornstein, P., *Cell-matrix interactions: the view from the outside.* Methods Cell Biol, 2002. **69**: p. 7-11.

11. Reed, M.J., et al., *Differential expression of SPARC and thrombospondin 1 in wound repair: immunolocalization and in situ hybridization.* J Histochem Cytochem, 1993. **41**(10): p. 1467-77.

12. Podhajcer, O.L., et al., *The role of the matricellular protein SPARC in the dynamic interaction between the tumor and the host.* Cancer Metastasis Rev, 2008. **27**(4): p. 691-705.

13. Pen, A., et al., *Molecular markers of extracellular matrix remodeling in glioblastoma vessels: microarray study of laser-captured glioblastoma vessels.* Glia, 2007. **55**(6): p. 559-72.

14. Mendis, D.B., G.O. Ivy, and I.R. Brown, *SPARC/osteonectin mRNA is induced in blood vessels following injury to the adult rat cerebral cortex.* Neurochem Res, 1998. **23**(8): p. 1117-23.

15. Yan, Q., et al., *Alterations in the lens capsule contribute to cataractogenesis in SPARC-null mice.* J Cell Sci, 2002. **115**(Pt 13): p. 2747-56.

16. Bradshaw, A.D., et al., *SPARC-null mice display abnormalities in the dermis characterized by decreased collagen fibril diameter and reduced tensile strength.* J Invest Dermatol, 2003. **120**(6): p. 949-55.

17. Sage, H., et al., *SPARC, a secreted protein associated with cellular proliferation, inhibits cell spreading in vitro and exhibits Ca+2-dependent binding to the extracellular matrix.* J Cell Biol, 1989. **109**(1): p. 341-56.

18. Sasaki, T., et al., *Crystal structure and mapping by site-directed mutagenesis of the collagen-binding epitope of an activated form of BM-40/SPARC/osteonectin.* EMBO J, 1998. **17**(6): p. 1625-34.

19. Sasaki, T., N. Miosge, and R. Timpl, *Immunochemical and tissue analysis of protease generated neoepitopes of BM-40 (osteonectin, SPARC) which are correlated to a higher affinity binding to collagens.* Matrix Biol, 1999. **18**(5): p. 499-508.

20. Bradshaw, A.D., et al., *Primary mesenchymal cells isolated from SPARC-null mice exhibit altered morphology and rates of proliferation.* Mol Biol Cell, 1999. **10**(5): p. 1569-79.

21. Nie, J., et al., *IFATS collection: Combinatorial peptides identify alpha5beta1 integrin as a receptor for the matricellular protein SPARC on adipose stromal cells.* Stem Cells, 2008. **26**(10): p. 2735-45.

22. Weaver, M.S., G. Workman, and E.H. Sage, *The copper binding domain of SPARC mediates cell survival in vitro via interaction with integrin beta1 and activation of integrin-linked kinase.* J Biol Chem, 2008. **283**(33): p. 22826-37.

23. Raines, E.W., et al., *The extracellular glycoprotein SPARC interacts with platelet-derived growth factor (PDGF)-AB and -BB and inhibits the binding of PDGF to its receptors.* Proc Natl Acad Sci U S A, 1992. **89**(4): p. 1281-5.

24. Kupprion, C., K. Motamed, and E.H. Sage, *SPARC (BM-40, osteonectin) inhibits the mitogenic effect of vascular endothelial growth factor on microvascular endothelial cells.* J Biol Chem, 1998. **273**(45): p. 29635-40.

25. Hasselaar, P. and E.H. Sage, *SPARC antagonizes the effect of basic fibroblast growth factor on the migration of bovine aortic endothelial cells.* J Cell Biochem, 1992. **49**(3): p. 272-83.

26. Francki, A., et al., *SPARC regulates TGF-beta1-dependent signaling in primary glomerular mesangial cells.* J Cell Biochem, 2004. **91**(5): p. 915-25.

27. Chin, D., et al., *Novel markers for poor prognosis in head and neck cancer.* Int J Cancer, 2005. **113**(5): p. 789-97.

28. Choi, P., et al., *Examination of oral cancer biomarkers by tissue microarray analysis.* Arch Otolaryngol Head Neck Surg, 2008. **134**(5): p. 539-46.

29. Kato, Y., et al., *Expression of SPARC in tongue carcinoma of stage II is associated with poor prognosis: an immunohistochemical study of 86 cases.* Int J Mol Med, 2005. **16**(2): p. 263-8.

30. Xue, L.Y., et al., *Tissue microarray analysis reveals a tight correlation between protein expression pattern and progression of esophageal squamous cell carcinoma.* BMC Cancer, 2006. **6**: p. 296.

31. Cheetham, S., et al., *SPARC promoter hypermethylation in colorectal cancers can be reversed by 5-Aza-2'deoxycytidine to increase SPARC expression and improve therapy response.* Br J Cancer, 2008. **98**(11): p. 1810-9.

32. Yang, E., et al., *Frequent inactivation of SPARC by promoter hypermethylation in colon cancers.* Int J Cancer, 2007. **121**(3): p. 567-75.

33. Mok, S.C., et al., *SPARC, an extracellular matrix protein with tumor-suppressing activity in human ovarian epithelial cells.* Oncogene, 1996. **12**(9): p. 1895-901.

34. Kahn, S.L., et al., *Quantitative methylation-specific PCR for the detection of aberrant DNA methylation in liquid-based Pap tests.* Cancer, 2008. **114**(1): p. 57-64.

35. Sova, P., et al., *Discovery of novel methylation biomarkers in cervical carcinoma by global demethylation and microarray analysis.* Cancer Epidemiol Biomarkers Prev, 2006. **15**(1): p. 114-23.

36. Wang, Y., et al., *Survey of differentially methylated promoters in prostate cancer cell lines.* Neoplasia, 2005. **7**(8): p. 748-60.

37. Wong, S.Y., et al., *Analyses of the role of endogenous SPARC in mouse models of prostate and breast cancer.* Clin Exp Metastasis, 2008. **25**(2): p. 109-18.

38. Sato, N., et al., *SPARC/osteonectin is a frequent target for aberrant methylation in pancreatic adenocarcinoma and a mediator of tumor-stromal interactions.* Oncogene, 2003. **22**(32): p. 5021-30.

39. Infante, J.R., et al., *Peritumoral fibroblast SPARC expression and patient outcome with resectable pancreatic adenocarcinoma.* J Clin Oncol, 2007. **25**(3): p. 319-25.

40. Rodriguez-Jimenez, F.J., et al., *Overexpression of SPARC protein contrasts with its transcriptional silencing by aberrant hypermethylation of SPARC CpG-rich region in endometrial carcinoma.* Oncol Rep, 2007. **17**(6): p. 1301-7.

41. Suzuki, M., et al., *Aberrant methylation of SPARC in human lung cancers.* Br J Cancer, 2005. **92**(5): p. 942-8.

42. Brekken, R.A., et al., *Enhanced growth of tumors in SPARC null mice is associated with changes in the ECM.* J Clin Invest, 2003. **111**(4): p. 487-95.

43. Puolakkainen, P.A., et al., *Enhanced growth of pancreatic tumors in SPARC-null mice is associated with decreased deposition of extracellular matrix and reduced tumor cell apoptosis.* Mol Cancer Res, 2004. **2**(4): p. 215-24.

44. Arnold, S., et al., *Forced expression of MMP9 rescues the loss of angiogenesis and abrogates metastasis of pancreatic tumors triggered by the absence of host SPARC.* Exp Biol Med (Maywood), 2008. **233**(7): p. 860-73.

45. Morgan, S.M., et al., *Biochemical characterization and molecular cloning of a novel endothelial-specific sialomucin.* Blood, 1999. **93**(1): p. 165-75.

46. Liu, C., et al., *Human endomucin is an endothelial marker.* Biochem Biophys Res Commun, 2001. **288**(1): p. 129-36.

47. Ran, S., et al., *Evaluation of novel antimouse VEGFR2 antibodies as potential antiangiogenic or vascular targeting agents for tumor therapy.* Neoplasia, 2003. **5**(4): p. 297-307.

48. Brekken, R.A., et al., *Vascular endothelial growth factor as a marker of tumor endothelium.* Cancer Res, 1998. **58**(9): p. 1952-9.

49. Hallmann, R., et al., *Novel mouse endothelial cell surface marker is suppressed during differentiation of the blood brain barrier.* Dev Dyn, 1995. **202**(4): p. 325-32.

50. Bernstein, E.F., et al., *Long-term sun exposure alters the collagen of the papillary dermis. Comparison of sun-protected and photoaged skin by northern*

analysis, immunohistochemical staining, and confocal laser scanning microscopy. J Am Acad Dermatol, 1996. **34**(2 Pt 1): p. 209-18.

51. Bernstein, E.F., et al., *Differential expression of the versican and decorin genes in photoaged and sun-protected skin. Comparison by immunohistochemical and northern analyses.* Lab Invest, 1995. **72**(6): p. 662-9.

52. Reed, C.C. and R.V. Iozzo, *The role of decorin in collagen fibrillogenesis and skin homeostasis.* Glycoconj J, 2002. **19**(4-5): p. 249-55.

53. McCarthy, J.B. and L.T. Furcht, *Laminin and fibronectin promote the haptotactic migration of B16 mouse melanoma cells in vitro.* J Cell Biol, 1984. **98**(4): p. 1474-80.

54. Ohnishi, T., et al., *Fibronectin-mediated cell migration promotes glioma cell invasion through chemokinetic activity.* Clin Exp Metastasis, 1997. **15**(5): p. 538-46.

55. Ohnishi, T., et al., *Role of fibronectin-stimulated tumor cell migration in glioma invasion in vivo: clinical significance of fibronectin and fibronectin receptor expressed in human glioma tissues.* Clin Exp Metastasis, 1998. **16**(8): p. 729-41.

56. Kaplan, R.N., et al., *VEGFR1-positive haematopoietic bone marrow progenitors initiate the pre-metastatic niche.* Nature, 2005. **438**(7069): p. 820-7.

57. Kim, W.H., et al., *Laminin-1-adherent cancer cells show increased proliferation and decreased apoptosis in vivo.* Anticancer Res, 1999. **19**(4B): p. 3067-71.

58. Wang, H., et al., *Tumor cell alpha3beta1 integrin and vascular laminin-5 mediate pulmonary arrest and metastasis.* J Cell Biol, 2004. **164**(6): p. 935-41.

59. Murdoch, C., et al., *The role of myeloid cells in the promotion of tumour angiogenesis.* Nat Rev Cancer, 2008. **8**(8): p. 618-31.

60. Sica, A., et al., *Macrophage polarization in tumour progression.* Semin Cancer Biol, 2008. **18**(5): p. 349-55.

61. Mantovani, A., et al., *Macrophage polarization: tumor-associated macrophages as a paradigm for polarized M2 mononuclear phagocytes.* Trends Immunol, 2002. **23**(11): p. 549-55.

62. Baluk, P., H. Hashizume, and D.M. McDonald, *Cellular abnormalities of blood vessels as targets in cancer.* Curr Opin Genet Dev, 2005. **15**(1): p. 102-11.

63. Morikawa, S., et al., *Abnormalities in pericytes on blood vessels and endothelial sprouts in tumors.* Am J Pathol, 2002. **160**(3): p. 985-1000.

64. Gerhardt, H. and H. Semb, *Pericytes: gatekeepers in tumour cell metastasis?* J Mol Med, 2008. **86**(2): p. 135-44.

65. Xian, X., et al., *Pericytes limit tumor cell metastasis.* J Clin Invest, 2006. **116**(3): p. 642-51.

66. Juliano, R.L., *Signal transduction by cell adhesion receptors and the cytoskeleton: functions of integrins, cadherins, selectins, and immunoglobulin-superfamily members.* Annu Rev Pharmacol Toxicol, 2002. **42**: p. 283-323.

67. Engbring, J.A. and H.K. Kleinman, *The basement membrane matrix in malignancy.* J Pathol, 2003. **200**(4): p. 465-70.

68. Ioachim, E., et al., *Immunohistochemical expression of extracellular matrix components tenascin, fibronectin, collagen type IV and laminin in breast cancer: their prognostic value and role in tumour invasion and progression.* Eur J Cancer, 2002. **38**(18): p. 2362-70.

69. Timar, J., et al., *Proteoglycans and tumor progression: Janus-faced molecules with contradictory functions in cancer.* Semin Cancer Biol, 2002. **12**(3): p. 173-86.

70. Bingle, L., N.J. Brown, and C.E. Lewis, *The role of tumour-associated macrophages in tumour progression: implications for new anticancer therapies.* J Pathol, 2002. **196**(3): p. 254-65.

71. Guweidhi, A., et al., *Osteonectin influences growth and invasion of pancreatic cancer cells.* Ann Surg, 2005. **242**(2): p. 224-34.

72. Pardali, K. and A. Moustakas, *Actions of TGF-beta as tumor suppressor and pro-metastatic factor in human cancer.* Biochim Biophys Acta, 2007. **1775**(1): p. 21-62.

73. Truty, M.J. and R. Urrutia, *Basics of TGF-beta and pancreatic cancer.* Pancreatology, 2007. **7**(5-6): p. 423-35.

74. Mahadevan, D. and D.D. Von Hoff, *Tumor-stroma interactions in pancreatic ductal adenocarcinoma.* Mol Cancer Ther, 2007. **6**(4): p. 1186-97.

75. Zhou, X., et al., *Small interfering RNA inhibition of SPARC attenuates the profibrotic effect of transforming growth factor beta1 in cultured normal human fibroblasts.* Arthritis Rheum, 2005. **52**(1): p. 257-61.

76. Brune, K., et al., *Genetic and epigenetic alterations of familial pancreatic cancers.* Cancer Epidemiol Biomarkers Prev, 2008. **17**(12): p. 3536-42.

77. Hong, S.M., et al., *Multiple genes are hypermethylated in intraductal papillary mucinous neoplasms of the pancreas.* Mod Pathol, 2008. **21**(12): p. 1499-507.

78. Norose, K., et al., *SPARC deficiency leads to early-onset cataractogenesis.* Invest Ophthalmol Vis Sci, 1998. **39**(13): p. 2674-80.

79. Bruns, C.J., et al., *In vivo selection and characterization of metastatic variants from human pancreatic adenocarcinoma by using orthotopic implantation in nude mice.* Neoplasia, 1999. **1**(1): p. 50-62.

80. Murphy, C.L. and M.J. Lever, *A ratiometric method of autofluorescence correction used for the quantification of Evans blue dye fluorescence in rabbit arterial tissues.* Exp Physiol, 2002. **87**(2): p. 163-70.

81. *A language and environment for statistical computing*. 2005, Vienna, Austria: R Foundation for Statistical Computing.

CHAPTER FOUR

TGFβ1 inhibition is sufficient to extend survival and curtail metastasis of pancreatic carcinoma in SPARC-null mice

Shanna A. Arnold[1], Lee B. Rivera[1], Juliet G. Carbon[1], Chi-Lun Chang[1], Sean P. Dineen[1], Amy D. Bradshaw[2] and Rolf A. Brekken*[1].

[1]Hamon Center for Therapeutic Oncology Research, Departments of Surgery and Pharmacology, University of Texas Southwestern Medical Center, Dallas, TX 75390 USA.

[2]Department of Medicine, Medical University of South Carolina, Charleston, SC 29412.

Running header 'TGFβ1 rescues survival of *SPARC-null* mice'

*Corresponding Author:
Rolf A. Brekken, PhD
Hamon Center for Therapeutic Oncology Research
UT-Southwestern Medical Center
6000 Harry Hines Blvd.
Dallas, TX 75390-8593
Tel: 214 648 5151 Fax: 214 648 4940
e-mail address: rolf.brekken@utsouthwestern.edu

Supported in part by The Effie Marie Cain Scholarship in Angiogenesis Research (to RAB.) and the NIH (R01 CA118240 to RAB). SA was supported in part by a training grant from the NIH (GM007062).

Abstract

Pancreatic adenocarcinoma is the fourth leading cause of cancer-related death in the Western industrialized world, owing to rapid primary tumor growth and ensuing metastasis. Desmoplasia, local invasion and metastasis are prominent characteristics of pancreatic adenocarcinoma. SPARC is a matricellular protein that governs ECM deposition and maturation during tissue remodeling, particularly, during wound healing and tumorigenesis. In the present study, we sought to determine the mechanism by which the lack of host SPARC alters the tumor microenvironment and enhances invasion and metastasis of an orthotopic model of pancreatic cancer. We identified that active TGFβ1 levels were increased significantly in tumors grown in *SPARC-null* mice. TGFβ1 contributes to many aspects of tumor development including metastasis, endothelial cell permeability, inflammation and fibrosis, all of which are altered in the absence of endogenous SPARC. Given these results, we performed a survival study to assess the contribution of increased TGFβ1 activity to tumor progression in *SPARC-null* mice using losartan, an angiotensin II type 1 receptor antagonist that diminishes TGFβ1 expression and activation *in vivo*. Tumors grown in *SPARC-null* mice progressed more quickly than those grown in *wild-type* littermates leading to a significant reduction in median survival. However, median survival of *SPARC-null* animals treated with losartan was extended to that displayed by losartan-treated *wild-type* controls. In addition, losartan treatment reduced local invasion and metastasis, decreased vascular permeability and altered the immune profile of tumors grown in *SPARC-null* mice. This data supports the concept that aberrant TGFβ1-activation in the absence of host SPARC contributes significantly to tumor progression and suggests that SPARC, by controlling ECM deposition and maturation, can regulate cytokine availability and activation.

Key words:

extracellular matrix, metastasis, osteonectin, pancreatic cancer, SPARC, TGFβ1

Introduction

In 2009, it is estimated that 43,000 people will be diagnosed with pancreatic adenocarcinoma in the United States, while 35,000 patients will die from the disease [SEER]. The five year survival rate is a dismal 5.5% due to the fact that only 7% of patients are diagnosed while the cancer is locally confined [SEER]. Therefore, it is imperative to understand the mechanisms driving invasion and metastasis in pancreatic adenocarcinoma to develop new approaches to combat the disease in the high percentage of cases whose tumor has already spread beyond its local borders.

SPARC (secreted protein acidic and rich in cysteine) is a glycoprotein that belongs to the matricellular class of proteins, a functional family of extracellular proteins involved in the regulation of extracellular matrix (ECM) deposition and remodeling. Although principally non-structural, matricellular proteins influence the structural integrity and composition of the ECM. SPARC expression, after development, is limited to areas of high ECM turnover, such as bone and gut [1]. However, SPARC expression is upregulated during wound-healing, angiogenesis and tumorigenesis [1-5]. *SPARC-null* (*SPARC-/-*) mice display characteristics suggestive of ECM defects, such as early cataract development, progressive osteopenia, lax skin and a curly tail [6]. In fact, collagen deposition and fibrillogenesis were found to be disrupted in the lens capsule and dermis of *SPARC-/-* mice [7, 8]. These data suggest that SPARC is required for and mediates ECM deposition and tissue remodeling.

In addition to its function in ECM assembly, SPARC either directly binds to or indirectly regulates several growth factors including platelet-derived growth factor (PDGF), fibroblast growth factor (FGF), vascular endothelial growth factor (VEGF) and

transforming growth factor β (TGFβ) [9-12]. Like SPARC, TGFβ is multifunctional signaling protein implicated in wound-healing and fibrosis, as well as tumor progression and metastasis [13-15]. In fact, data suggests that there is a reciprocal regulatory feedback loop between SPARC and TGFβ, whereby TGFβ induces the expression of SPARC and, in turn, SPARC modulates the expression and activity of TGFβ [12, 16-20]. Additionally, SPARC may modulate growth factor signaling indirectly is by regulating the deposition and composition of the ECM which, subsequently, controls the bioavailability of chemokines including TGFβ.

Previously, we demonstrated that in an orthotopic murine model of pancreatic adenocarcinoma, invasion and metastasis was increased in the absence of host SPARC. Consequently, tumor-bearing *SPARC-/-* mice experienced increased morbidity and decreased survival. In addition, we observed a clear reduction in the deposition of fibrillar collagens I and III, basement membrane collagen IV and the collagen-associated proteoglycan decorin in tumors grown in *SPARC-/-* mice. Paradoxically, tumors grown in *SPARC-/-* mice displayed a significant decrease in microvessel density and pericyte recruitment despite increases in invasion and metastasis. Enhanced vascular permeability and perfusion due to alterations in the vascular basement membrane led to decreased hypoxia in tumors established in the absence of host SPARC. Lastly, tumors grown in *SPARC-/-* mice displayed enhanced recruitment of fibroblasts and alternatively-activated (M2) macrophages [Arnold et al. in press DMM, Thesis Chapter 3].

In the current study, we discovered that PAN02 tumors grown orthotopically in *SPARC-/-* mice have significantly increased levels of active TGFβ1 relative to those grown in *wild-type* (*SPARC+/+)* counterparts. To assess the contribution of excess active

TGFβ1 on invasion, metastasis, survival, angiogenesis and immune modulation in the absence of host SPARC, TGFβ1 expression and activation was inhibited by treatment with the angiotensin II type 1 receptor antagonist, losartan. We now report that losartan decreased invasion and metastasis, abrogated vasodilation, restricted permeability and regulated immune tolerance in tumor-bearing *SPARC*-/- mice, which effectively restored median survival to that of *SPARC*+/+ mice. We have provided evidence that the aberrant activation of TGFβ1 in the tumor microenvironment lacking host SPARC contributes significantly to the phenotypic alterations observed during progression of orthotopic PAN02 tumors. We conclude that TGFβ1 is predominantly responsible for the increased tumor dissemination and decreased survival observed in tumor-bearing *SPARC*-/- animals.

Results

There is enhanced activation of transforming growth factor beta in tumors grown in SPARC-null mice.

We previously showed that orthotopic pancreatic tumor growth of PAN02 cells is more invasive and metastatic in the absence of host SPARC and that this confers a decrease in the survival of *Sparc-null* (*SPARC-/-*) mice relative to *wild-type* (*SPARC+/+*) littermates [Arnold et al. in press DMM, Thesis Chapter 3]. In addition, tumors grown in *SPARC-/-* mice displayed alterations in angiogenesis, extracellular matrix (ECM) deposition and immune cell recruitment. Specifically, although microvessel density was reduced in tumors grown in the absence of host SPARC, the vascular basement membrane was compromised leading to enhanced permeability and decreased hypoxia. Collagen deposition and fibrillogenesis was also decreased. Furthermore, tumors grown in *SPARC-/-* mice displayed increased recruitment and activation of fibroblasts and alternatively-activated macrophages (M2). These alterations are summarized in Table 1.

Table 1. Summary of Tumor-Associated Effects in SPARC-/- Mice

Tumor Growth	**Tumor Weight**	**NC**
	Invasion & Metastasis	↑
	Survival	↓
Microvascular Properties	**Microvessel Density**	↓
	Pericyte Coverage	↓
	Vascular Basement Membrane Density	↓
	Permeability	↑
	Hypoxia	↓
Extracellular Matrix	**Collagen Deposition**	↓
	Collagen Fibrillogenesis	↓
	Decorin Content	↓
Immune Response	**Fibroblasts**	↑
	Neutrophils	**NC**
	Total Macrophages	↑
	M1 Macrophages	**NC**
	M2 Macrophages	↑

Table summarizing the tumor-associated effects previously analyzed in the PAN02 orthotopic tumor model. Arrows indicate whether *SPARC-/-* mice displayed an increase (↑) or decrease (↓) compared to *SPARC+/+* mice. NC indicates no change.

Although we discovered many changes in the tumor microenvironment of *SPARC-/-* compared to *SPARC+/+* animals, the underlying cause for increased invasion/metastasis and decreased survival remained elusive. An initial finding was that tumors grown in the absence of host SPARC displayed reduced deposition of the collagen-binding proteoglycan, decorin, presumably due to diminished deposition of collagen. We validated and quantified this result with fluorescence immunohistochemistry and found that decorin deposition in tumors grown in *SPARC-/-* mice was significantly reduced, not only within tumors, but at the tumor capsule (Figure 1A, $p=0.0051$). Decorin and other ECM proteins have been shown to bind, contribute to the bioavailability and modulate the activation of growth factors and cytokines [21]. We suspected that the diminished ECM associated with the absence of host SPARC might enhance tumor progression by altering growth factor localization and availability. In particular, it is established that decorin can directly bind and regulate the activity of transforming growth factor-beta (TGFβ) [22-25]. Immunohistochemistry was performed utilizing antibodies directed against biologically active and total TGFβ1. The results revealed that, although there was no change in total TGFβ1 (Figure 1C), there was a significant increase in active TGFβ1 in tumors grown in the absence of host SPARC (Figure 1B, $p<0.0001$). This was particularly apparent in spontaneous abnormal ducts in the PAN02 tumors. In addition, an ELISA specific for active TGFβ1 was performed on *SPARC+/+* and *SPARC-/-* tumor lysates. By ELISA, active TGFβ1 was increased by nine-fold in tumors grown in *SPARC-/-* compared to *SPARC+/+* mice (Figure 1B, bottom center, $p<0.0001$).

Therefore, the deposition of ECM proteins such as collagen and decorin, essential to the modulation of growth factors, is diminished during tumor progression in SPARC-/- mice. Contrary to what was expected if ECM proteins act as a repository for growth factors, active TGFβ1 was increased in tumors grown in *SPARC*-/- mice. We suspect that this increase is due to reduced sequestration of total TGFβ1 by the ECM, which would allow enhanced binding and activation of TGFβ1 at the cell surface. This is supported by the fact that the majority of the active TGFβ1 is found localized to ductal structures within the tumor (Figure 1B, dotted lines).

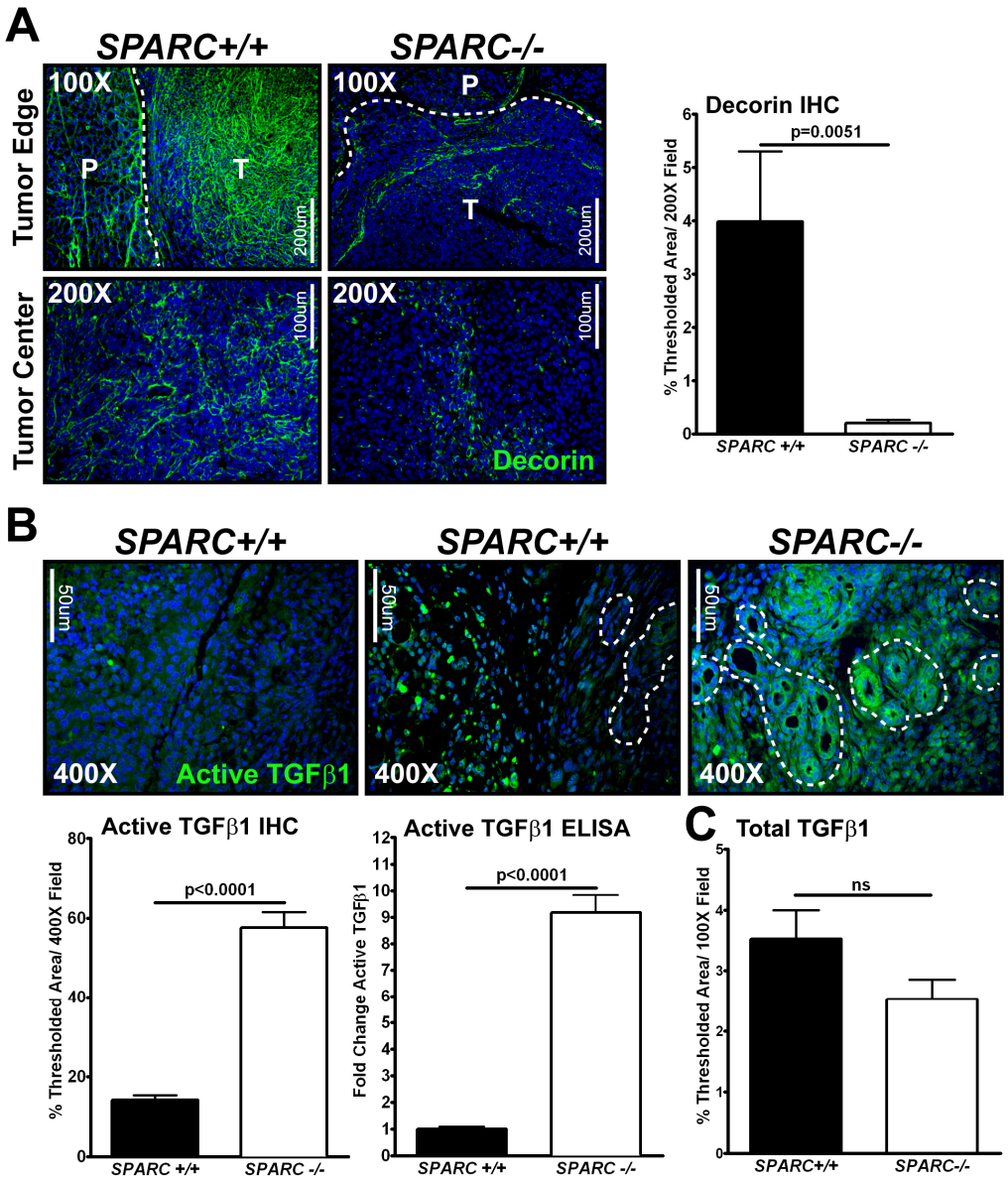

Figure 1. TGFβ1 and the TGFβ Binding Proteoglycan, Decorin, in Orthotopic PAN02 Tumors. Fluorescence immunohistochemistry was utilized to quantify the amount of active and total TGFβ1, as well as decorin in tumors grown in *SPARC*+/+ and *SPARC*-/- mice (A-C). (A) Tumor sections were stained with antibody goat anti-decorin (green) and percent thresholded area quantified. DAPI (blue) marks cell nuclei. Images were taken at the tumor edge (top panels) and the tumor center (bottom panels). Total magnification is 100X and 200X as indicated. Dotted lines indicate the border between the tumor (T) and normal pancreas (P). (B) Tumor sections were stained with an antibody rabbit anti-TGFβ1 (green) specific for the active form and percent thresholded area

quantified. DAPI (blue) marks cell nuclei. Total magnification is 400X as indicated. Dotted lines indicate spontaneous abnormal ducts arising from the PAN02 cells within the tumor. The amount of active TGFβ1 in tumor lysates was also measured using a commercial sandwich ELISA kit (G7591 Promega). Data represents two independent assays that are combined by normalizing all samples to *SPARC*+/+ and recorded as fold change. 50ug of total protein was loaded per well and samples were run in either duplicate or quadruplicate. (C) Total TGFβ1 protein within tumors was assessed with antibody rabbit anti-TGFβ1,2 and percent thresholded area quantified. All p-values were calculated with a Student's t-test. ns, not significant.

Attenuation of TGFβ1 via an angiotensin II type 1 receptor antagonist rescues survival of SPARC-null mice.

Many of the phenotypic changes observed during tumor progression in *SPARC*-/- mice, such as enhanced vascular permeability, increased metastasis, decreased survival and immune tolerance, mimic effects identified downstream of TGFβ1 [14, 15, 26, 27]. A survival study was performed to determine the extent of which augmented activation of TGFβ1 within the tumor microenvironment contributes to tumor progression, metastasis and survival in *SPARC*-/- mice [Arnold et al. in press DMM, Thesis Chapter 3]. Mice bearing orthotopic PAN02 tumors were treated with an angiotensin II type 1 receptor antagonist, losartan, shown to be effective at inhibiting the expression and activation of TGFβ1 [28-30]. As previously reported, *SPARC*-/- mice succumbed to tumor burden more rapidly than their SPARC+/+ counterparts with a median survival of 28.0 days compared to 35.5 days (Figure 2A, p=0.0184). Although targeting TGFβ1 with losartan had no significant effect on survival of *SPARC*+/+ animals, the median survival of *SPARC*-/- mice was extended from 28.0 days without to 40.0 days with treatment (Figure 2A, p=0.0129). In fact, Losartan therapy was able to rescue the survival of *SPARC*-/-

mice bearing orthotopic PAN02 tumors, with a median survival equivalent to losartan-treated *SPARC*+/+ mice (Figure 2A). Losartan treatment delayed but was unable to prevent invasive and metastatic progression, as every animal exhibited extensive and aggressive tumor burden at time of sacrifice. Figure 2B reveals the typical aggressive behavior of the PAN02 orthotopic model, with local invasion into adjacent organs such as the spleen, visceral adipose, abdominal muscle and intestine, as well as distant metastasis to the liver. Losartan therapy, however, reduced the splenomegaly associated with PAN02 tumor progression (Figure 2B, graph). The splenomegaly appeared to be a result of local tumor invasion and accumulation of immune cells.

Therefore, aberrant activation of TGFβ1 contributes significantly to augmented tumor progression in the absence of host SPARC as inhibition of TGFβ1 with losartan effectively rescued the survival of *SPARC*-/- mice.

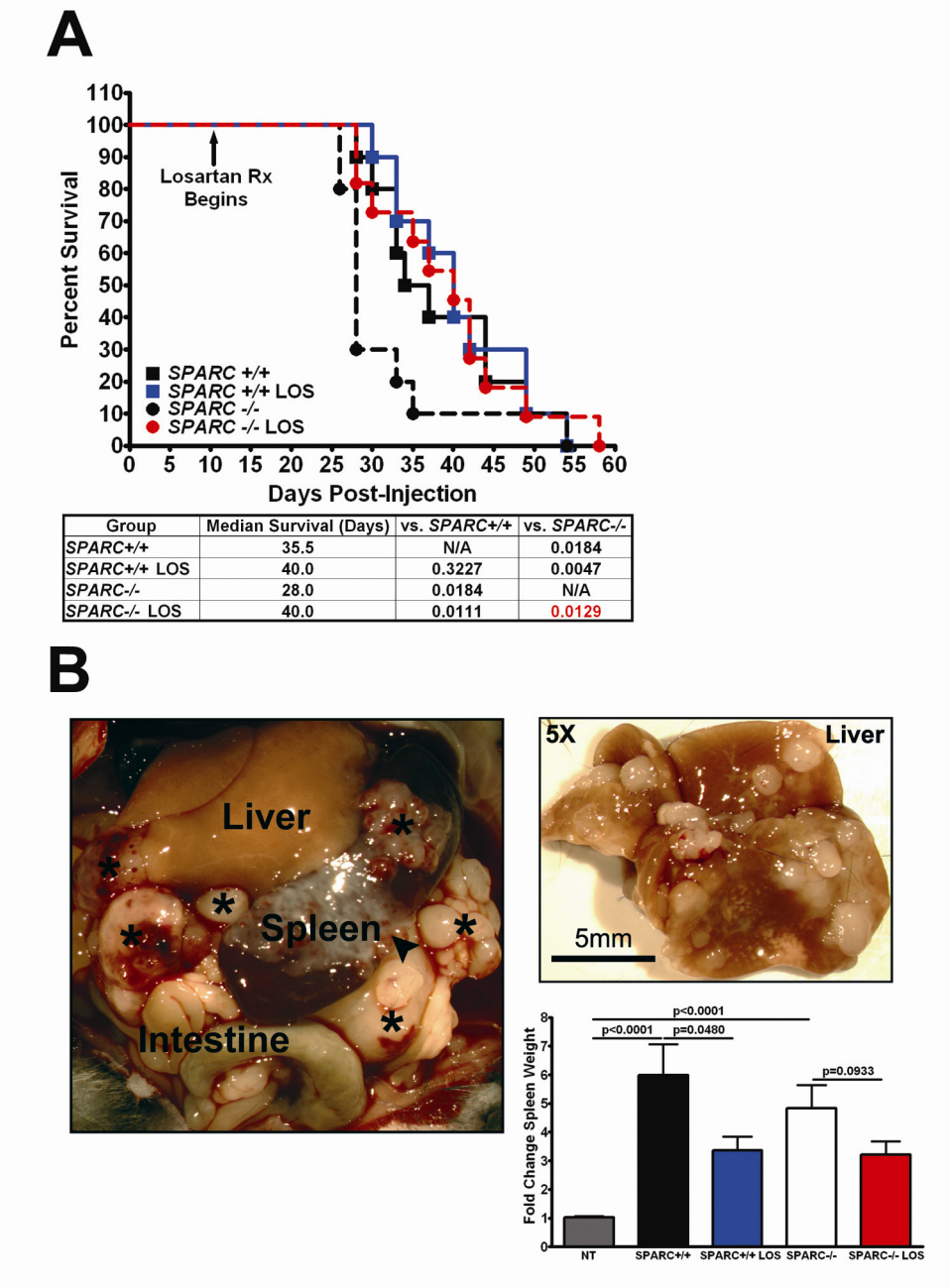

Group	Median Survival (Days)	vs. *SPARC*+/+	vs. *SPARC*-/-
SPARC+/+	35.5	N/A	0.0184
SPARC+/+ LOS	40.0	0.3227	0.0047
SPARC-/-	28.0	0.0184	N/A
SPARC-/- LOS	40.0	0.0111	0.0129

Figure 2. Orthotopic PAN02 Survival Study. 1x10^6 PAN02 cells were injected into the tail of the pancreas of *SPARC*+/+ and *SPARC*-/- mice. Tumors were allowed to grow for 10 days prior to initiation of losartan therapy (600 mg/L) via drinking water *ad libitum* in 2% sucrose. A) Survival curve of *SPARC*+/+ and *SPARC*-/- mice treated with losartan (LOS). The table lists the median survival and associated p-values calculated with the

Gehan-Breslow-Wilcoxon test (n=10/group). (B, left) Low power (5X) *ex vivo* image of typical PAN02 tumor progression. Tumor nodules (*) are extensive throughout the abdomen and splenic invasion (arrowhead) is common. (B, right) Liver metastasis also occurs frequently and is shown in this *ex vivo*, low magnification (5X) shot. Scale bar (5 mm) is indicated. (C) Spleens were weighed and the fold change calculated based on the weight of spleens taken from non-tumor bearing (NT) mice. Significance was determined by a Student's t-test and all significant p-values are indicated.

Attenuation of TGFβ1 via an angiotensin II type 1 receptor antagonist reduces invasion and metastasis in SPARC-null mice.

To adequately assess the affect of TGFβ1 inhibition on tumor progression, local invasion and metastasis, an endpoint study was performed, whereby, losartan treatment was initiated the day following PAN02 tumor injection and all animals were sacrificed at four weeks, regardless of tumor burden or health status. This endpoint study revealed that losartan treatment was able to control both local invasion and metastasis in *SPARC*+/+ and *SPARC*-/- mice. Although there were no differences in tumor/pancreas weights between genotypes or treatment groups (data not shown), the tumor growth appeared more isolated and controlled in the losartan-treated groups compared to untreated counterparts, whereby, more residual pancreas was retained (Figure 3A). Furthermore, losartan therapy reduced the number of animals in each group with signs of local invasion (invasion incidence) and the number of adjacent organs involved (total invasive events) (Table 2). The effect of losartan on local invasion was apparent in the *SPARC*-/- mice, but not observed in *SPARC*+/+ mice (Table 2). Local invasion occurred predominantly in the visceral adipose, abdominal muscle, intestine/mesentery and spleen (Figure 3B). *SPARC*+/+ and *SPARC*-/- mice responded to therapy with a reduction in the number of

animals in each group with metastatic dissemination (metastatic incidence) and a diminution in the number of macroscopic metastatic lesions (total invasive events) (Table 2). Metastasis occurred predominantly in the mesenteric lymph nodes and liver (Figure 3C). Importantly, although invasion and metastatic incidence and events were increased in *SPARC-/-* compared to *SPARC+/+* mice, as previously reported, losartan was able to "normalize" tumor progression in *SPARC-/-* mice to that observed in *SPARC+/+* counterparts (Table 2 and 3).

Therefore, local invasion and metastasis was effectively controlled by TGFβ1 inhibition, which could account for the survival benefit observed with losartan-treated compared to untreated SPARC-/- mice. This is further evidence that excess TGFβ1 is responsible for the accelerated tumor progression and altered tumor microenvironment of orthotopic PAN02 tumors grown in the absence of host SPARC.

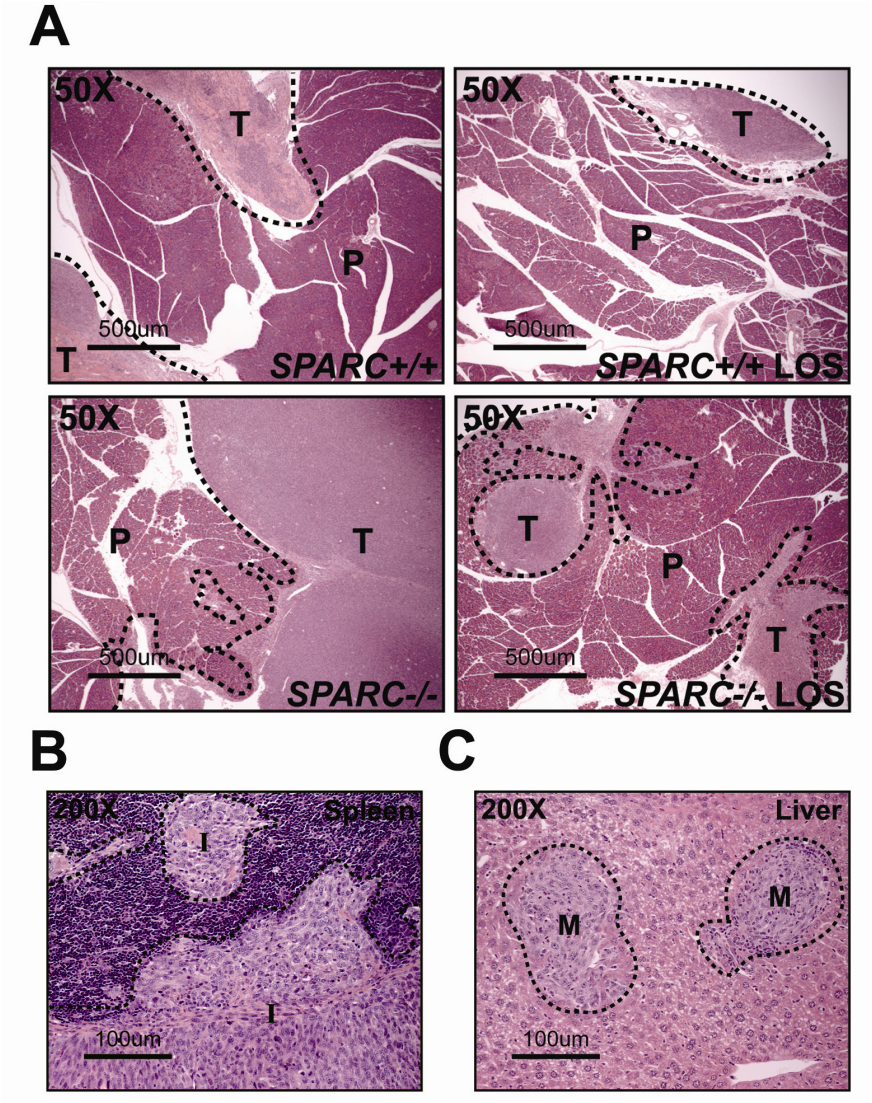

Figure 3. Losartan Reduces Local Invasion and Metastasis of PAN02 Tumors. $1x10^6$ PAN02 cells were injected into the tail of the pancreas of *SPARC*+/+ and *SPARC*-/- mice. Losartan therapy (600 mg/L) via drinking water *ad libitum* in 2% sucrose was initiated 24 hours after tumor cell injection and mice were sacrificed 28 days later. (A) Images of H&E stained primary tumor sections show residual pancreas and the primary tumor border of untreated and losartan-treated (LOS) *SPARC*+/+ and *SPARC*-/- mice. Dotted lines demarcate the normal adjacent pancreas (P) from the primary tumor (T). Total magnification (50X) and scale bars (500 μm) are indicated. (B) H&E section of a spleen displaying disruption of the splenic capsule and local tumor invasion (I). Total magnification (200X) and scale bars (100 μm) are shown. (C) Image of an H&E stained liver section revealing the common site for distant metastasis (M). Total magnification (200X) and scale bars (100 μm) are indicated.

Table 2. Losartan Effect on Tumor Invasion

Invasion Incidence		
Group	**n=**	**Total**
SPARC+/+	10	8 (80%)
SPARC+/+ LOS	8	8 (100%)
SPARC-/-	8	8 (100%)
SPARC-/- LOS	8	4 (50%)

Total Invasive Events			
Group	**n=**	**Total**	**Mean**
SPARC+/+	10	25	2.50
SPARC+/+ LOS	8	20	2.50
SPARC-/-	8	28	3.50
SPARC-/- LOS	8	14	1.75

Animals bearing orthotopic PAN02 tumors were treated with losartan (600 mg/L) via drinking water *ad libitum* in 2% sucrose. Therapy began immediately and the entire group sacrificed 28 days later. Local invasion was defined as tumor growth into adjacent organs with attachment to the primary tumor. Invasion incidence is the number of animals in each group with signs of local invasion. Invasion incidence rates (%) were calculated by dividing the invasion incidence by the total number of mice in the group. Total invasive events were recorded as the total number of organs affected by local invasion and mean invasive events were calculated by dividing the total invasive events by the number of mice in that group.

Table 3. Losartan effect on tumor metastasis

Metastatic Incidence										
Group	n=	Lung	Kidney	Liver	Spleen	Diaphragm	Intestine	I.P.	Other	Total
SPARC+/+	10	0	0	1 (10%)	0	2 (20%)	6 (60%)	4 (40%)	1 (10%)	7 (70%)
SPARC+/+ LOS	8	0	0	0	1 (13%)	0	2 (25%)	2 (25%)	1 (13%)	4 (50%)
SPARC-/-	8	0	0	1 (13%)	1 (13%)	0	7 (88%)	0	1 (13%)	8 (100%)
SPARC-/- LOS	8	0	1 (13%)	0	0	0	6 (75%)	1 (13%)	0	6 (75%)

Total Metastatic Events											
Group	n=	Lung	Kidney	Liver	Spleen	Diaphragm	Intestine	I.P.	Other	Total	Mean
SPARC+/+	10	0	0	1	0	2	15	6	2	26	2.60
SPARC+/+ LOS	8	0	0	0	1	0	4	2	1	8	1.00
SPARC-/-	8	0	0	2	2	0	23	0	1	28	3.50
SPARC-/- LOS	8	0	1	0	0	0	10	3	0	14	1.75

Mice bearing orthotopic PAN02 tumors were treated with losartan (600 mg/L). Therapy began immediately and the entire group sacrificed 28 days later. Metastatic incidences were recorded as the number of mice bearing metastasis in each organ. Metastatic incidence rates (%) were calculated by dividing the metastatic incidence by the total number of mice in the group. Metastatic events were recorded as the total number of individual metastases in each organ. Mean metastatic events were calculated by dividing the total metastatic events by the number of mice in each group.

The angiotensin II type 1 receptor antagonist effectively reduces TGFβ pathway activation in SPARC-null mice.

Although losartan, an angiotensin II type 1 receptor antagonist, has been successfully utilized to inhibit the expression and activation of TGFβ1 in several animal models and in humans, we wanted to validate in our hands that TGFβ1 expression and downstream activation of TGFβ1 response genes were effectively inhibited in our orthotopic model of pancreatic adenocarcinoma. This was accomplished by performing real-time quantitative reverse-transcriptase polymerase chain reaction (qPCR). First, we analyzed the mRNA expression of TGFβ1, TGFβ2, TGFβ3 and thrombospondin-1 (TSP-1). Thrombospondin-1 is a matricellular protein that can function as a co-activator of latent TGFβ family members. TGFβ1 and TSP-1 are induced by the activation of angiotensin II type 1 receptor signaling and it is through reduction in TSP-1 expression that losartan is suspected to reduce the activation of latent TGFβ1 [31, 32]. Although not quite significant due to low sample number, a trend was observed for TGFβ1 in that expression was increased by two-fold in tumors grown in *SPARC-/-* compared to *SPARC+/+* mice (Figure 4A). However, this change was undetectable at the protein level by immunohistochemistry (Figure 1C). Furthermore, losartan abrogated this increase such that mRNA levels in tumors grown in losartan-treated *SPARC-/-* mice were identical to levels detected in both untreated and losartan-treated *SPARC+/+* mice (Figure 4A). TGFβ2 mRNA was undetectable with our current taqman probes (data not shown). On the other hand, TGFβ3 mRNA levels followed a trend similar to TGFβ1, albeit with increased variability and only minimal response to losartan (Figure 4A). The expression

of TSP-1 was similar between *SPARC*+/+ and *SPARC*-/- mice, but as expected with angiotensin II type 1 receptor blockade, it was decreased in losartan-treated compared to untreated tumors in both genotypes (Figure 4A).

Once it was established that losartan reduced not only the expression of TGFβ1 but the expression of a one of its co-activators, TSP-1, the next step was to determine if this inhibition effectively blocked TGFβ1 signaling. To broadly assess losartan effects on TGFβ1 signaling, we chose to perform the commercially available RT^2 Profiler™ PCR Array (PAMM-035; SABiosciences, Frederick, MD). This array measures the mRNA levels of 84 TGFβ response genes. Consistent with the decrease in expression and activation of TGFβ1, many TGFβ response genes revealed altered expression (Table 4). As expected, since tumors grown in the absence of host SPARC harbor increased active TGFβ1, a majority of TGFβ target genes in tumors from *SPARC*-/- mice were elevated more than two-fold compared to tumors from *SPARC*+/+ mice (Table 4, *SPARC*-/- vs. *SPARC*+/+). Relative to untreated counterparts, tumors grown in losartan-treated *SPARC*+/+ and *SPARC*-/- animals showed more than a two-fold decrease of a majority of TGFβ target genes (Table 4, *SPARC*+/+ LOS vs. *SPARC*+/+ and *SPARC*-/- LOS vs. *SPARC*-/-). Most importantly, losartan treatment restored the mRNA expression profile of tumors grown in the absence of host SPARC to similar levels observed in untreated *SPARC*+/+ mice (Figure 4B and Table 4, *SPARC*-/- LOS vs. *SPARC*+/+). Figure 4B shows the cluster analysis performed by the online RT^2 Profiler™ PCR Array software provided by SABiosciences. Notice that the most closely associated TGFβ gene profiles are from tumors grown in *SPARC*+/+ and losartan-treated *SPARC*-/- mice (Figure 4B).

As a visual, Figure 4C shows heatmaps of the TGFβ response genes listed in Table 4, where each box represents a separate gene in the PCR array and each map is a relative comparison between two groups. For example, as stated above, tumors from *SPARC-/-* mice had increased regulation of TGFβ response genes in comparison to *SPARC+/+* mice so in this heatmap many boxes are red for increased fold regulation (Figure 4C). Likewise, many boxes are green in the heatmap comparing tumors from losartan-treated to untreated *SPARC-/-* animals due to down-regulation of TGFβ1 signaling (Figure 4C).

Therefore, it is clear that losartan was able to effectively reduce the expression, activation and signaling of TGFβ1 during tumor progression in the absence of host SPARC. However, further validation is needed to prove that it is through the inhibition of TGFβ1 and not angiotensin II that tumor progression is decelerated in *SPARC-/-* mice. This will be accomplished by repeating the survival and endpoint studies utilizing 1D11, a neutralizing monoclonal antibody specific for TGFβ1, and comparing the results to losartan therapy.

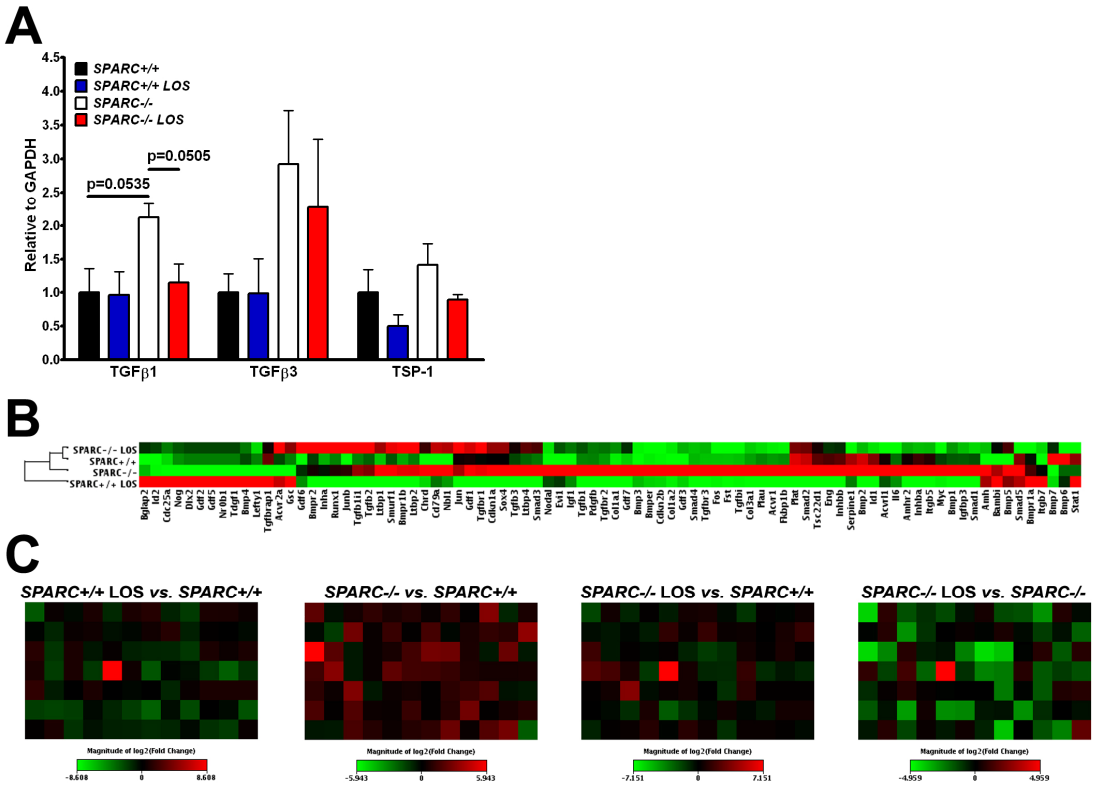

Figure 4. Losartan Effectively Inhibits TGFβ1 Expression and Signaling in Tumors from *SPARC-/-* Mice. (A) The mRNA expression of TGFβ1, TGFβ3 and TSP-1 in tumors from *SPARC*+/+ and *SPARC*-/- mice treated with losartan was assessed with taqman-based qPCR. n=3/group and p-values were calculated with the Student's t-test. (B) Clustergram results from the RT^2 Profiler™ PCR Array (PAMM-035; SABiosciences). Green indicates negative fold-regulation, whereas red indicates positive fold-regulation relative to six internal control genes. (C) Heatmaps from the RT^2 Profiler™ PCR Array displaying the TGFβ response genes listed in Table 4. Each box represents a separate gene in the PCR array and each map is a relative comparison between two groups as indicated. Fold change log^2 scales are shown below each heatmap.

Table 4. Losartan effect on TGFβ signaling pathways

Fold Regulation				
	Relative to *SPARC*+/+			Relative to *SPARC*-/-
Gene Symbol	*SPARC*+/+ LOS	*SPARC*-/-	*SPARC*-/- LOS	*SPARC*-/- LOS
Acvr1	-7.7947	4.4878	-3.8591	-17.3186
Acvr2a	1.3264	-1.2968	1.3926	1.8059
Acvrl1	-1.2488	1.4369	-2.0424	-2.9348
Amh	1.9419	2.1406	1.1382	-1.8807
Amhr2	-2.5412	1.5347	-1.7535	-2.6912
Bambi	1.9419	1.7888	1.4507	-1.2331
Bglap2	2.4394	1.1884	1.5853	1.3340
Bmp1	-2.2447	2.1332	-1.2819	-2.7344
Bmp2	-3.8464	1.0703	-2.7497	-2.9429
Bmp3	1.9419	8.4679	1.1382	-7.4397
Bmp4	1.8207	-1.8113	-1.1347	1.5963
Bmp5	1.3943	1.5168	1.3321	-1.1386
Bmp6	-1.1507	-1.1867	-1.2908	-1.0877
Bmp7	-2.3030	-2.5263	-1.5511	1.6287
Bmper	1.3027	6.0966	-1.1698	-7.1317
Bmpr1a	1.4727	1.1567	-1.6973	-1.9633
Bmpr1b	-1.4285	2.4470	2.5328	1.0351
Bmpr2	-1.1781	1.0673	1.2507	1.1718
Cd79a	1.5226	2.9588	2.7165	-1.0892
Cdc25a	2.3842	-1.1243	1.2761	1.4347
Cdkn1a	-2.1265	1.5199	1.2993	-1.1698
Cdkn2b	1.0729	2.2423	-1.0198	-2.2867
Chrd	1.0684	1.9386	1.5765	-1.2297
Col1a1	-1.3375	10.1683	2.7967	-3.6357
Col1a2	2.5571	61.5207	3.2193	-19.1099
Col3a1	-3.3323	4.1039	-1.5350	-6.2996
Dlx2	1.9419	-1.4671	1.1382	1.6699
Eng	-1.6466	1.2134	-1.1787	-1.4302
Evi1	1.1814	1.4661	1.1549	-1.2695
Fkbp1b	-2.0958	2.9241	-1.9069	-5.5761
Fos	-2.3158	6.4666	-3.0743	-19.8801
Fst	-2.4360	5.9587	-2.3591	-14.0573
Gdf1	-3.4617	1.5922	1.4915	-1.0675
Gdf2	1.9419	-1.4671	1.1382	1.6699
Gdf3	1.3732	5.3815	1.6503	-3.2609
Gdf5	1.9419	-1.4671	1.1382	1.6699
Gdf6	1.9419	2.7378	5.2954	1.9342
Gdf7	-4.1224	8.8581	3.7862	-2.3396
Gsc	1.9419	-1.4671	1.6595	2.4347
Id1	-3.4738	1.2303	-3.0089	-3.7019
Id2	390.3163	4.5694	142.0987	31.0980

Igf1	1.4305	2.9201	1.5186	-1.9229
Igfbp3	-7.1975	2.8324	-2.1042	-5.9597
Il6	-1.1659	2.3603	-2.2042	-5.2027
Inha	-1.4444	1.6358	2.7240	1.6653
Inhba	-3.4762	1.4419	-2.2883	-3.2995
Inhbb	-9.0223	1.4231	-1.5318	-2.1799
Itgb5	-2.8709	1.4845	-1.9852	-2.9470
Itgb7	3.0791	2.0069	1.1390	-1.7620
Jun	-1.8954	1.2675	1.4179	1.1186
Junb	-1.0292	8.0055	12.9938	1.6231
Lefty1	1.9650	-1.4600	-1.3007	1.1225
Ltbp1	-1.0313	1.2535	1.2006	-1.0441
Ltbp2	-1.1929	1.4479	1.4781	1.0208
Ltbp4	-1.0313	1.0703	1.0380	-1.0311
Myc	-2.3612	2.0111	-2.5602	-5.1488
Nbl1	1.2759	2.4351	2.2203	-1.0968
Nodal	1.9419	3.7166	1.1382	-3.2654
Nog	1.9419	-1.3557	1.1382	1.5430
Nr0b1	1.9419	-1.4671	1.1382	1.6699
Pdgfb	-4.1916	3.3566	1.0576	-3.1739
Plat	-4.6767	1.0504	-1.2069	-1.2677
Plau	-4.3575	3.6100	-2.3090	-8.3354
Runx1	-1.2566	1.2675	1.6299	1.2859
Serpine1	-2.3384	1.1728	-5.7328	-6.7237
Smad1	-4.2442	2.4829	-2.5075	-6.2258
Smad2	-9.5566	1.1111	-1.2161	-1.3512
Smad3	-1.3972	1.7826	1.4023	-1.2713
Smad4	-5.6197	6.0629	-1.1690	-7.0874
Smad5	1.0486	1.1196	-1.5684	-1.7559
Smurf1	-1.3127	1.4784	1.4547	-1.0162
Sox4	-6.7388	1.8417	1.4874	-1.2382
Stat1	1.1348	-1.4379	-1.9456	-1.3531
Tdgf1	1.9419	-1.4671	1.1382	1.6699
Tgfb1	-3.2344	3.2087	1.2779	-2.5110
Tgfb1i1	-1.5310	1.7789	2.0630	1.1597
Tsc22d1	-2.0929	1.2483	-1.1105	-1.3863
Tgfb2	-2.1924	1.7715	2.2065	1.2455
Tgfb3	-2.6935	2.1053	1.3147	-1.6013
Tgfbi	-2.2792	5.5328	-2.5320	-14.0087
Tgfbr1	-1.2393	1.1950	1.2064	1.0096
Tgfbr2	-3.1372	3.8185	1.2868	-2.9675
Tgfbr3	-3.8974	6.5933	1.1311	-5.8290
Tgfbrap1	1.3191	-4.4816	-1.2271	3.6522

RT^2 Profiler™ PCR Array (SABiosciences) analysis of mRNA fold regulation of 84 TGFβ response genes in tumors from *SPARC*+/+ and *SPARC*-/- mice treated with

losartan. Greater than negative two-fold regulation is indicated in green, while greater than positive two-fold regulation is indicated in red.

The angiotensin II type 1 receptor antagonist fails to restore angiogenesis and blood vessel maturation but leads to vasoconstriction and reduced permeability in tumors grown in SPARC-null mice.

We have previously reported that tumors grown in *SPARC-/-* mice demonstrated reduced microvessel density and pericyte recruitment, as well as increased permeability [Arnold et al. in press DMM, Thesis Chapter 3]. TGFβ1 has been shown to control angiogenesis, pericyte recruitment and blood vessel function during tumorigenesis [26, 33]. Therefore, we were interested in how excess TGFβ1 in the tumor microenvironment of *SPARC-/-* mice contributed to the aforementioned vascular changes. Microvessel density and pericyte recruitment were assessed by fluorescence immunohistochemistry. Staining with the pan endothelial cell marker, Meca-32, validated that microvessel density was significantly decreased in tumors grown in *SPARC-/-* mice compared to *SPARC+/+* controls (Figure 5A, $p<0.0001$). However, thresholded area was increased in the absence of host SPARC and many vessels appeared dilated (Figure 5A, $p<0.0001$). Therefore, the area of individual blood vessels or mean blood vessel area was assessed. Indeed, blood vessels were significantly larger and dilated in tumors grown in the absence of host SPARC accounting for the increase in thresholded area despite a decrease in microvessel density (Figure 5A, $p<0.0001$). Losartan treatment significantly reduced microvessel density in tumors from *SPARC+/+* mice ($p=0.0473$), but neither restored nor reduced

further the microvessel density of tumors from *SPARC*-/- mice (Figure 5A). On the other hand, TGFβ1 inhibition significantly reduced the mean blood vessel area in tumors grown in the absence of host SPARC, essentially restoring the blood vessel size to that found in tumors from *SPARC*+/+ animals (Figure 5A, $p<0.0001$). Therefore, losartan treatment decreased microvessel density in tumors grown in *SPARC*+/+ mice, but constricted blood vessels in tumors from *SPARC*-/- mice.

Colocalization of Meca-32 and a pericyte marker, NG2, confirmed that pericyte recruitment was significantly diminished in tumors grown in *SPARC*-/- mice compared to *SPARC*+/+ controls (Figure 5B, $p=0.0173$). However, losartan therapy failed to restore blood vessel maturation in tumors from either *SPARC*-/- or *SPARC*+/+ mice. In fact, although not significant, losartan further reduced pericyte recruitment in tumors grown in both *SPARC*-/- or *SPARC*+/+ mice.

In addition to alterations in microvessel density and maturity, tumors grown in *SPARC*-/- mice exhibited enhanced vascular permeability relative to tumors from *SPARC*+/+ controls [Arnold et al. in press DMM, Thesis Chapter 3]. The permeability of fluorescein isothiocyanate-labeled dextran (FITC-Dextran) ($2x10^6$ kDa) was determined for tumors grown in mice treated with losartan (Figure 6). This experiment validated that tumors grown in the absence of host SPARC display increases in permeability to macromolecules (Figure 6, $p=0.0834$). More importantly, losartan treatment abrogated this increase in FITC-Dextran in tumors grown in *SPARC*-/- mice and restored permeability to levels equivalent to that observed in tumors grown in untreated *SPARC*+/+ mice (Figure 6, $p=0.0249$).

Therefore, aberrant TGFβ1 activation in tumors grown in the absence of host SPARC contributes to vasodilation and enhanced blood vessel permeability during tumorigenesis, but not to reduced microvessel density or pericyte recruitment.

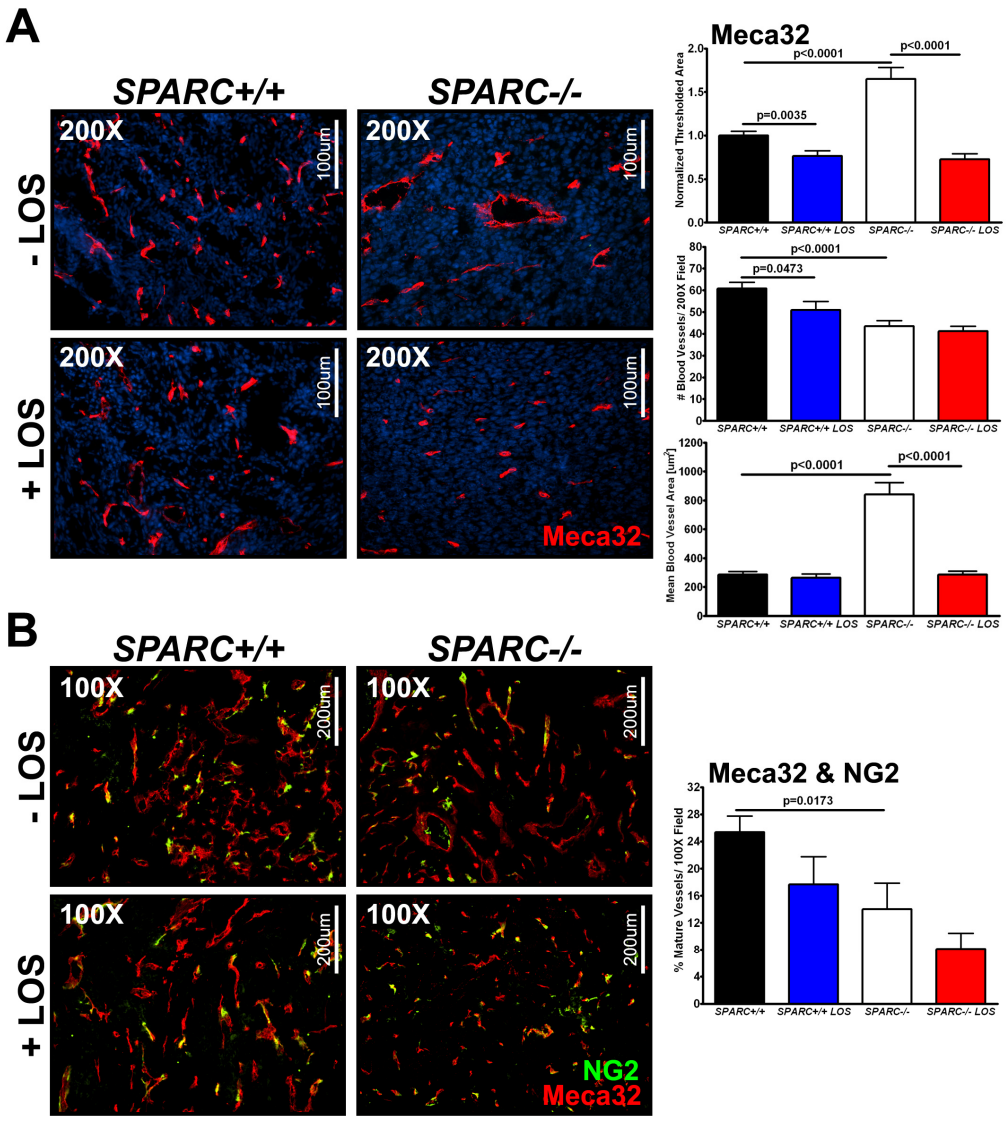

Figure 5. Losartan Effect on Microvessel Density and Pericyte Recruitment. Fluorescence immunohistochemistry was utilized to quantify microvessel density and pericyte recruitment in PAN02 orthotopic tumors grown in *SPARC*+/+ and *SPARC*-/- mice treated with losartan (A-B). (A) Tumor sections were stained with rat anti-mouse endothelial cell Meca-32 (red) [34]. DAPI (blue) marks cell nuclei. The percent thresholded area normalized to untreated *SPARC*+/+, number of blood vessels and mean blood vessel area were quantified. Total magnification (200X) and scale bars (100μm) are indicated. (B) Sections were stained with Meca-32 and rabbit anti-NG2. Percent mature vessels were calculated as the number of Meca-32 & NG2 colocalized vessels divided by the total number of Meca-32 positive vessels. Total magnification (100X) and scale bars (200μm) are shown. All p-values were calculated with the Student's t test.

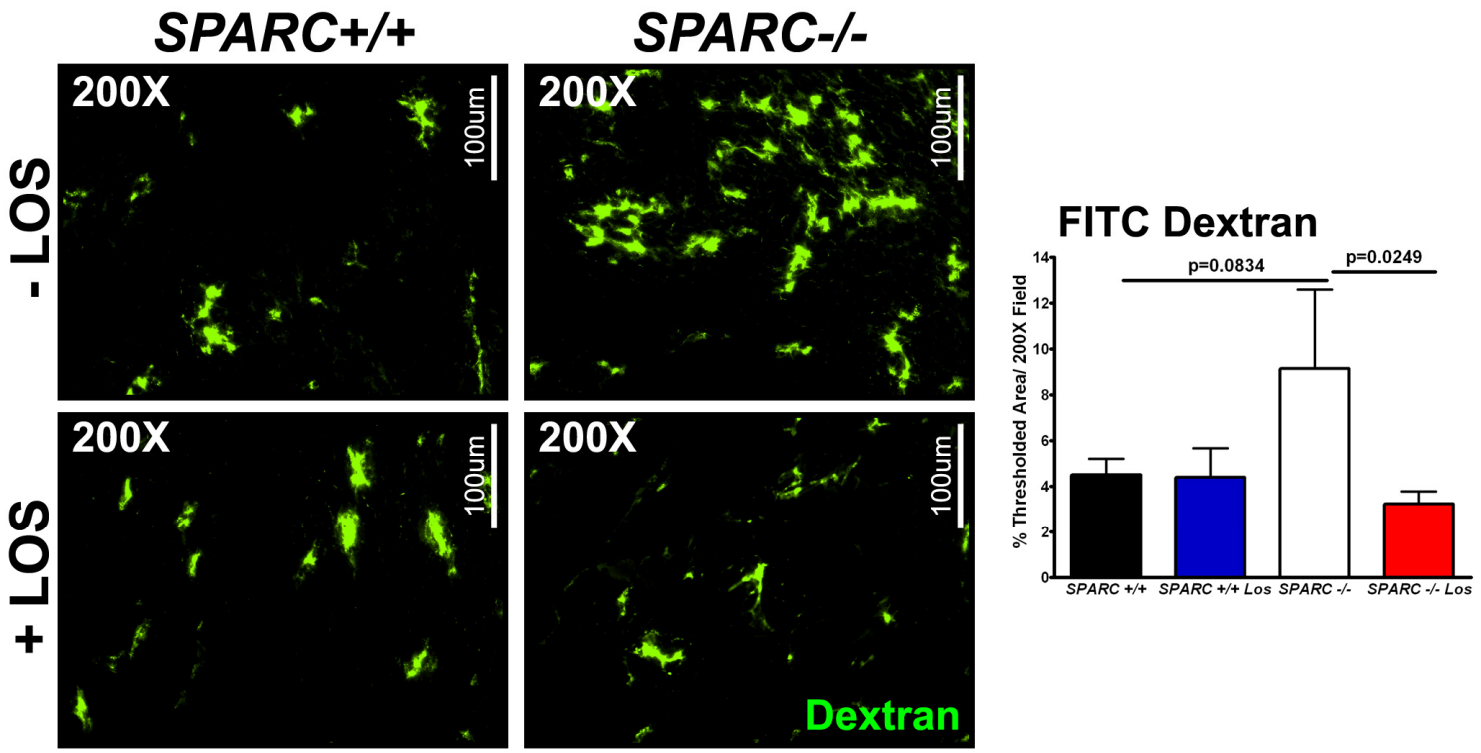

Figure 6. Losartan Effect on Permeability and Vascular Function. *SPARC+/+* and *SPARC-/-* mice bearing orthotopic PAN02 tumors and treated with losartan were injected intravenously with fluorescein isothiocyanate-conjugated dextran (FITC-Dextran) (25 mg/ml) ($2x10^6$mw; D7137; Molecular Probes/Invitrogen) in 0.9% sterile saline at a dose of 200 µl/mouse. The fluorescent dextran was allowed to circulate 10 minutes before the mice were euthanized. Tissue was snap-frozen, sectioned (10 µm) and immediately analyzed by fluorescence microscopy. Percent thresholded area was quantified. Total magnification (200X) and scale bars (100µm) are indicated. All p-values were calculated with the Student's t test.

Collagen deposition and fibrillogenesis in tumors grown in SPARC-null mice is reduced further by the angiotensin II type 1 receptor antagonist.

Previous studies have shown that tumors grown in *SPARC-/-* mice have reduced collagen deposition and fibrillogenesis [Arnold et al. in press DMM, Thesis Chapter 3] [35, 36]. Although this was a consistent observation, the question still remained as to whether alterations in the collagen matrix influenced metastasis and/or survival of *SPARC-/-* mice bearing orthotopic PAN02 tumors. Due to the fact that losartan treatment was able to rescue survival and abrogate metastasis in *SPARC-/-* mice, the next step was to determine if inhibiting TGFβ1 could restore proper collagen deposition and maturation. Mason's trichrome staining confirmed that tumors grown in the absence of host SPARC display reduced collagen deposition (Figure 7A). However, losartan treatment failed to restore collagen deposition in tumors grown in *SPARC-/-* mice (Figure 7A). Furthermore, the amount of collagen production was unaffected by either genotype or losartan therapy as measured by hydroxyproline analysis (Figure 7B). When collagen deposition and maturation in orthotopic PAN02 tumors was quantified by second harmonic generation (SHG), it was found that not only was collagen deposition and maturation decreased in tumors grown in the absence of host SPARC, but that losartan augmented this effect resulting in an even further decrease in collagen deposition and maturation (Figure 7C). The deposition of immature (red), mature (green) and total collagen (both) were all significantly reduced in losartan-treated

compared to untreated SPARC-/- mice (Figure 7C, p=0.0053, p=0.0001, p=0.0002, respectively).

Therefore, we can conclude that although collagen deposition and maturation is disrupted, it does not directly contribute to orthotopic pancreatic tumor progression in *SPARC-/-* mice. Rather, we propose that the decrease in collagen deposition indirectly effects metastasis and survival by reducing the repository for TGFβ1, leading to its enhanced bioavailability and subsequent activation.

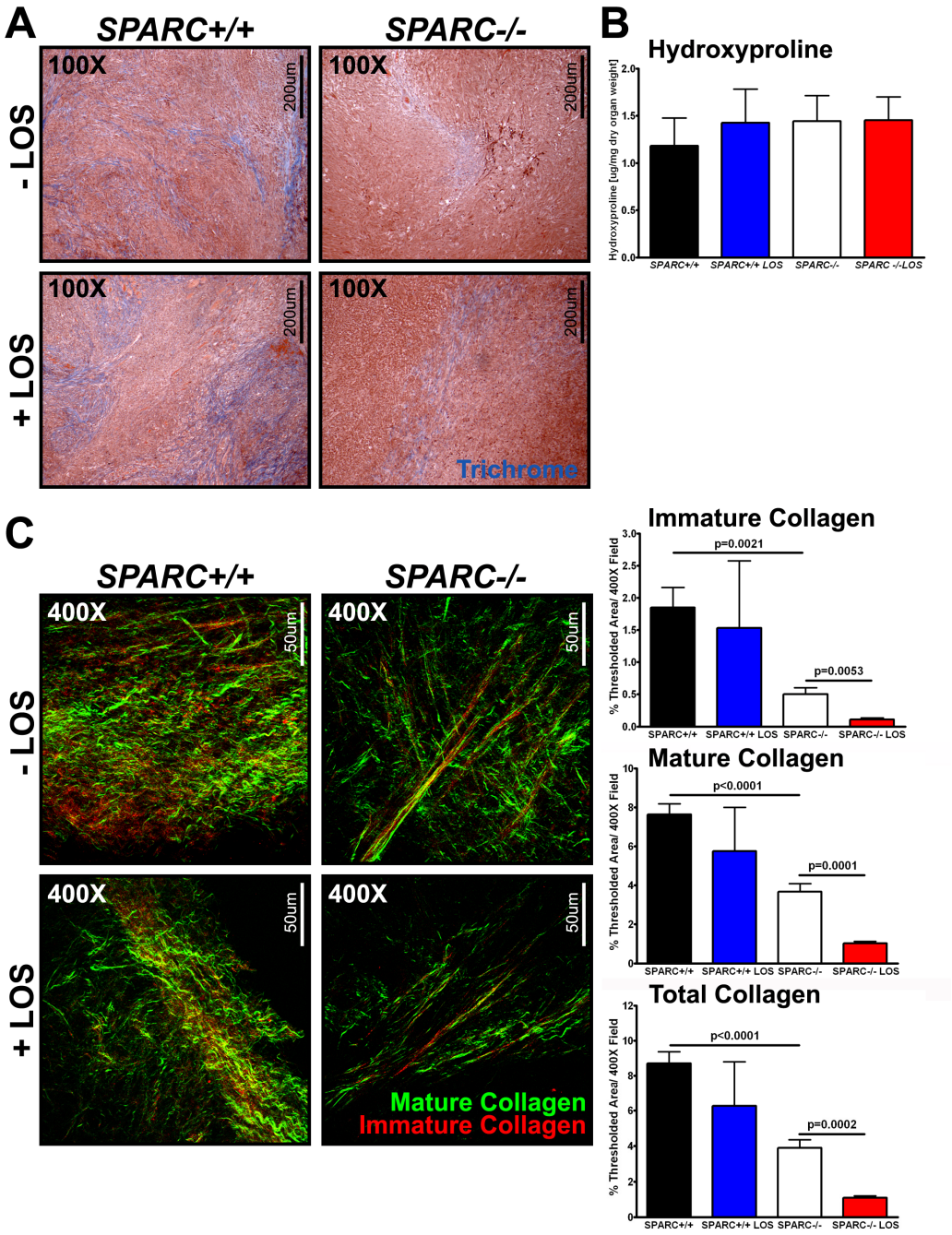

Figure 7. Losartan Effect on Collagen Deposition and Maturation. The amount of collagen production, deposition and maturation was assessed in PAN02 orthotopic tumors grown in *SPARC+/+* and *SPARC-/-* mice treated with losartan. (A) Masson's Trichrome staining shows the amount of fibrillar collagen (blue) deposited within tumors. Total magnification (100X) and scale bars (200µm) are indicated. (B) The amount of

collagen produced and secreted within tumors was quantified by hydroxyproline analysis. (C) Collagen content and maturity was quantified by second harmonic generation (SHG). Frozen tumor sections (50 μm) were mounted in PBS. Collagen fibers within the tumor sections were excited at 900 nm to generate a SHG signal which was then detected at 450 nm. Both forward scattered signal, indicative of mature collagen (green) and backward scattered signal, indicative of immature collagen (red) was detected. Percent thresholded area of immature, mature and total collagen was quantified. Total magnification (400X) and scale bars (50 μm) are indicated. All p-values were calculated with the Student's t test.

The angiotensin II type 1 receptor antagonist fails to reduce the activation of alternatively-activated macrophages or myeloid derived suppressor cells.

Previously, we identified that tumors grown in the absence of host SPARC exhibited an increase in macrophage recruitment and, more specifically, an increase in alternatively-activated macrophages (M2) [Arnold et al. in press DMM, Thesis Chapter 3]. Based on this result we hypothesized that the tumor microenvironment in *SPARC-/-* mice was "immune tolerant", which could be leading to increased metastasis and decreased survival. As a result, we assessed macrophage recruitment and activation after losartan treatment. Immunohistochemistry for classically activated macrophage (M1) using iNos and M2 macrophage using CD163 and the mouse mannose receptor (MMR) validated that the ratio of M2 to M1 macrophage in tumors grown in the absence of host SPARC was significantly increased relative to those grown in *SPARC+/+* controls (Figure 8A, p=0.0321). However, losartan therapy did not reduce the number of M2 macrophages in either genotype (Figure 8A). In fact, tumors grown in losartan-treated mice exhibited an

even larger increase in the ratio of M2 to M1 macrophage (Figure 8A, *SPARC*+/+ vs. *SPARC*+/+ LOS, p=0.0576 and *SPARC*-/- vs. *SPARC*-/- LOS, p=0.0040).

Myeloid-derived suppressor cells (MDSCs) have also been shown to activate tumor-associated immune tolerance [37]. Therefore, we performed fluorescence immunohistochemistry with antibodies targeting CD11b and GR-1, two markers that when colocalized serve to identify the MDSC population. Quantification of the number of CD11b+GR-1+ cells in tumor sections revealed that neither genotype nor losartan treatment significantly altered the recruitment of MDSCs (Figure 8B). Therefore, losartan restores survival and diminishes metastasis without reducing two populations, M2 macrophage and MDSC, known to lead to immunosuppression.

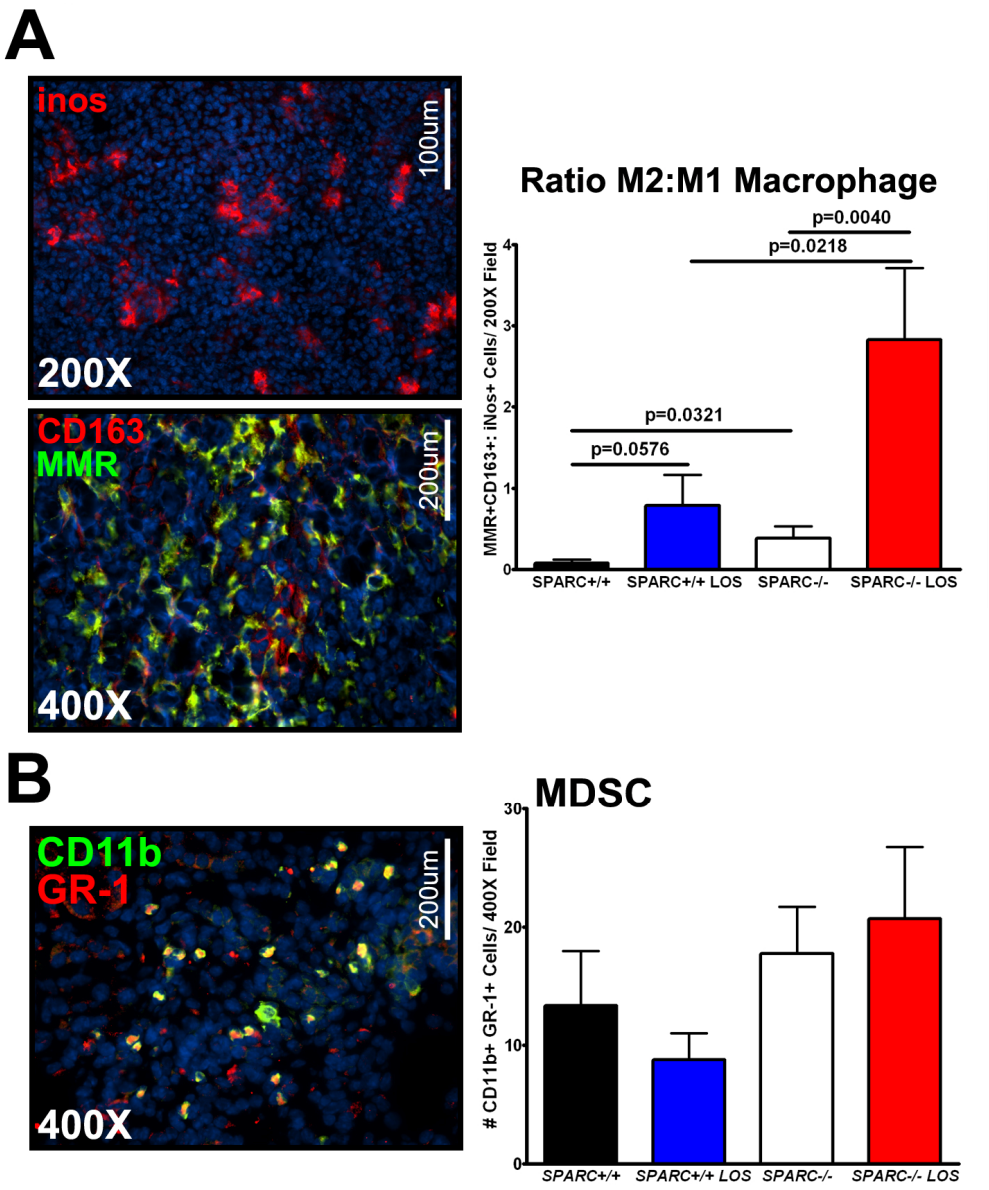

Figure 8. Losartan Effects on Macrophage Activation and MDSC. Fluorescence immunohistochemistry was utilized to assess macrophage and myeloid derived suppressor cell (MDSC) recruitment in tumors grown in PAN02 orthotopic tumors grown in *SPARC*+/+ and *SPARC*-/- mice treated with losartan (A-B). (A) Frozen tumor sections were stained with either antibody rabbit anti inos (red) for detection of M1 macrophage or antibody rabbit anti CD163 (red) and antibody rat anti MMR (green) for detection of M2 macrophage. DAPI (blue) marks cell nuclei. The number of inos positive cells and

the number of CD163 and MMR double positive cells was counted and the ratio of M2 to M1 calculated. Total magnification (200X, 400X) and scale bars (100 μm, 200 μm) are indicated. (B) Frozen tumor sections were stained with antibodies FITC-conjugated rat anti CD11b (green) and CY3-conjugated rat anti GR-1 (red). DAPI (blue) marks cell nuclei. The number of CD11b and GR-1 double positive cells was counted. Total magnification (400X) and scale bars (200 μm) are indicated. All p-values were calculated with the Student's t test.

The angiotensin II type 1 receptor antagonist reduces the activation of regulatory T-cells in tumors and spleens of SPARC-null mice.

A third population of immune cells implicated in immune tolerance is the regulatory T-cell [38-40]. We had never assessed the recruitment of either activated or regulatory T-cells in our model. Therefore, we chose to perform fluorescence immunohistochemistry to assess the recruitment of both activated and regulatory T-cells. Co-staining with the general T-cell marker, CD3, and the activated T-cell marker, CD69, allowed the quantification of percent activated T-cells or the number of CD3+CD69+ double positive cells divided by the total number of CD3+ cells. In general, the percent activated T-cells was not significantly different, although there was a marked trend towards decreased activated T-cells in tumors grown in the absence of host SPARC, regardless of losartan treatment (Figure 9A, $p=0.0507$). On the other hand, the percent regulatory T-cells, assessed by colocalization of CD25 and foxp3, was significantly increased in tumors grown in *SPARC-/-* compared to *SPARC+/+* mice (Figure 9B, $p<0.0001$). More importantly, losartan treatment abrogated this increase in regulatory T-cells (Figure 9B, $p=0.0003$). Since T-cell mediated immunosuppression is dependent on the balance

between activated and regulatory T-cells, the ratio of regulatory CD25+foxp3+ T-cells to activated CD3+CD69+ T-cells was calculated (Figure 9C). Identical to the results for the percent regulatory T-cells, tumors from SPARC-/- mice had an increase in the ratio of regulatory T-cells to activated T-cells relative to those from SPARC+/+ mice and losartan therapy was able to neutralize this effect (Figure 9C, *SPARC*+/+ vs. *SPARC*-/-, $p<0.0001$ and *SPARC*-/- vs. *SPARC*-/- LOS, $p<0.0001$). T-cell recruitment and mobilization to the spleen was also determined (Figure 9D). Losartan treatment reduced the number of CD3+CD69+ double positive activated T-cells mobilized to the spleen in *SPARC*-/- mice (Figure 9D, $p=0.0017$). In addition, although there were no changes in regulatory T-cell recruitment to the spleens of *SPARC*-/- compared to *SPARC*+/+ mice, losartan therapy significantly reduced the number of CD25+foxp3+ double positive regulatory T-cells in both genotypes (Figure 9D, *SPARC*+/+ vs. *SPARC*+/+ LOS, $p=0.0042$ and *SPARC*-/- vs. *SPARC*-/- LOS, $p=0.0401$).

Therefore, tumors grown in the absence of host SPARC display enhanced activation and recruitment of regulatory T-cells compared to those from *SPARC*+/+ mice. Furthermore, losartan therapy was able to abrogate this increase and reduce the recruitment and mobilization of regulatory T-cells to the tumor and the spleen. As a result, it is possible that losartan reduced metastasis and rescued survival of SPARC-/- mice by rebalancing immunosuppression within the tumor microenvironment.

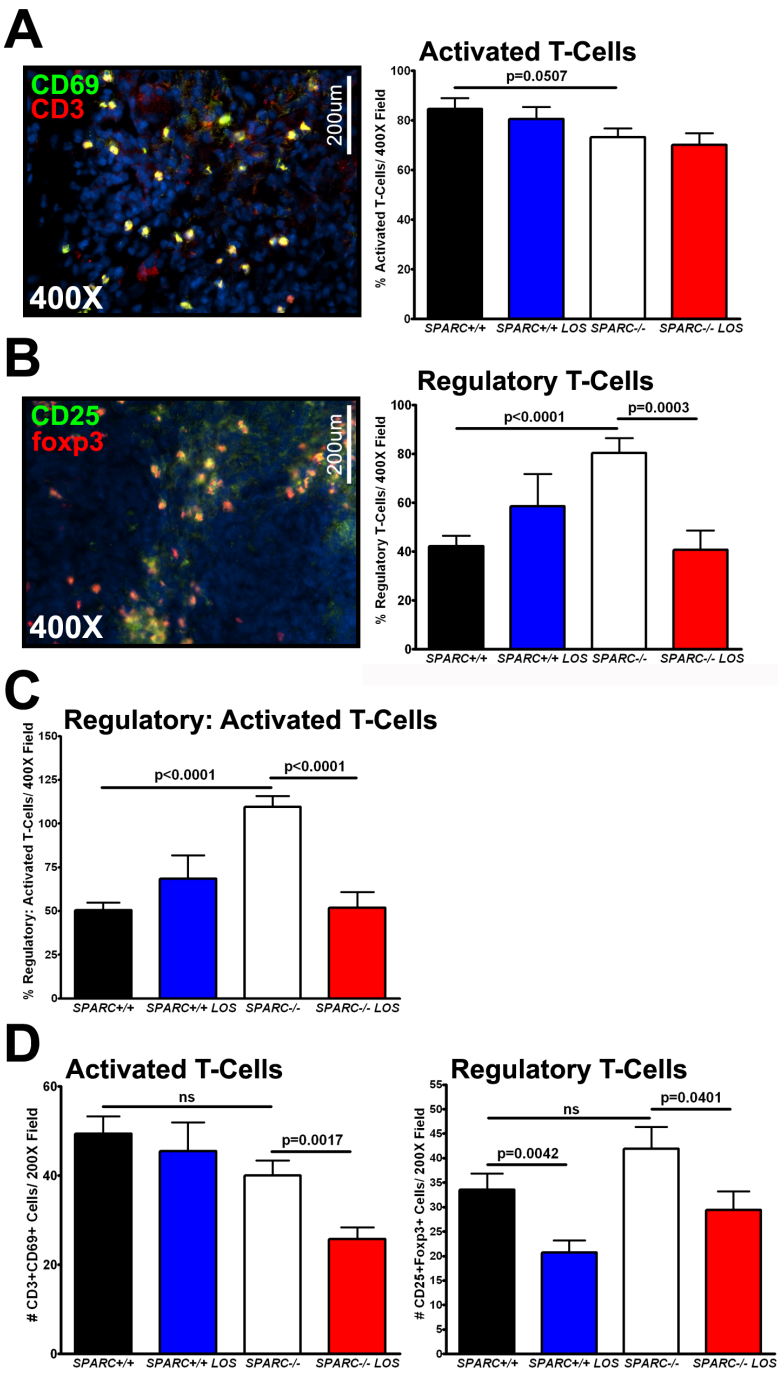

Figure 9. Losartan Effects on T-Cell Activation. Fluorescence immunohistochemistry was utilized to assess the recruitment of activated and regulatory T-cells in PAN02 orthotopic tumors (A-C) or spleens (D) in *SPARC+/+* and *SPARC-/-* mice treated with losartan. (A) Frozen tumor sections were stained with antibody rat anti CD3 (red) and

antibody armenian hamster anti CD69 (green) for detection of activated T-cells. DAPI (blue) marks cell nuclei. Percent activated T-cells was calculated by dividing the number of CD3 and CD69 double positive cells by the total number of CD3 positive cells. Total magnification (400X) and scale bars (200 μm) are indicated. (B) Frozen tumor sections were stained with antibody CY3-conjugated rat anti foxp3 (red) and antibody FITC-conjugated rat anti CD25 (green) for detection of regulatory T-cells. DAPI (blue) marks cell nuclei. Percent regulatory T-cells was calculated by dividing the number of foxp3 and CD25 double positive cells by the total number of CD3 positive cells. Total magnification (400X) and scale bars (200 μm) are indicated. (C) The ratio of regulatory T-cells to activated T-cells was calculated by dividing the number of CD3 and CD69 double positive cells by the number of foxp3 and CD25 double positive cells. Data was recorded as percent. (D) Frozen splenic sections were stained for activated and regulatory T-cells as described in A and B. The number of activated and regulatory T-cells was counted. ns, not significant. All p-values were calculated with the Student's t test.

PAN02 cells in vitro and in vivo are undergoing epithelial-to-mesenchymal transition.

An observation was made *in vitro* and *in vivo*, that although PAN02 cells were derived from pancreatic ductal epithelial cells, they exhibit many mesenchymal characteristics such as an elongated cell shape in culture with no signs of the cobblestone pattern characteristic of epithelial monolayers. This is important because TGFβ1 has been shown to have a dichotomous effect on tumor cell proliferation and migration depending on the epithelial versus mesenchymal nature of the cell [41]. Not only does TGFβ1 induce epithelial to mesenchymal transition (EMT) but, once a cell is mesenchymal, it no longer responds to TGFβ1 with immobility and quiescence [41, 42]. Instead, TGFβ1 induces the migration and proliferation of mesenchymal-like fibroblastoid tumor cells [41]. To determine if PAN02 cells have undergone EMT, we stained tumor sections with E-cadherin, an epithelial marker, and vimentin, a mesenchymal marker. The majority of the

PAN02 tumors were negative for E-cadherin. The only positive stain within the tumors arose from spontaneous *de novo* ducts derived from the PAN02 cells (Figure 10A). These ducts were abnormal albeit expressed E-cadherin that was appropriately localized to cell-cell junctions (Figure 10A, Zoom). This suggests that PAN02 cells are in the process of undergoing EMT, but still possess the ability to return to an epithelial-like state. Furthermore, PAN02 tumors displayed high expression of vimentin, which confirms that the PAN02 cells are behaving like mesenchymal cells. As additional evidence, immunocytochemistry of PAN02 cells *in vitro*, reveals that β–catenin is completely localized to the nucleus.

Therefore, the fact that PAN02 cells have undergone or are in the process of EMT, suggests that the excess TGFβ1 during tumor progression in *SPARC-/-* mice might have direct effects on the PAN02 cells, stimulating their migration and subsequent metastasis.

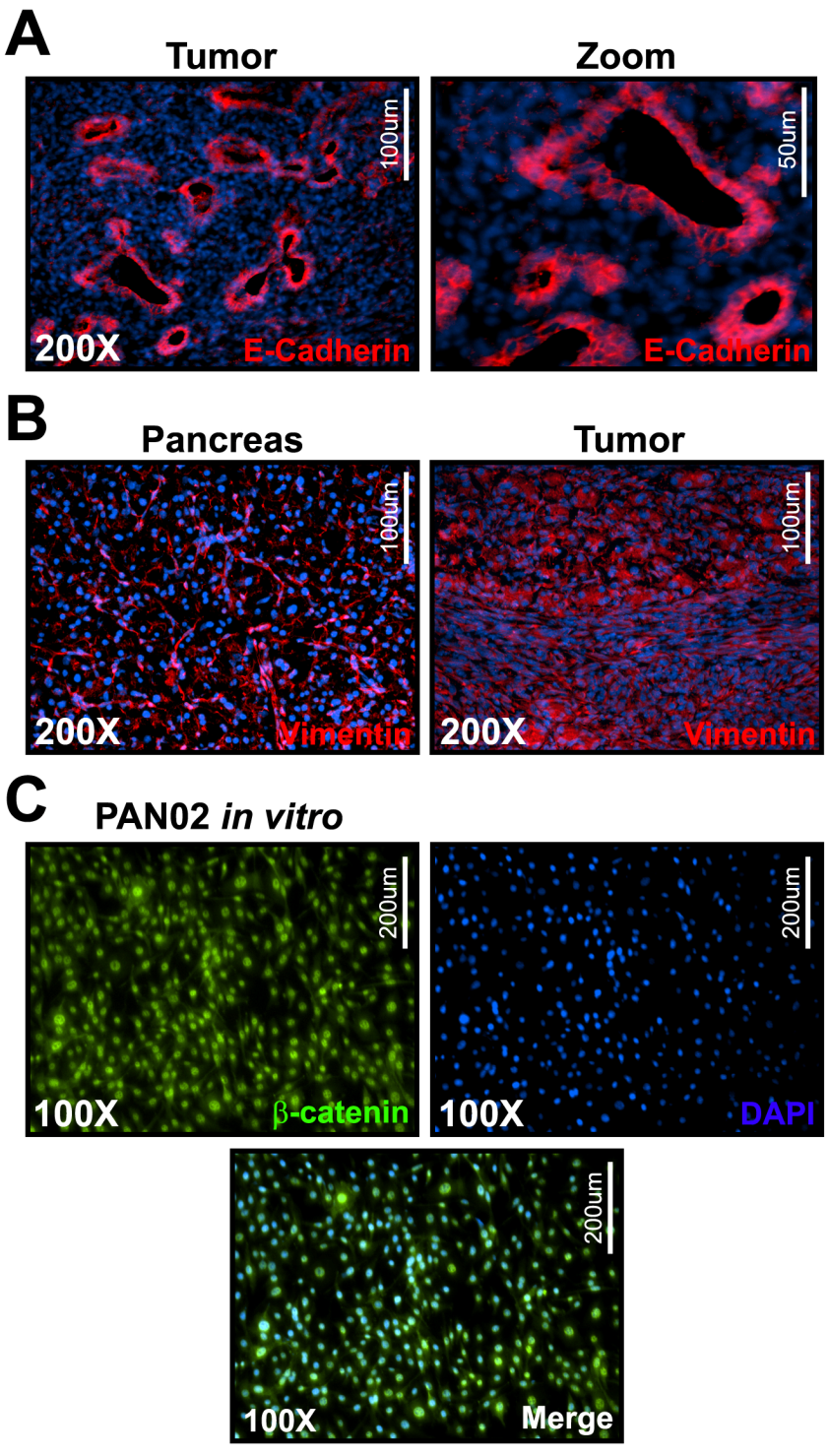
A
Tumor
Zoom
100um
50um
200X
E-Cadherin
E-Cadherin
B
Pancreas
Tumor
100um
100um
200X
Vimentin
200X
Vimentin
C
PAN02 in vitro
200um
200um
100X
β-catenin
100X
DAPI
200um
100X
Merge

Figure 10. Mesenchymal Characteristics of PAN02 Cells. Fluorescence immunohistochemistry (A-B) and immunocytochemistry (C) were utilized to assess the epithelial versus mesenchymal nature of PAN02 cells. (A) Frozen tumor sections were stained with antibody rabbit anti E-Cadherin (red) to mark epithelial cells. DAPI (blue) marks cell nuclei. Total magnification (200X) and scale bars (100 μm and 50 μm) are indicated. (B) Frozen pancreas and tumor sections were stained with antibody goat anti Vimentin (red) to mark mesenchymal cells. DAPI (blue) marks cell nuclei. Total magnification (200X) and scale bars (100 μm) are indicated. (C) PAN02 cells were stained with antibody rabbit anti β-catenin (red) to visualize its cellular localization. DAPI (blue) marks cell nuclei. Total magnification (100X) and scale bars (200 μm) are indicated.

SPARC and TGFβ1 enhance PAN02 cell migration.

To determine if PAN02 cell migration is influenced by SPARC and/or TGFβ1, wound healing assays were performed. PAN02 cells were treated with either 0.1% FBS alone or in combination with recombinant SPARC (10 μg/ml), recombinant TGFβ1 (250 ng/ml), both SPARC and TGFβ1, or anti-TGFβ1,2,3 (10 μg/ml). Wound width was measured six hours after wound initiation. PAN02 cells treated with either SPARC or TGFβ1 exhibited a significant increase in wound closure or decrease in wound width relative to 0.1% FBS alone (Figure 11A, both $p<0.0001$). Furthermore, the combination of SPARC and TGFβ1 significantly accelerated wound closure compared to either treatment alone (Figure 11A, SPARC vs. SPARC + TGFβ1 $p<0.0001$ and TGFβ1 vs. SPARC + TGFβ1 $p=0.0002$). Lastly, neutralizing TGFβ signaling with an anti-$TGF\beta_{1,2,3}$ antibody significantly delayed wound closure compared to 0.1% FBS alone (Figure 11A, $p=0.0028$). It is important to note that PAN02 cells express and secrete measurable amounts of SPARC (Figure 11A, top right panel). Therefore, if SPARC and TGFβ1 act concurrently to enhance PAN02

cell migration, then the secretion of SPARC by the PAN02 cells *in vivo* is enhancing the pro-migratory effects of excess TGFβ1. To validate that SPARC and TGFβ1 induce the migration of PAN02 cells, transwell migration assays were utilized. PAN02 cells migrated towards 0.5% FBS and were treated with recombinant SPARC (10 and 30 μg/ml), recombinant TGFβ1 (50, 250 and 500 ng/ml) or SPARC (10 μg/ml) in combination with anti-TGFβ1,2,3 (10 μg/ml). TGFβ1 dose-dependently enhanced PAN02 migration (Figure 11B, left graph). Likewise, SPARC also dose-dependently activated PAN02 migration (Figure 11B, right graph). Moreover, SPARC-induced migration was dependent on TGFβ1 because addition of the anti-$TGF\beta_{1,2,3}$ completely abrogated SPARC activation of migration (Figure 12B, right graph, SPARC (10 μg/ml) vs. SPARC (10 μg/ml) + anti-$TGF\beta_{1,2,3}$ $p<0.0001$).

Therefore, PAN02 migration is enhanced by both SPARC and TGFβ1, whereby SPARC-induced migration is dependent on TGFβ1. This data provides plausible evidence that TGFβ1 in the tumor microenvironment is directly regulating the migration of PAN02 cells and stimulating their dissemination.

Figure 11

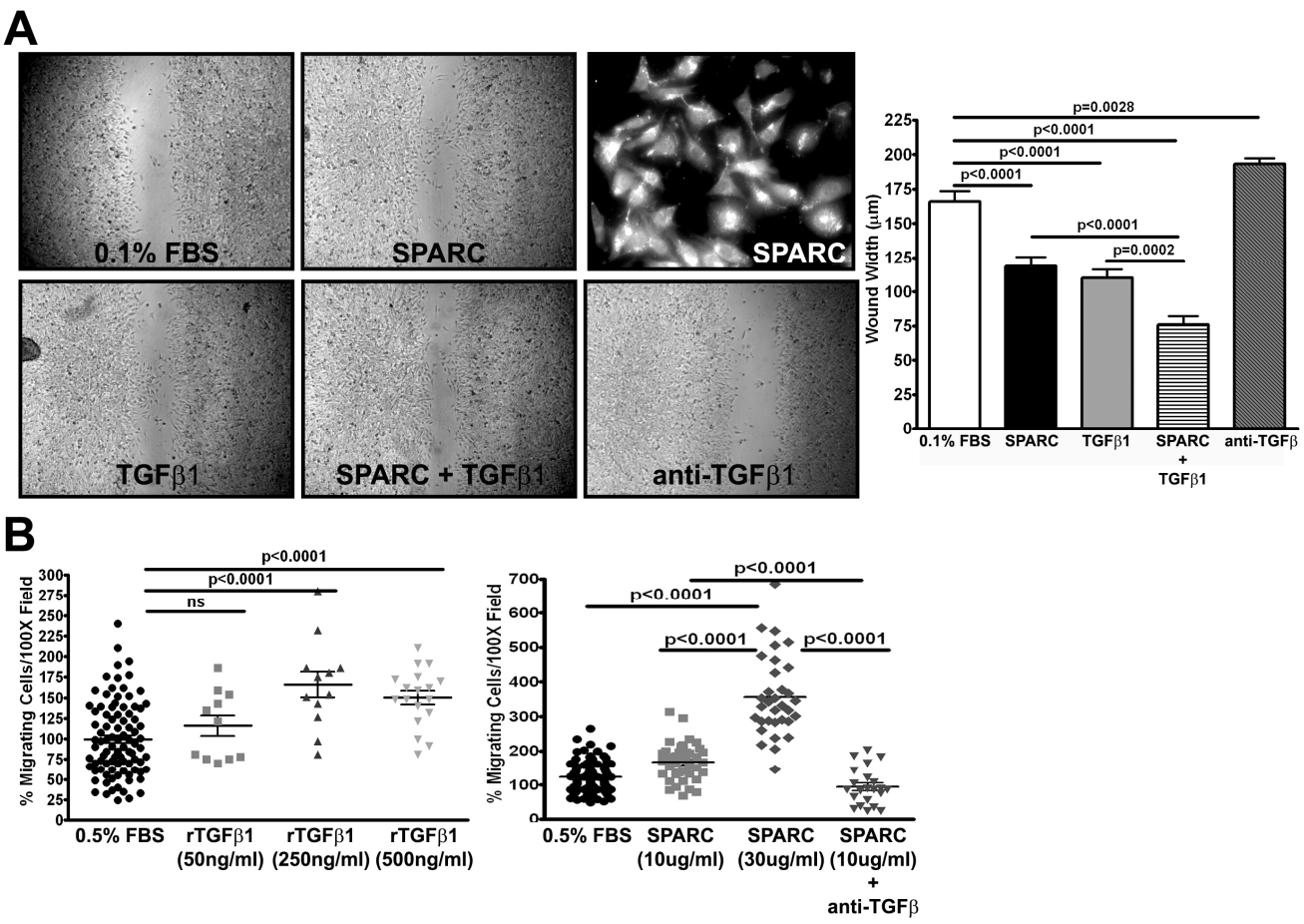
A
0.1% FBS
SPARC
SPARC
TGFβ1
SPARC + TGFβ1
anti-TGFβ1
Wound Width (μm)
p=0.0028
p<0.0001
p<0.0001
p<0.0001
p<0.0001
p=0.0002
0.1% FBS
SPARC
TGFβ1
SPARC + TGFβ1
anti-TGFβ
B
% Migrating Cells/100X Field
p<0.0001
p<0.0001
ns
0.5% FBS
rTGFβ1 (50ng/ml)
rTGFβ1 (250ng/ml)
rTGFβ1 (500ng/ml)
% Migrating Cells/100X Field
p<0.0001
p<0.0001
p<0.0001
p<0.0001
0.5% FBS
SPARC (10ug/ml)
SPARC (30ug/ml)
SPARC (10ug/ml) + anti-TGFβ

Figure 11. Influence of SPARC and TGFβ1 on PAN02 Migration. The ability of SPARC and TGFβ1 to control PAN02 cell migration *in vitro* was assessed. (A) A wound-healing assay was utilized to determine if SPARC and TGFβ1 could act concomitantly to enhance PAN02 migration. Cells were plated at a density of 1.5 X 10^5 cells per well in 96-well plates and allowed to grow to 100% confluency. A scratch was made and cells allowed to migrate into the wound. Recombinant SPARC (10μg/ml), recombinant TGFβ1 (250ng/ml) and anti-TGFβ1,2,3 (10μg/ml) were prepared in DMEM 0.1% FBS. The wound width (μm) was measured after 6 hours. Inset of immunocytochemistry with antibody goat anti-mouse SPARC reveals that PAN02 cells do express SPARC. (B) A transwell migration assay was performed as an additional means to assess SPARC and TGFβ1 effect on PAN02 migration, as well as, to determine if SPARC effect on PAN02 migration is TGFβ dependent. Cells were serum-starved overnight then seeded at 20,000 cells per 24-well 0.8 μm cell culture insert (BD Falcon). DMEM 0.1% FBS served as the chemoattractant. Recombinant SPARC (10 and 30 μg/ml) was added to the upper chamber, while recombinant TGFβ1 (50, 250 and 500 ng/ml) and anti-TGFβ1,2,3 (5μg/ml) were added to the bottom chamber. Cells were allowed to migrate 24 hours at 37°C in 5% CO_2. Migrated cells were fixed, stained and counted. Cell counts were normalized to DMEM 0.1% FBS and recorded as % migrating cells. ns, not significant. All p-values were calculated with the Student's t test.

Discussion

We have provided evidence that suggests that enhanced metastasis and decreased survival of *SPARC*-/- mice is a result of aberrant activation of TGFβ1. Inhibition of the expression and activation of TGFβ1 with the angiotensin II type 1 receptor antagonist, losartan, rescued survival of *SPARC*-/- mice challenged with PAN02 orthotopic tumors. Most likely, median survival of *SPARC*-/- mice was extended because local invasion and metastatic burden was reduced by losartan treatment.

Previously identified alterations in the tumor microenvironment between *SPARC*+/+ and *SPARC*-/- mice were reassessed after losartan therapy. We found that

vasodilation and blood vessel permeability are influenced by the excess active TGFβ1 detected in tumors grown in the absence of host SPARC and, therefore, may contribute to metastasis and survival. On the other hand, decreased microvessel density and pericyte recruitment were not restored with losartan treatment and are unlikely causes for the enhanced metastatic burden in *SPARC-/-* mice. Not surprising, considering that SPARC is required for proper collagen deposition and fibrillogenesis, losartan was unable to restore collagen deposition in tumors grown in the absence of host SPARC. In fact, the inhibition of TGFβ1 led to a further decrease in collagen deposition and maturation in tumors from *SPARC-/-* mice. Regulatory T-cells contribute to tumor immune tolerance by neutralizing inflammatory responses and have been shown to correlate with worse clinical outcomes [40]. We observed that regulatory T-cell recruitment was increased in tumors established in the absence of host SPARC and that this increase was negated with losartan treatment. An imbalance in immunosuppressive and inflammatory cells provides another explanation for enhanced metastasis and decreased survival of *SPARC-/-* mice.

Although losartan was able to effectively reduce the expression, activation and signaling of TGFβ1, further validation is needed to prove that it is through the inhibition of TGFβ1 and not angiotensin II that tumor progression is inhibited in *SPARC-/-* mice. Specific targeting of TGFβ1 will be achieved with a neutralizing TGFβ1 monoclonal antibody, 1D11. Survival, invasion, metastatic burden, vasodilation, blood vessel permeability and the immune profile will then be reevaluated after treatment with 1D11 and compared to the results of the losartan studies.

What is clear is that TGFβ1 is the predominant regulator of metastasis and survival in SPARC-/- mice. What is not completely clear is how inhibition of the expression and activation of TGFβ1 abrogates metastasis and rescues survival of mice lacking SPARC. Several possibilities exist, including "normalization" of the vasculature by constricting the blood vessels and reducing permeability, as well as rebalancing the immune compartment by reducing regulatory T-cells. Another major possibility is that TGFβ1 is directly affecting the migration and dissemination of PAN02 cells. Furthermore, at this point, we can only speculate as to why TGFβ1 is aberrantly activated in the absence of host SPARC. We hypothesize that alterations in the ECM such as decreased collagen deposition and reduced decorin, increase the bioavailable pool of latent TGFβ1, leaving more to bind and get activated at the cell surface.

Materials and Methods

Tissue Culture

The murine pancreatic adenocarcinoma cell line (PAN02, also known as Panc02) was purchased from the Developmental Therapeutics Program, Division of Cancer Treatment and Diagnosis, National Cancer Institute (Frederick, MD), and grown in high glucose Dulbecco's Modified Eagles Medium (DMEM + GlutaMAX™-1, Invitrogen, Carlsbad, CA) supplemented with 5% fetal bovine serum (FBS, Life Technologies, Grand Island, NY). The PAN02 cell line was tested (Impact III PCR profiles; MU Research Animal Diagnostic Laboratory, Columbia, MO) and was found to be pathogen-free.

Orthotopic Tumor Model

B6;129S-*Sparc*^{tm1Hwe} mice were generated as described previously [44] and backcrossed into C57BL/6J a minimum of 10 generations. The mice were housed in a pathogen-free facility and experiments were conducted under a protocol approved by the Institutional Animal Care and Use Committee of UT Southwestern Medical Center (Dallas, TX). All experiments were performed with *Sparc-null* (*SPARC-/-*) and *wild-type* (*SPARC+/+*) littermates. For injections, confluent cultures of PAN02 cells (>90% viable) were trypsinized, pelleted in DMEM 5% FBS, washed twice in phosphate buffered saline (PBS) and resuspended in 0.9% sterile saline (Sigma, St. Louis, MO). Tumor cells ($1x10^6$) were injected directly into the tail of the pancreas to establish orthotopic tumors as previously described [35, 45]. For the survival study, individual mice were monitored daily and were euthanized when they displayed signs of tumor-associated morbidity such as excessive weight gain or loss, ascites, lethargy and/or distress. Bulk tumor growth was monitored through abdominal palpation. For the endpoint study, the entire cohort of mice was euthanized four weeks after tumor cell injection. The liver, heart, lung, kidney, brain, spleen and pancreas, including the tumor, were removed and weighed. Tumor could not be separated from the pancreas so tumor weights include residual pancreas. Metastasis and local invasion into surrounding organs was assessed macroscopically by visual examination. Suspected metastases were fixed, stained with H&E and verified as metastatic lesions histologically. Therefore, only visible macroscopic metastatic and locally invasive lesions were counted towards incidence and burden.

TGFβ Inhibition with an Angiotensin II Type 1 Receptor Antagonist

Animals bearing orthotopic PAN02 tumors were treated with the angiotensin II type 1 receptor antagonist, losartan potassium (Cozaar, Merck, Whitehouse Station, NJ), shown to also inhibit the expression and activation of TGFβ. Therapy was given via drinking water *ad libitum* at a dose of 600mg/L in 2% sucrose solution. The drinking solution was changed 3 times a week. Animals were randomized into treatment groups matched for age and sex. For the survival study, therapy began 10 days after tumor cell injection and continued the entire duration of the experiment. Therapy began immediately for the endpoint study and continued for 4 weeks until the entire group was sacrificed. Local invasion was defined as tumor growth into surrounding organs that remained attached to the primary tumor, while a nodule was considered a metastasis if it was located in a distant organ or clearly had no connection to the primary tumor.

Immunohistochemistry

Fixed Tissue: Tissues were fixed in either Methyl Carnoy's solution (60% methanol, 30% chloroform, 10% glacial acetic acid) and sent to the Molecular Histopathology Laboratory at UT Southwestern Medical Center (Dallas, TX) for paraffin-embedding and sectioning. The Molecular Histopathology Laboratory also performed staining with hematoxylin & eosin or Masson's trichrome. Tissue sections were deparaffinized and rehydrated in PBS containing 0.2% Tween-20 (PBSt) prior to staining.

Frozen Tissue: Tissues were snap-frozen in liquid nitrogen, embedded in optimal cutting temperature compound (OCT) (Tissue-Tek®), cut into 10 μm thick sections, air-dried overnight, fixed for 2 minutes in acetone and washed in PBSt prior to staining.

Fluorescence Detection: Deparaffinized and rehydrated sections were blocked in 20% AquaBlock (East Coast Biologics), incubated with primary antibody overnight at 40^0C, incubated with fluorophore-conjugated (FITC or Cy3) secondary antibody (Jackson Immunoresearch) (1:500) for 1-2 hours at room temperature and mounted with ProLong Gold Antifade Reagent with DAPI (Invitrogen).

Antibody Specifics: Primary antibodies used for IHC are listed in Supplemental Table S1 [34]. Antigen retrieval was performed, where indicated, by digesting with 20 μg/ml proteinase K for 5 minutes at room temperature.

Supplemental Table S1. Primary Antibodies and Applications

Antibody Information					Application				
Antigen	Antibody Clone or Catalog # (Ref)	Species	Source	Target	Dilution or Concentration	Frozen	Methyl Carnoy's	Retrieval PK Digest	FL
β-Catenin	6B3	Rabbit	Cell Signaling Technology, Danvers, MA	EMT	1:50	√			√
CD11b (Mac-1)	M1/70	Rat	AbD Serotec, Raleigh, NC	Monocytes/Macs/MDSCs	15ug/ml	√			√
CD163	M-96	Rabbit	Santa Cruz Biotechnology Inc., Santa Cruz, CA	M2 Macs	1:50-1:100	√			√
CD25 (IL-2Ra)	PC61.5	Rat	ebioscience, San Diego, CA	T-Regs	1:50-1:100	√			√
CD3	KT3	Rat	ebioscience, San Diego, CA	Total T-Cells	1:50-1:100	√			√
CD69 (VEA)	H1.2F3	Arm. Hamster	ebioscience, San Diego, CA	Active T-Cells	1:50-1:100	√			√
Decorin	AF1060	Goat	R&D Systems, Minneapolis, MN	Proteoglycan	10-15ug/ml		√		√
E-Cadherin	sc-7870	Rabbit	Santa Cruz Biotechnology Inc., Santa Cruz, CA	Epithelial Junctions	15ug/ml	√			√
Foxp3	FJK-16S	Rat	ebioscience, San Diego, CA	T-Regs	1:50-1:100	√			√
GR-1	RB6-8C5	Rat	Biolegend, San Diego, CA	PMNs/MDSCs	1:100	√			√
iNOS	NB120-15323	Rabbit	Novus Biologicals, Littleton, CO	M1 Macs	1:50-1:100	√			√
Mannose Receptor (MMR) (CD206)	MR5D3	Rat	Biolegend, San Diego, CA	M2 Macs	1:100-1:200	√			√
NG2 chondroitin sulfate proteoglycan	AB5320	Rabbit	Chemicon International Inc., Temecula, CA	Pericytes	1:200	√			√
Pan Endothelial Cell Marker	Meca-32*	Rat	Developmental Studies Hybridoma Bank, University of Iowa, Iowa City, IA	Endothelial Cells	5-10ug/ml	√			√
SPARC (mouse)	AF942	Goat	R&D Systems, Minneapolis, MN	Mouse SPARC Specific	1:50	√			√
TGFβ1	G122A	Rabbit	Promega	Active TGFβ1	1:50		√	√	√
TGFb1,2	sc-146	Rabbit	Santa Cruz Biotechnology Inc., Santa Cruz, CA	Total TGFb	1:50	√			√
Vimentin	AB1620	Goat	Chemicon International Inc., Temecula, CA	Mesenchymal/EMT	1:40	√			√

Primary antibodies used for immunohistochemistry, tissue fixation methods, retrieval protocols and detection procedures are listed. Frozen tissue was fixed 5 minutes with cold acetone. Antigen retrieval was performed by digesting with 20 μg/ml proteinase K for 5 minutes at room temperature (Retrieval PK Digest). (FL) fluorescence detection. * (Hallmann et al., 1995). All primary antibodies are incubated overnight at 4 degree C and secondary (1:500) 1-2hr room temperature.

Imaging and Quantification

Tissue sections were analyzed with a Nikon Eclipse E600 microscope (Nikon, Lewisville, TX). Color images were captured with a Nikon Digital Dx1200me camera and Act1 software (Universal Imaging Corporation, Downington, PA). Fluorescence images were captured with a Photometric Coolsnap HQ camera and were captured randomly throughout the entire tumor, including the center and border, and under identical conditions including magnification and exposure time to allow quantification of signal intensities, object counts, percent thresholded area and colocalization with NIS Elements AR 2.30 software (Nikon). Images were thresholded to exclude background signal from secondary antibody alone. An average of ten images per tumor and a minimum of three tumors per group were used for each target.

TGFβ1 enzyme-linked immunosorbent assay (ELISA)

Tumors were homogenized in lysis buffer (20 mM Tris-HCl pH 7.5, 150 mM NaCl, 1% Triton X-100) containing proteinase inhibitors (Complete Proteinase Inhibitor Cocktail Tablets, Roche, Indianapolis. IN). Tissue debris was pelleted and the resulting supernatant was used in subsequent analysis. Total protein was determined with a BCA protein assay (Pierce, Rockford, IL). An ELISA for active TGFβ1 (TGF beta 1 Emax ImmunoAssay System, Promega, Madison, WI) was performed on 50μg of total protein per well according to the manufacturer's protocol. A minimum of 4 tumors per group was analyzed in duplicate. Data were normalized to *SPARC*+/+.

Real-Time Quantitative Reverse-Transcriptase Polymerase Chain Reaction (qPCR)

RNA Isolation and Purification

RNA was isolated from tumors collected in the survival study utilizing TRIzol® (Invitrogen) reagent according to the manufacturer's protocol. Four milliliters of TRIzol® was used to isolate RNA from 100mg of tumor. RNAse inhibitor (Roche) was then added to the isolated RNA and treated with DNAse (DNA Free Kit; Ambion, Austin, TX). The RNA was then further purified with the RNeasy Mini Kit (Qiagen, Valencia, CA). The samples were then eluted in RNAse/DNAse free water and utilized for subsequent cDNA synthesis.

Standard qPCR:

Purified RNA, three samples per group, was reverse transcribed into cDNA using the iScript™ cDNA synthesis kit (Bio-Rad, Hercules, CA). Taqman probes for mouse GAPDH, transforming growth factor beta 1 (TGFβ1), transforming growth factor beta 3 (TGFβ3) and thrombospondin-1 (TSP-1) were purchased from Applied Biosystems (Foster City, CA). Real-time qPCR was performed with iTaq™ Supermix with ROX (Bio-Rad). The fold change was calculated as $2^{-\Delta CT}$ where CT is the cycle threshold and ΔCT is the difference between the CT of the desired probe and the CT of GAPDH. Fold changes were then normalized to the *SPARC*+/+ group for each probe.

TGFβ qPCR Array:

The expression of 84 genes related to the TGFβ signaling pathway was assessed with the RT^2 Profiler™ PCR Array (PAMM-035; SABiosciences, Frederick, MD). Synthesis of cDNA and real-time PCR was performed according to the manufacturer's protocol using the RT² First Strand Kit (SABiosciences) and RT² qPCR Master Mix (SABiosciences).

Three RNA samples were pooled for each group prior to cDNA synthesis. Therefore, only one array was performed for each group. Cycle thresholds (CT) were uploaded to SABiosciences' online PCR array data analysis software allowing for the calculation of fold change/regulation and production of the clustergram and heatmaps. http://www.sabiosciences.com/pcr/arrayanalysis.php

Fluorescent Dextran Permeability

Prior to sacrifice, mice were injected intravenously (tail vein) with fluorescein isothiocyanate-conjugated dextran (FITC-Dextran) (25 mg/ml) ($2x10^6$mw; D7137; Molecular Probes/Invitrogen, Eugene, OR) in 0.9% sterile saline at a dose of 200 µl/mouse. The fluorescent dextran was allowed to circulate 10 minutes before the mice were euthanized. Organs were removed, weighed, snap frozen, embedded in OCT and cut into 10 µm thick sections. FITC-dextran permeability was immediately assessed by fluorescence microscopy. A minimum of ten random photographs was taken of each tumor section, with an average of three animals per group. Results were recorded as mean percent thresholded area.

Hydroxyproline Analysis

Mice were anesthetized with isoflurane and organs were removed and weighed as described before. Organs were then snap frozen, lyophilized, weighed (dry weight), pulverized and subjected to complete acid hydrolysis with 6 N HCl for 18 hours at 120°C. Each sample was then neutralized to pH7 with 4N NaOH. One ml of Chloramine T was added to 2 ml volumes of collagen sample and incubated at room temperature for

20 minutes. One ml of Ehrlich's Reagent (60% perchloric acid, 15 ml 1-propanol, 3.75 g p-dimethyl-amino-benzaldehyde in 25 ml) was added and samples were incubated at 60°C for 20 minutes. Absorbance at 558 λ was read on a spectrophotometer. Collagen was quantified as μg hydroxyproline per mg dry weight of starting material.

Second Harmonic Generation Collagen Quantification

Frozen tumor sections (50μm) were mounted in PBS and coverslipped. A Zeiss LSM510 META NLO using an Achroplan 40x/0.8W objective lens (Zeiss, Roslyn, New York) was used to visualize the tissue sections. Collagen fibers within the tumor sections were excited at 900nm with a Chameleon XR pulsed Ti:sapphire laser (Coherent, California) to generate a second harmonic generation (SHG) signal which was then detected at 450nm. Excitation light was removed by a HQ 450 sp-2p filter (Chroma Technology, Vermont) and forward scattered signal, indicative of mature collagen, was detected with the transmitted light detector. A 680nm short-pass dichroic mirror was utilized to remove backscattered excitation light. Backward scattered signal, indicative of immature collagen, was detected with a non-descanned detector placed at the illumination port of the wide-field epifluorescence light path. Two z-stack (10-step) images, at the areas of greatest collagen deposition, were taken for each tumor (n=2) per group and the percent thresholded area quantified independently for every stack.

Immunocytochemistry.

PAN02 cells were plated on ibidi 8-well μslides (Applied Biophysics, San Diego, CA) at 10,000 cells per well. Cells were allowed to adhere overnight at 37^{o}C 5% CO_2. Cells

were fixed in 10% formalin for 10 minutes at room temperature then permeabilized with 0.1% Triton X-100 for 5 minutes at room temperature. The slides were blocked for 1 hour in 20% Aquablock (East Coast Bio, North Berwick, ME) before incubation with primary antibodies rabbit anti-βcatenin (Cell Signaling Technology, Danvers, MA) or goat anti-mouse SPARC (R&D Systems, Minneapolis, MN) overnight at 4^{o}C. Slides were incubated with secondary antibody (1:500) for 1 hour at room temperature then mounted with DAPI ProLong® Gold antifade reagent (Invitrogen).

Wound Healing Assay

Cells were plated at a density of 1.5 X 10^5 cells per well in 96-well plates and allowed to grow to 100% confluency. Serum containing media was removed, wells washed twice and replaced with serum-free DMEM. A scratch was then made down the center of each well with an extra long p10 pipette tip. The most uniform and consistent scratches were marked and used in the final analysis. Recombinant SPARC (10μg/ml), recombinant TGFβ1 (250ng/ml) and anti-TGFβ1,2,3 (10μg/ml) were prepared in DMEM 0.1% FBS and added to the appropriate wells. Treatments were performed in duplicate. Images from the center of each well were taken at times 0 and 6 hours. The wound width (μm) was measured at a minimum of 20 locations along the wound for each replicate using NIS Elements AR 2.30 software. The initial wound width was used to verify consistency in scratches.

Transwell Migration Assay

Cells were serum-starved overnight then plated in duplicate at 20,000 cells/ well in 100 µl of serum-free DMEM in the upper chamber of a 24-well 0.8 µm cell culture insert (BD Falcon, San Jose, CA). The lower chamber of the 24-well plate received 300µl DMEM 0.1% FBS as the chemoattractant. Recombinant SPARC (10 and 30 µg/ml) was added to the upper chamber, while recombinant TGFβ1 (50, 250 and 500 ng/ml) and anti-TGFβ1,2,3 (5µg/ml) were added to the bottom chamber. Cells were allowed to migrate 24 hours at 37°C in 5% CO_2. Cells were removed from the upper chamber with cotton swabs. Invading cells located on the under-side of the membrane were then fixed in 100% cold methanol 10 minutes and stained with hematoxylin and eosin. Membranes were removed and mounted on slides with Cytoseal (Thermo Fisher Scientific). A minimum of 10 images per replicate were taken at 100X total magnification and the number of invaded cells per field was counted. Cell counts were normalized to DMEM 0.1% FBS and recorded as % migrating cells.

Statistical Analyses

Statistical analyses were performed using GraphPad Prism (GraphPad Software, San Diego, CA). Immunohistochemistry quantification and all *in vitro* assays were analyzed with the unpaired Student's t test where a p-value less than 0.05 was considered significant. The survival curves were analyzed with the Gehan-Breslow-Wilcoxon test.

Acknowledgements

We gratefully acknowledge the laboratory of Dr. Mala Mahendroo and Meredith Akins for their assistance in collecting and analyzing the collagen second harmonic generation data.

Competing Interests Statement

The authors declare no competing interests.

Author Contributions

SAA contributed to the design and execution of all experiments, performed the data analysis and wrote the manuscript. LBR assisted with animal studies. JGC assisted in the maintenance of the animal colony and contributed to the animal studies. CLC performed the standard qPCR assays. SPD performed surgical implantation of tumor cells and assisted in animal studies. ADB performed hydroxyproline analysis and contributed to interpretation of results. RAB oversaw the design, execution, and interpretation of the experiments and writing of the manuscript.

References

1. Bornstein, P., *Cell-matrix interactions: the view from the outside.* Methods Cell Biol, 2002. **69**: p. 7-11.

2. Reed, M.J., et al., *Differential expression of SPARC and thrombospondin 1 in wound repair: immunolocalization and in situ hybridization.* J Histochem Cytochem, 1993. **41**(10): p. 1467-77.

3. Podhajcer, O.L., et al., *The role of the matricellular protein SPARC in the dynamic interaction between the tumor and the host.* Cancer Metastasis Rev, 2008. **27**(4): p. 691-705.

4. Pen, A., et al., *Molecular markers of extracellular matrix remodeling in glioblastoma vessels: microarray study of laser-captured glioblastoma vessels.* Glia, 2007. **55**(6): p. 559-72.

5. Mendis, D.B., G.O. Ivy, and I.R. Brown, *SPARC/osteonectin mRNA is induced in blood vessels following injury to the adult rat cerebral cortex.* Neurochem Res, 1998. **23**(8): p. 1117-23.

6. Framson, P.E. and E.H. Sage, *SPARC and tumor growth: where the seed meets the soil?* J Cell Biochem, 2004. **92**(4): p. 679-90.

7. Yan, Q., et al., *Alterations in the lens capsule contribute to cataractogenesis in SPARC-null mice.* J Cell Sci, 2002. **115**(Pt 13): p. 2747-56.

8. Bradshaw, A.D., et al., *SPARC-null mice display abnormalities in the dermis characterized by decreased collagen fibril diameter and reduced tensile strength.* J Invest Dermatol, 2003. **120**(6): p. 949-55.

9. Raines, E.W., et al., *The extracellular glycoprotein SPARC interacts with platelet-derived growth factor (PDGF)-AB and -BB and inhibits the binding of PDGF to its receptors.* Proc Natl Acad Sci U S A, 1992. **89**(4): p. 1281-5.

10. Kupprion, C., K. Motamed, and E.H. Sage, *SPARC (BM-40, osteonectin) inhibits the mitogenic effect of vascular endothelial growth factor on microvascular endothelial cells.* J Biol Chem, 1998. **273**(45): p. 29635-40.

11. Hasselaar, P. and E.H. Sage, *SPARC antagonizes the effect of basic fibroblast growth factor on the migration of bovine aortic endothelial cells.* J Cell Biochem, 1992. **49**(3): p. 272-83.

12. Francki, A., et al., *SPARC regulates TGF-beta1-dependent signaling in primary glomerular mesangial cells.* J Cell Biochem, 2004. **91**(5): p. 915-25.

13. Verrecchia, F. and A. Mauviel, *Transforming growth factor-beta and fibrosis.* World J Gastroenterol, 2007. **13**(22): p. 3056-62.

14. de la Cruz-Merino, L., et al., *Role of transforming growth factor Beta in cancer microenvironment.* Clin Transl Oncol, 2009. **11**(11): p. 715-20.

15. Kelly, R.J. and J.C. Morris, *Transforming growth factor-beta: A target for cancer therapy.* J Immunotoxicol, 2009.

16. Schiemann, B.J., J.R. Neil, and W.P. Schiemann, *SPARC inhibits epithelial cell proliferation in part through stimulation of the transforming growth factor-beta-signaling system.* Mol Biol Cell, 2003. **14**(10): p. 3977-88.

17. Ford, R., et al., *Modulation of SPARC expression during butyrate-induced terminal differentiation of cultured human keratinocytes: regulation via a TGF-beta-dependent pathway.* Exp Cell Res, 1993. **206**(2): p. 261-75.

18. Reed, M.J., et al., *TGF-beta 1 induces the expression of type I collagen and SPARC, and enhances contraction of collagen gels, by fibroblasts from young and aged donors.* J Cell Physiol, 1994. **158**(1): p. 169-79.

19. Pavasant, P., et al., *The synergistic effect of TGF-beta and 1,25-dihydroxyvitamin D3 on SPARC synthesis and alkaline phosphatase activity in human pulp fibroblasts.* Arch Oral Biol, 2003. **48**(10): p. 717-22.

20. Wrana, J.L., C.M. Overall, and J. Sodek, *Regulation of the expression of a secreted acidic protein rich in cysteine (SPARC) in human fibroblasts by transforming growth factor beta. Comparison of transcriptional and post-transcriptional control with fibronectin and type I collagen.* Eur J Biochem, 1991. **197**(2): p. 519-28.

21. Macri, L., D. Silverstein, and R.A. Clark, *Growth factor binding to the pericellular matrix and its importance in tissue engineering.* Adv Drug Deliv Rev, 2007. **59**(13): p. 1366-81.

22. Tufvesson, E. and G. Westergren-Thorsson, *Tumour necrosis factor-alpha interacts with biglycan and decorin.* FEBS Lett, 2002. **530**(1-3): p. 124-8.

23. Takeuchi, Y., Y. Kodama, and T. Matsumoto, *Bone matrix decorin binds transforming growth factor-beta and enhances its bioactivity.* J Biol Chem, 1994. **269**(51): p. 32634-8.

24. Hausser, H., et al., *Selective inactivity of TGF-beta/decorin complexes.* FEBS Lett, 1994. **353**(3): p. 243-5.

25. Schonherr, E., et al., *Decorin core protein fragment Leu155-Val260 interacts with TGF-beta but does not compete for decorin binding to type I collagen.* Arch Biochem Biophys, 1998. **355**(2): p. 241-8.

26. Pardali, E. and P. ten Dijke, *Transforming growth factor-beta signaling and tumor angiogenesis.* Front Biosci, 2009. **14**: p. 4848-61.

27. Mumm, J.B. and M. Oft, *Cytokine-based transformation of immune surveillance into tumor-promoting inflammation.* Oncogene, 2008. **27**(45): p. 5913-9.

28. Agarwal, R., et al., *Add-on angiotensin II receptor blockade lowers urinary transforming growth factor-beta levels.* Am J Kidney Dis, 2002. **39**(3): p. 486-92.

29. Laviades, C., N. Varo, and J. Diez, *Transforming growth factor beta in hypertensives with cardiorenal damage.* Hypertension, 2000. **36**(4): p. 517-22.

30. Matt, P., et al., *Circulating transforming growth factor-beta in Marfan syndrome.* Circulation, 2009. **120**(6): p. 526-32.

31. Zhou, Y., et al., *Thrombospondin 1 mediates angiotensin II induction of TGF-beta activation by cardiac and renal cells under both high and low glucose conditions.* Biochem Biophys Res Commun, 2006. **339**(2): p. 633-41.

32. Naito, T., et al., *Angiotensin II induces thrombospondin-1 production in human mesangial cells via p38 MAPK and JNK: a mechanism for activation of latent TGF-beta1.* Am J Physiol Renal Physiol, 2004. **286**(2): p. F278-87.

33. Mazzocca, A., et al., *Inhibition of transforming growth factor beta receptor I kinase blocks hepatocellular carcinoma growth through neo-angiogenesis regulation.* Hepatology, 2009. **50**(4): p. 1140-51.

34. Hallmann, R., et al., *Novel mouse endothelial cell surface marker is suppressed during differentiation of the blood brain barrier.* Dev Dyn, 1995. **202**(4): p. 325-32.

35. Arnold, S., et al., *Forced expression of MMP9 rescues the loss of angiogenesis and abrogates metastasis of pancreatic tumors triggered by the absence of host SPARC.* Exp Biol Med (Maywood), 2008. **233**(7): p. 860-73.

36. Brekken, R.A., et al., *Enhanced growth of tumors in SPARC null mice is associated with changes in the ECM.* J Clin Invest, 2003. **111**(4): p. 487-95.

37. Ostrand-Rosenberg, S. and P. Sinha, *Myeloid-derived suppressor cells: linking inflammation and cancer.* J Immunol, 2009. **182**(8): p. 4499-506.

38. Galgani, M., et al., *The Yin and Yang of CD4(+) Regulatory T Cells in Autoimmunity and Cancer.* Curr Med Chem, 2009.

39. Beyer, M. and J.L. Schultze, *Regulatory T cells: major players in the tumor microenvironment.* Curr Pharm Des, 2009. **15**(16): p. 1879-92.

40. Cao, X., *Regulatory T cells and immune tolerance to tumors.* Immunol Res, 2009.

41. Wendt, M.K., T.M. Allington, and W.P. Schiemann, *Mechanisms of the epithelial-mesenchymal transition by TGF-beta.* Future Oncol, 2009. **5**(8): p. 1145-68.

42. Xu, J., S. Lamouille, and R. Derynck, *TGF-beta-induced epithelial to mesenchymal transition.* Cell Res, 2009. **19**(2): p. 156-72.

43. Bingle, L., N.J. Brown, and C.E. Lewis, *The role of tumour-associated macrophages in tumour progression: implications for new anticancer therapies.* J Pathol, 2002. **196**(3): p. 254-65.

44. Norose, K., et al., *SPARC deficiency leads to early-onset cataractogenesis.* Invest Ophthalmol Vis Sci, 1998. **39**(13): p. 2674-80.

45. Bruns, C.J., et al., *In vivo selection and characterization of metastatic variants from human pancreatic adenocarcinoma by using orthotopic implantation in nude mice.* Neoplasia, 1999. **1**(1): p. 50-62.

CHAPTER FIVE: DISCUSSION AND FUTURE DIRECTIONS

SPARC can modulate ECM assembly, integrin activity and growth factor signaling; thereby, controlling a range of cellular functions including adhesion, proliferation, survival and migration. Therefore, it is not surprising that the expression of SPARC is dysregulated in many human cancers and that this dysregulation contributes to patient outcome. Although there is no unifying mechanism, as yet, for the effects of SPARC in tumorigenesis, this protein clearly influences the microenvironment and signaling pathways involved in disease progression. The concept that SPARC regulates cell function through modulation of integrin binding and activation is provocative, since integrin receptors have also been implicated in each of the cellular processes influenced by SPARC. To date, no bona fide signaling receptor has been identified for SPARC. However, given that SPARC directly binds to the ECM, integrins and growth factor/receptor complexes, we propose that SPARC functions as an extracellular scaffolding protein; whereby, SPARC dictates the activating threshold at which integrin and growth factor-signaling processes propagate cellular events (Figure 1). It is known that there is extensive cross-talk between integrin- and growth factor -signaling pathways, and that integrin signaling is required for proper cellular responses to cytokine stimulation [1-4]. In addition, integrins can associate directly with growth factor receptors [1-4]. By controlling the clustering and activation of integrins, as well as, the association and cross-talk with growth factor receptors, SPARC might function as a rheostat for cellular signaling and behavior. Thus, factors controlling the effects of

SPARC on any particular cell would consist of the ECM composition, integrin profile, cytokine milieu, cell type (e.g. mesenchymal, endothelial or epithelial), and SPARC concentration/cell-surface localization. This concept provides a potential explanation for how SPARC modulates so many cellular events, and for why the considerable data collected in regard to SPARC during tumorigenesis have failed to elucidate any specific and consistent mechanism.

It is difficult to determine a mechanism when numerous confounding factors are involved, and when many groups publish seemingly contradictory data on the function of SPARC. However, we propose that this collection of incongruous data is a result of the dependence of SPARC function on multiple factors associated with its role as an extracellular scaffolding protein and signaling rheostat. Future experiments should aim to validate whether SPARC controls the formation of integrin- and growth factor-receptor complexes and, if so, to clarify how these associations control cellular responses to various cytokines. Additionally, it is pertinent to determine how SPARC dictates the activities of each cell type in the tumor microenvironment. Given that SPARC contributes to such a diverse and conflicting range of activities, targeting SPARC globally in human cancer has the potential to present with adverse off-target effects. Therefore, clarification of the molecular mechanisms that involve the role of SPARC during tumorigenesis is necessary in order to develop effective strategies that can target SPARC therapeutically and exploit the idea of manipulating the tumor microenvironment to control cancer growth and metastasis.

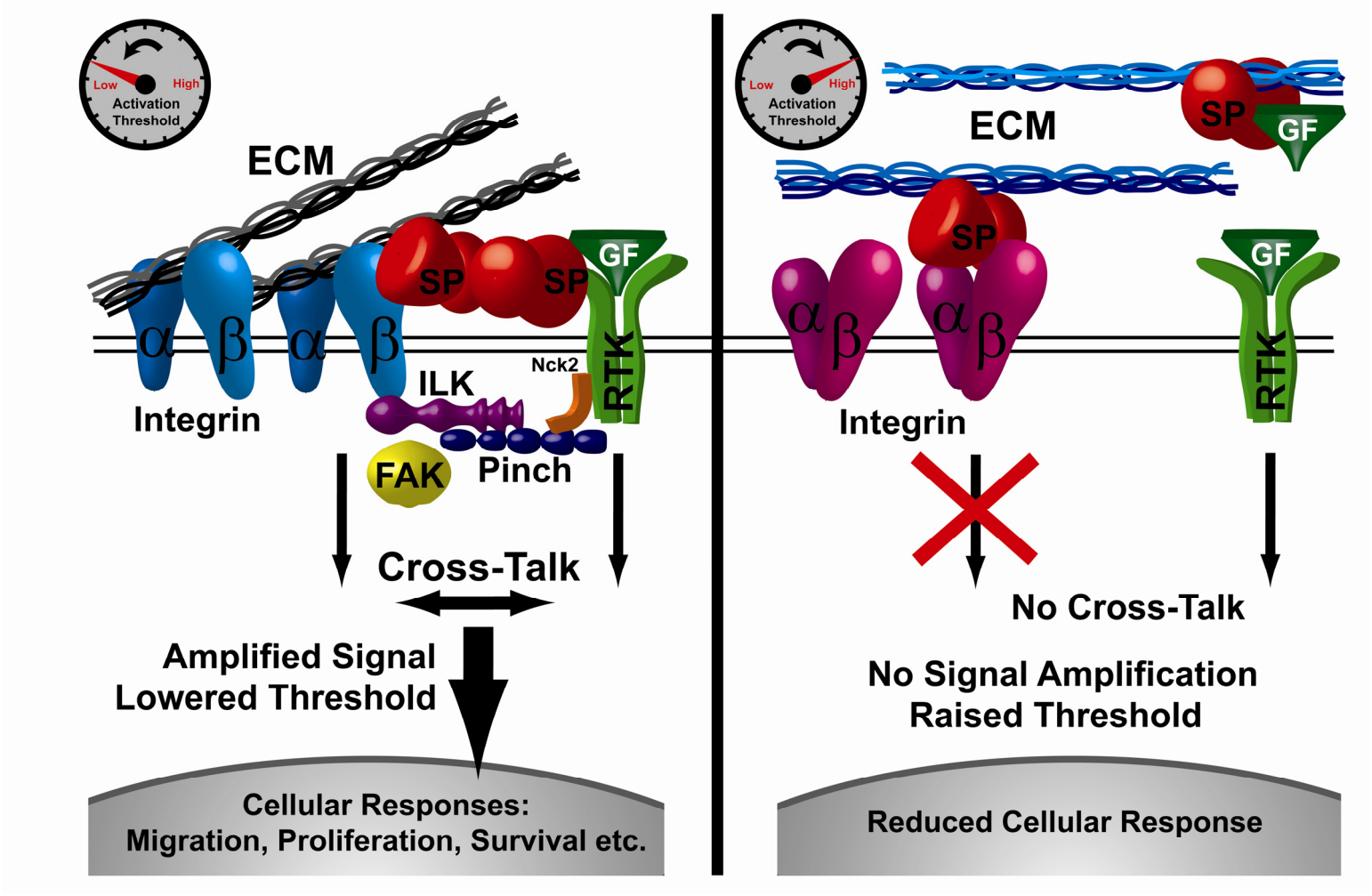
Low
High
Activation Threshold
ECM
SP
SP
GF
α
β
α
β
Integrin
ILK
Nck2
RTK
FAK
Pinch
Cross-Talk
Amplified Signal
Lowered Threshold
Cellular Responses:
Migration, Proliferation, Survival etc.
Low
High
Activation Threshold
ECM
SP
GF
SP
GF
α
β
α
β
Integrin
RTK
No Cross-Talk
No Signal Amplification
Raised Threshold
Reduced Cellular Response

Figure 1. SPARC as an Extracellular Scaffolding Protein and Rheostat. We propose that SPARC (SP) acts as an extracellular scaffolding protein; whereby, SPARC controls the interactions and cross-talk between the extracellular matrix (ECM), integrins (α, β) and growth factor receptors (RTK). By controlling integrin clustering and activation, as well as, integrin communication with growth factor receptors, SPARC can function as a rheostat for signaling and cellular response. (Left) SPARC may decrease the activating threshold of certain growth factors (GF) by enhancing complex formation and cross-talk between integrins and growth factor receptors. Integrin-linked kinase (ILK), Pinch, and Nck2 link integrins and growth factor receptors, intracellularly, to form localized signaling cascades, while SPARC acts as an extracellular scaffold to reinforce this complex. Focal adhesion kinase (FAK) is just one example of a signaling molecule located downstream of both integrins and growth factor receptors whose activation is influenced by SPARC. Ultimately, integrin-growth factor receptor cross-talk leads to signal amplification and enhanced cellular responses. (Right) SPARC may also increase the activating threshold of integrins and growth factors by inhibiting the binding of certain integrins to the ECM, opposing integrin-growth factor receptor clustering, and/or sequestering growth factors in the extracellular milieu. All of these effects result in a loss of communication and signal amplification of integrins and growth factor receptors, which reduces cellular responses. ECM composition, integrin profile, cytokine profile, cell-type and SPARC concentration/cell-surface localization are all factors dictating this differential response to SPARC.

References

1. Eliceiri, B.P., *Integrin and growth factor receptor crosstalk.* Circ Res, 2001. **89**(12): p. 1104-10.

2. Porter, J.C. and N. Hogg, *Integrins take partners: cross-talk between integrins and other membrane receptors.* Trends Cell Biol, 1998. **8**(10): p. 390-6.

3. Somanath, P.R., A. Ciocea, and T.V. Byzova, *Integrin and growth factor receptor alliance in angiogenesis.* Cell Biochem Biophys, 2009. **53**(2): p. 53-64.

4. Streuli, C.H. and N. Akhtar, *Signal co-operation between integrins and other receptor systems.* Biochem J, 2009. **418**(3): p. 491-506.

ACKNOWLEDGEMENTS

Foremost, I would like to express my gratitude to a wonderful mentor, Rolf Brekken, for his patience and guidance. Rolf's passion for science and ability to provide hands-on mentorship has made my graduate studies exciting and memorable. His "open-door" policy and continual support has gently guided me through the challenges of graduate school, all while inspiring me to become an independent scientist. His concern, empathy and thoughtfulness for his graduate students are unwavering and inspiring. I could not have asked for a better mentor.

I would like to acknowledge my thesis committee members Kristine E. Kamm, Philip E. Thorpe and Michelle Tallquist Seidel for their amazing direction and motivation. Challenging questions, detailed discussion and thoughtful insight were never lacking.

Of course, none of this would be possible without the assistance and encouragement from the entire Brekken laboratory. The Brekken lab has inspired friendships and scientific partnerships that will last a life-time.